



UNIVERSITY OF READING

DEPARTMENT OF MATHEMATICS AND STATISTICS

**Computational and theoretical
modelling of self-healable polymer
materials**

Dipesh Amin

Thesis submitted for the degree of
Doctor of Philosophy

June 2016

Abstract

In this thesis we study self-healing polymeric materials, these are materials which can autonomously heal upon fracture (showing a partial or full recovery of mechanical strength). While there are a number of approaches to self-healing we focus on modelling supramolecular polymer networks. These are formed by physical association of linear or branched polymers via reversible and highly directional non-covalent bonds. We carry out hybrid molecular dynamics/Monte Carlo simulations of supramolecular networks formed by unentangled telechelic chains. The association of stickers leads to the formation of a transient network. At high bonding energies, the majority of stickers are fully reacted and the fraction of open stickers is less than 1%. We find the dynamical behaviour of such systems is dominated by a partner exchange mechanism in which stickers exchange their associated partners by the association and disassociation of sticker clusters. We propose a phantom chain hopping model to describe chain relaxation dynamics in supramolecular networks, which provides numerical predictions in reasonably good agreement with our simulation results. These systems are then studied under both shear and planar extensional flows. The presence of transient networks leads to a huge increase in viscosity. We find strain hardening behaviour in start-up flow for shear rates higher than the reciprocal of the average bond lifetime which we conclude results from the non-Gaussian stretching of polymer chains. An overall reduction in the number of network strands is also seen which ultimately leads to shear thinning behaviour in steady-state. We also carry out simulations of mildly entangled monodisperse polymer chains under planar extensional flow by taking advantage of the computational benefits afforded by using GPUs in scientific computing. The method developed is found to be 10 times faster than a CPU approach while providing similar accuracy. These simulations are

shown alongside experiments of uniaxial extension and provide qualitatively similar behaviour (both showing extensional thickening at intermediate rates).

Declaration of Authorship

I confirm that this is my own work and the use of all material from other sources has been properly and fully acknowledged.

Dipesh Amin

Acknowledgements

I would like to thank my supervisors Dr. Zuowei Wang and Prof. Alexei E. Likhtman for their patience and insight during my PhD. Prof. Alexei E. Likhtman sadly passed away before it's completion. His energy and focus were an inspiration to all his students, and he will be sorely missed. I also want to thank the other members of the Theoretical Polymer Physics group for their knowledge and guidance.

Finally, I would like to thank my family and friends for their support and encouragement during my research.

Contents

List of Figures	v
1 Introduction	1
1.1 Motivation	1
1.2 Overview	4
1.3 Molecular Rheology	4
1.3.1 Microscopic definition of stress	4
1.3.2 Viscoelasticity	6
1.4 Polymer dynamics	7
1.4.1 Brownian motion	7
1.4.2 Freely jointed chains	9
1.4.3 Gaussian chains	10
1.4.4 Rouse model	10
1.4.5 Tube model	14
1.5 Theory of associating polymers	17
1.5.1 Sticky Rouse	18
1.5.2 Sticky Reptation	19
1.5.3 Self-healing	20
1.6 Network theory	21
1.6.1 Affine network model	22

1.6.2	Phantom network model	22
1.7	Molecular dynamics	23
1.7.1	Periodic boundary conditions	23
1.7.2	Pair interactions	25
1.7.3	Numerical integration scheme	26
1.8	Monte Carlo methods	28
1.8.1	Metropolis Hastings algorithm	28
1.8.2	Association dynamics	29
2	Dynamics in supramolecular polymers	32
2.1	Introduction	32
2.2	Models and Simulation Methods	36
2.3	Results and Discussions	39
2.3.1	Static properties: reversible network analysis	39
2.3.2	Dynamic and rheological properties	50
2.3.3	Theoretical models	66
2.4	Conclusions	72
3	Non-linear rheology	75
3.1	Introduction	75
3.1.1	Supramolecular polymers	77
3.2	Time-dependent rheology	80
3.3	Equations of motion	81
3.4	Thermostat	83
3.4.1	Simulation parameters	84
3.5	Shear flow	85
3.6	Extensional flow	86
3.6.1	KR boundary conditions	87

3.7	Results	90
3.7.1	Viscosity	90
3.7.2	Chain stretching and network structure	96
3.7.3	Steady state properties	100
3.8	Conclusions	103
4	Extensional flow of entangled polymers	105
4.1	Introduction	105
4.2	System mapping and linear viscosity	108
4.3	GPU simulations	112
4.3.1	Motivation	112
4.3.2	Hardware	112
4.3.3	Implementation	114
4.4	Results	118
4.5	Conclusions	123
5	Conclusions	125
5.1	Conclusions	125
5.2	Future Work	128

List of Figures

1.1	Illustration of simple shear flow.	6
1.2	N -step freely jointed random walk.	10
1.3	Illustration of a Rouse chain.	11
1.4	A chain in a fixed network of obstacles. The tube is depicted by dashed lines.	15
1.5	Illustration showing 2D periodic boundary conditions.	24
1.6	A graph showing the potentials experienced by a sticker eq. 1.15 . . .	30
2.1	Snapshot of a transient network formed by associating telechelic chains of length $N = 25$ and sticky bonding energy $\varepsilon = 10k_B T$. The red spheres represent the stickers at the chain ends.	39
2.2	Weight-averaged chain cluster size as a function of the extent of reaction p as obtained in supramolecular polymer systems with sticker functionality $f = 3$. The simulations were performed using different box sizes and so different number of parent chains N_{ch}	41
2.3	Average fractions of stickers that are in open, partially reacted and fully reacted states as a function of sticky bonding energy ε . The chain length is $N = 25$	42

2.4	(a) Probabilities for finding a sticker in a sticker cluster of size N_{clu} in the systems with sticky bonding energy $\varepsilon = 10k_B T$. The dashed curves illustrate the analytical results given by eq. (2.8). (b) Average sticker cluster size as a function of sticky bonding energy.	43
2.5	(a) Fraction of elastically ineffective strands, ϕ_{ineff} , in the supramolecular networks obtained by using different cutoffs to identify fully contracting chains in the PPA-type analysis. The inset presents the probability distributions of the chain end-to-end distances in the fixed networks with both excluded volume interactions and thermal fluctuations switched off. (b) Direct MD simulation results on the stress relaxation of fixed polymer networks that are generated by fixing the topological structures of transient networks obtained from hybrid MD/MC simulations. All results are averaged over 100 statistically independent network configurations, and the error bars show the standard deviation of the mean. The polymer chain length is $N = 25$. . .	47
2.6	Average sticky bond lifetime τ_b , partner exchange time τ_{pe} , and cluster exchange time τ_{ce} with respect to sticky bonding energy ε for the systems with two different chain lengths and $\tau_{MC} = 0.01\tau_{LJ}$	52
2.7	(a) Schematic demonstration of a partner exchange event which has a characteristic time τ_{pe} ; (b) Probability distributions of the partner exchange time τ_{pe} and cluster exchange time τ_{ce} for supramolecular systems with chain length $N = 25$ and bonding energy $\varepsilon = 10k_B T$. . .	55

2.8	(a) Sketch of a partner exchange event via the sticker cluster association-dissociation process. (b) Right-stochastic matrix that measures the probability for a sticker initially in a cluster of size i (i th row) to transfer into a final cluster of size j (j th column) for the system with $\varepsilon = 10k_B T$ and $N = 25$. The two solid lines indicate the high probabilities for the cluster sizes to change by ± 3 stickers.	58
2.9	(a) Mean-square displacements of stickers in supramolecular systems with different sticky bonding energies ε . The black dotted-dashed curve shows results obtained from fixed polymer networks whose configurations were taken from simulations of supramolecular systems with $\varepsilon = 12k_B T$. For reference the Rouse time τ_R and the sticker partner exchange time at $\varepsilon = 10T$ are given by the two vertical dashed lines on the right. (b) MSD of sticker clusters with different sizes $N_{clu} \leq 6$ at $\varepsilon = 10k_B T$. The parent chain length is $N = 25$ in all cases.	62
2.10	Stress relaxation (a) and chain end-to-end vector correlation functions (b) in the systems with $N = 25$ and various bonding energies ε . The dotted-dashed curves present the results obtained from fixed polymer networks whose configurations were taken from simulations of supramolecular systems with $\varepsilon = 12k_B T$	63
2.11	Simulation results on the terminal relaxation times of the stress and chain end-to-end vector correlation functions. The terminal relaxation times predicted by eq. (2.12) using simulation data on the sticker partner exchange time and hopping distance are also included.	64
2.12	Stress relaxation functions of supramolecular systems with and without a upper cap N_{clu}^* for the sticker cluster sizes. The system parameters are $\varepsilon = 10k_B T$ and $N = 25$	66

2.13	Sketch of the phantom hopping model. The red circles represent the stickers at the ends of the target chain.	67
2.14	Simulation results of the phantom chain hopping model on the end-to-end vector correlation function $\Phi(t)$ (a) and the sticker mean square displacement (b) of the target chains. The symbols are the results obtained from hybrid MD/MC simulations of supramolecular networks with polymer chain length $N = 25$ at various bonding energies ϵ . The simulation times in both the PCHM and supramolecular systems have been rescaled by the Rouse times of the corresponding polymer chains. The dotted-dashed line in (a) presents the $\Phi(t)$ data of the fixed polymer network same as in Figure 2.10(b).	71
3.1	Illustration showing the deformation of a volume under the application of shear and planar extension.	76
3.2	The “M1” muddle described by James and Walters (1993). Shows the difference in extensional viscosity calculated for a single material using different experimental techniques.	77
3.3	Illustration of the Lees-Edwards sliding brick periodic boundary conditions for planar couette flow. The grey lines show the equivalent simulation box for Langragian-Rhomboid periodic boundaries.	86
3.4	Evolution of randomly positioned particles via the Kraynik-Reinelt (KR) lattice under planar extensional flow as a function of time. Only the x - and y -axis vary with time. At $\epsilon = \epsilon_p$ the lattice reproduces itself, and the particles are shown before the positions are folded back (c).	88

3.5	Simulations results for a melt system without stickers for a number of shear and extension rates. The black dot-dashed line highlights the linear viscosity curve calculated from the equilibrium stress autocorrelation function.	91
3.6	Simulation results for the supramolecular system with bonding energy $\varepsilon = 10$ for a number of shear and extension rates. The black dot-dashed line highlights the linear viscosity curve calculated from the equilibrium stress autocorrelation function.	94
3.7	The end-to-end vector and the fraction of open, partially- and fully-reacted stickers as a function of time.	97
3.8	Evolution of a chain configuration (taken from a simulation of $N = 45$, $N_{ch} = 400$ and $\varepsilon = 10k_B T$) with shear rate $\dot{\gamma} = 5 \times 10^{-3}/\tau_{LJ}$	99
3.9	Comparison of steady state viscosity with and without stickers present.	101
3.10	(a)-(b) The change in fraction of open, partially- and fully-reacted stickers as a function of deformation rate. (c)-(d) The change in bond lifetime and partner exchange time as a function of deformation rate.	102
4.1	Application of the orientation relaxation function to approximate the stress relaxation function following the stress-optical law.	110
4.2	Mapping of MD simulations using $N = 235$ using an approximation of the stress relaxation function derived via the stress-optical law to the experimental PS50K data. The time shift factor used in the mapping is 2.05×10^4	111
4.3	Illustration highlighting the difference in execution between GPUs and CPUs. This picture was adapted from a talk presented by James Balfour.	113
4.4	Illustration showing Z-order curve iterations in 3D. This image was created using Mathematica by Robert Dickau (2008).	115

4.5	The steps of a parallel reduction operation on four elements.	116
4.6	Comparison of transient viscosity results obtained from GPU (symbols) and CPU (lines) simulations.	118
4.7	Comparison of transient viscosity results obtained from GPU simulations of planar extension of $N = 235$ and experiments of uniaxial extension of PS50K.	119
4.8	Comparison of steady state viscosity results obtained from GPU simulations of planar extension of polymer melts with chain length $N = 235$ and experiments of uniaxial extension of PS50K.	121
4.9	Transient viscosity for a large number of extension rates with $N = 235$.	122
4.10	Comparison of steady state viscosities, $\bar{\eta}$, for a number of extension rates, $\dot{\epsilon}$, between molecular dynamics simulations and the Doi-Edwards tube theory.	123

Chapter 1

Introduction

1.1 Motivation

The word polymer derives from the ancient Greek word *polus* (many) and *meros* (parts). As this description suggests polymers are large molecules or macromolecules constructed of many repeated subunits known as monomers. These materials have become essential in all aspects of modern life due to their broad range of properties (*e.g.*, mechanical strength, temperature resistance, structure) and can be found in everyday items' from the polyethylene terephthalate used to make drinks bottles to the composite polymers used in the Airbus A380 'Superjumbo' airframe. While natural sources of polymers exist, the most widely used polymers are synthesised using petrochemical feedstocks which are in limited supply and subject to an ever increasing cost. This is where the development of materials which can be more easily recycled and which possess an increased lifespan will play an important role in reducing humanity's environmental cost.

One class of materials which stand out in this regard are those capable of autonomous healing. Self-healing materials are inspired by biological systems where damage results in an autonomous healing process which does not require external intervention (*e.g.*, blood clotting, bone repair) [1]. Self-healing materials are capable of repairing themselves upon damage with a full or partial recovery of mechanical strength. In recent years reversible chemical bonds have been exploited to produce healable materials which are more efficiently recycled. The production of materials which can heal either small cracks or fractures will dramatically improve the longevity of polymeric products. We are already starting to see the first commercially available examples in the form of healable coatings by manufacturers such as Nippon Paint and Bayer [1].

There are three primary approaches to self-healing [2]: 1) Intrinsic healing 2) Capsule based healing and 3) Vascular healing. Intrinsic healing relies on designing smart materials with temporary reversible bonds. These temporary bonds break when a fracture occurs but can subsequently autonomously reform. In capsule based approaches small capsules containing a repairing agent are embedded within the polymer matrix. These capsules then break open during fracture releasing their payload which fixes the material. Vascular self-healing approaches are most directly inspired by biological systems (the vascular system). These incorporate a healing agent in microchannels which run through the polymer matrix. In this thesis we focus on intrinsic self-healing as these materials are often designed using techniques of polymer physics. We study a class of materials known as supramolecular polymer networks.

Supramolecular polymer networks are formed by the physical association of linear or branched polymers via reversible non-covalent bonds [3, 4, 5, 6], such as hydrogen bonds [7, 8, 9, 10, 11, 12], $\pi - \pi$ stacking [13, 14], metal-ligand [15, 16, 17, 18] and

ionic interactions [19, 20, 21, 22]. The reversibility of crosslinking provides them unique abilities for working as self-healing, stimuli-sensitive and shape-memory materials (with the introduction of double networks). They also have superior processing and recycling properties over traditional polymers and chemical networks constructed from covalently crosslinked polymers owing to the sharp decrease in viscosity upon increasing temperature or decreasing concentration. The potential applications of supramolecular polymer networks have inspired strong interests in understanding the physical mechanisms underlying their structural, dynamical and mechanical properties.[3, 4, 5, 6]

The topological structures of supramolecular polymer networks are determined by the molecular composition of the parent polymers and the nature of the non-covalent interactions. For example, telechelic or triblock polymers with hydrophobic or hydrogen-bond-rich end blocks can associate into networks consisting of either flower-like micelles or large aggregates of attracting end groups bridged by flexible chains, depending on polymer concentration. [23, 24, 25] On the other hand, in transient networks formed by copolymers with many substituted associating groups, each chain is crosslinked with many other chains at well-separated bonding sites along its backbone. [12, 26, 19] In the latter case, each associating group is attached to two chain segments. The complicated topological structures, together with the interplay between the dynamics of the parent polymers and the breaking/reforming kinetics of the physical bonds, leads to the rich dynamical behavior of supramolecular networks.

1.2 Overview

This thesis is organised as follows: In the remainder of this chapter we review important aspects of polymer physics. In addition the methodology used in molecular dynamics simulations is outlined. As we wish to study associating polymers, this chapter also includes a description of the hybrid molecular dynamics and Monte Carlo approach we have adopted for modelling associating polymers. In Chapter 2 we study the equilibrium dynamics of associating polymer systems. The presence of associating monomers or stickers leads to the creation of a transient network at higher bonding energies, which consequently results in a dramatic slow-down in dynamic behaviour. In Chapter 3 we carry out non-equilibrium molecular dynamics simulations of these associating polymer system under both planar extensional flow and shear flow. Finally, in the last chapter we study the rheology of entangled polymer chains under start-up extension.

1.3 Molecular Rheology

1.3.1 Microscopic definition of stress

The stress tensor $\sigma_{\alpha\beta}$ (where α and β denote cartesian components x, y or z) is defined as the force per unit area in the α direction acting across a plane which is perpendicular to the β -axis. For a component $\sigma_{\alpha z}$ if we consider a volume V of fluid which is divided by a hypothetical plane perpendicular to the z -axis the stress tensor is given by the force S_α which the upper part exerts on the lower part through the plane along the α -direction

$$\sigma_{\alpha z} = \langle S_\alpha \rangle / A$$

where A is the area of the plane. In a polymer solution the force S_α consists of two parts, *i.e.*, the force which acts through the solvent S_α^s and the force which acts between the monomers or beads S_α^p . Therefore, the complete stress tensor can be written as

$$\sigma_{\alpha\beta} = \eta_s(\kappa_{\alpha\beta} + \kappa_{\beta\alpha}) + P\delta_{\alpha\beta} - \frac{1}{V} \sum_i F_i^\alpha R_i^\beta$$

where η_s denotes the solvent viscosity and $\kappa_{\alpha\beta}$ is the velocity gradient tensor. The final term is a summation over all particles in the system, and R_i denotes the i -th particle position and the total force $F_i = -\frac{\partial U}{\partial R_i}$ acting on this particle is given in terms of its potential energy U . The pressure tensor P is given by

$$P = \frac{1}{V} \left(\sum_i \frac{p_i p_i}{m_i} + \sum_i F_i^\alpha R_i^\beta \right)$$

where p_i denotes the peculiar velocity of a particle i and m_i is the mass of particle i . In dilute solutions, the major contribution to the stress is purely viscous, which is given by the first term. On the other hand, when the polymer concentration increases the last term begins to dominate. Thus, in dense polymer systems the total stress is simply given by [27]

$$\sigma_{\alpha\beta} = -\frac{1}{V} \sum_i F_i^\alpha R_i^\beta.$$

If the forces are pairwise this can conveniently be rewritten as

$$\sigma_{\alpha\beta} = -\frac{1}{V} \sum_{i<j} R_{ij}^\alpha F_{ij}^\beta \tag{1.1}$$

where $\mathbf{R}_{ij} = \mathbf{R}_i - \mathbf{R}_j$ and \mathbf{F}_{ij} is the force acting on particle i from particle j . Eq. (1.1) is used in the calculation of stress for polymer melts where no solvent is involved (as is the case for all systems studied in this thesis).

1.3.2 Viscoelasticity

Viscosity describes the resistance of a material to gradual deformation by shear stress. The stress response of a viscoelastic material to a small step strain γ is given by $\sigma_{xy}(t) = \gamma G(t)$ where $G(t)$ is defined as the stress relaxation function. In an equilibrium system, $G(t)$ is calculated from the stress auto-correlation function

$$G(t) = \frac{V}{k_B T} \langle \sigma_{xy}(t + \tau) \sigma_{xy}(\tau) \rangle \quad (1.2)$$

where xy are any two orthogonal directions and $G(t)$ is averaged over all pairs of orthogonal directions. The angular brackets $\langle \cdot \rangle$ denote an ensemble average, which is calculated with respect to the initial time, τ . In simulations of time-dependent correlation functions we make use of the multiple-tau correlator method [28] which allows us to calculate autocorrelation functions on the fly.

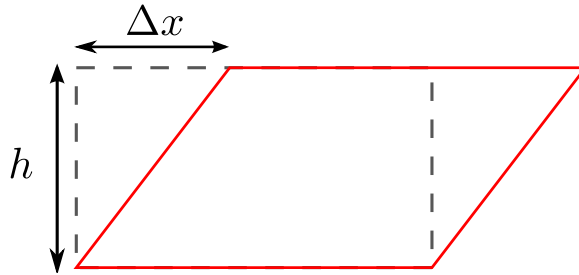


Figure 1.1: Illustration of simple shear flow.

If we now consider a fluid under simple shear, see Fig 1.1, the shear strain is given by $\gamma = \Delta x/h$. The shear stress σ_{xy} is then defined as the ratio of applied force in the x -direction and the cross-sectional surface area *i.e.*, $\sigma_{xy} = f/A$. Then from Newton's law of viscosity we know $\eta \frac{d\gamma}{dt} = f/A$, therefore, under simple shear the viscosity is defined in terms of the shear stress

$$\eta = \sigma_{xy} / \dot{\gamma}.$$

In this thesis we also consider planar extension, this is a deformation where the fluid expands in one direction and contracts in another direction with the remaining direction fixed. In our simulations the x -direction is expanding and the y -direction is contracting. Therefore, the planar extensional viscosity is defined as

$$\eta_E = \frac{\sigma_{xx} - \sigma_{yy}}{4\dot{\epsilon}}$$

where the factor of 4 in the denominator accounts for the Trouton ratio which allows for comparison between shear and planar extensional flows [29]. Here $\dot{\epsilon}$ denotes the extension rate. In the linear regime viscosity can be determined using the stress relaxation function eq. 1.2

$$\eta(t) = \int_0^t G(t') dt'$$

this will be calculated as additional validation of our procedure for the non-equilibrium regime. In Chapter 3 aspects of non-linear rheology are discussed further.

1.4 Polymer dynamics

1.4.1 Brownian motion

In 1872 the botanist Robert Brown [30] observed random motion of particles while examining grains of pollen suspended in water and he later observed the same motion of inorganic molecules, allowing him to rule out that this motion was due to living organisms.

This phenomenon was later termed Brownian motion and in 1905 Albert Einstein published a paper explaining in detail how the motion that Brown had observed was a result of pollen particles colliding with surrounding water molecules. This allowed him to derive the Einstein relation which describes the relationship between

a particles diffusion and it's friction (due to surrounding particles). Diffusion is the physical process by which particles spread steadily from regions of high concentration to regions of low concentration. Therefore, to understand the motion of an individual particle one must consider the concentration of particles. We can derive the Einstein relation in one dimension by considering the concentration $c(x, t)$ of particles at position x and time t . Then diffusion is described by Fick's Law which states that given a non-uniform concentration there is a flux which is proportional to the spatial gradient of concentration $j(x, t) = -D \frac{\partial c}{\partial x}$. In addition if there is an external potential $U(x)$ which exerts a force

$$F = -\frac{\partial U}{\partial x}$$

then an additional flux term is needed given by $j(x, t) = -\frac{c}{\zeta} \frac{\partial U}{\partial x}$ where ζ is known as the friction coefficient and describes mobility. Using the continuity equation

$$\frac{\partial c}{\partial t} = -\frac{\partial j}{\partial x}$$

we find

$$\frac{\partial c}{\partial t} = -\frac{\partial}{\partial x} \left(-D \frac{\partial c}{\partial x} - \frac{c}{\zeta} \frac{\partial U}{\partial x} \right).$$

At equilibrium the concentration of particles is given by the Boltzmann distribution

$$c_0 = A \exp(-U(x)/k_B T)$$

where k_B is the Boltzmann constant, T is the absolute temperature and A is a normalization factor. The flux term must then vanish at a concentration c_0 :

$$-D \frac{\partial c_0}{\partial x} - \frac{c_0}{\zeta} \frac{\partial U}{\partial x} = 0$$

which leads to the well-known Einstein relation

$$D = \frac{k_B T}{\zeta}.$$

The Einstein relation quantifies the diffusion of particles, allowing us to describe the random (Brownian) motion of particles. The Einstein relation is a special case of a more general theorem known as the fluctuation dissipation theorem [27]. Brownian motion plays an important role in modelling of polymer solutions and melts. In 3D the random motion of a particle can thus be modelled using a Wiener process

$$\zeta d\mathbf{r} = \sigma d\mathbf{W}$$

where $\sigma^2 = 2k_B T \zeta$ is the variance given by the Einstein relation and the left hand side term accounts for the frictional force experienced by a particle. Here the inertia term $m\ddot{r}$ has been ignored due to the high friction assumption.

1.4.2 Freely jointed chains

Firstly we consider the simplest representation of a polymer chain: an N -step random walk constructed of bonds with a fixed length b , see Figure 1.2. Each of these bonds points in a random direction which is uncorrelated with neighbouring bonds. The mean end-to-end vector is then simply $\langle \mathbf{R}_{ee} \rangle = 0$, however the mean squared end-to-end distance is given by

$$\langle \mathbf{R}_{ee}^2 \rangle = Nb^2.$$

As \mathbf{R}_{ee} is a sum of vectors with fixed length the central limit theorem tells us that for sufficiently large N the end-to-end vector can be described by a Gaussian distribution

$$\Psi(\mathbf{R}_{ee}) = \left(\frac{3}{2\pi Nb^2} \right)^{3/2} \exp \left(\frac{-3\mathbf{R}_{ee}^2}{2Nb^2} \right).$$

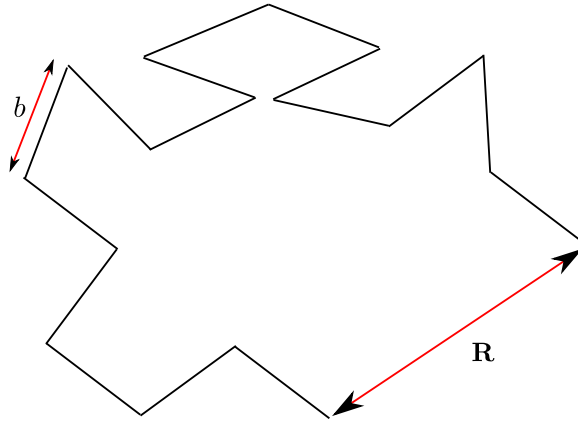


Figure 1.2: N -step freely jointed random walk.

1.4.3 Gaussian chains

The simplest model consistent with a Gaussian end-to-end vector distribution is one where every bond vector, \mathbf{r} , is itself Gaussian distributed

$$\psi(\mathbf{r}) = \left(\frac{3}{2\pi Nb^2} \right)^{3/2} \exp\left(\frac{-3\mathbf{r}^2}{2Nb^2} \right).$$

This is in contrast to the freely-jointed model discussed above where each bond had a fixed length. This approach is known as the Gaussian model and is often represented in terms of a model of ‘beads’ connected by harmonic springs with the same potential used in the Rouse model.

1.4.4 Rouse model

The Langevin equation describes the motion of a monomer which experiences regular forces due to interactions with other monomers in addition to random and friction forces due to interactions with surrounding media

$$\frac{d^2\mathbf{R}_i}{dt^2}m = -\nabla U(\mathbf{R}_1, \dots, \mathbf{R}_N) - \zeta \frac{d\mathbf{R}_i}{dt} + \sqrt{2k_B T \zeta} d\mathbf{W}_i, \quad (1.3)$$

where ζ is the friction coefficient, m is the monomer mass, $U(\mathbf{R}_1, \dots, \mathbf{R}_N)$ denotes the interaction potential which is dependent on all N monomers, and \mathbf{W}_i is a Wiener process for particle i .

The Rouse model [31] is often described as the cornerstone of polymer dynamics as it allows for a number of time-dependent properties to be calculated analytically, and most polymer models reduce to it on large length- or time-scales. In the Rouse

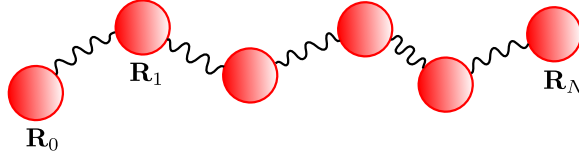


Figure 1.3: Illustration of a Rouse chain.

model a simple harmonic potential of the form

$$U_{Rouse}(\mathbf{R}_{i+1}, \mathbf{R}_i) = \frac{3k_B T}{2b^2} \sum_{i=0}^{N-1} (\mathbf{R}_{i+1} - \mathbf{R}_i)^2$$

acts between adjacent monomers \mathbf{R}_{i+1} and \mathbf{R}_i within a chain (see Figure 1.4), where the prefactor is chosen such that the average square of the bond length is

$$\langle (\mathbf{R}_{i+1} - \mathbf{R}_i)^2 \rangle = b^2.$$

In addition the Brownian dynamics assumption is used, which states the inertia term on the left hand side of eq. 1.3 becomes less important with time, therefore, this term is set to zero. The motion of a Rouse chain can then be described by a coupled system of stochastic differential equations (SDEs):

$$\zeta \frac{d\mathbf{R}_0}{dt} = \frac{3k_B T}{b^2} (\mathbf{R}_1 - \mathbf{R}_0) + \sqrt{2k_B T \zeta} d\mathbf{W}_0 \quad (1.4)$$

$$\zeta \frac{d\mathbf{R}_i}{dt} = \frac{3k_B T}{b^2} (\mathbf{R}_{i+1} + \mathbf{R}_{i-1} - 2\mathbf{R}_i) + \sqrt{2k_B T \zeta} d\mathbf{W}_i \quad (1.5)$$

$$\zeta \frac{d\mathbf{R}_N}{dt} = \frac{3k_B T}{b^2} (\mathbf{R}_{N-1} - \mathbf{R}_N) + \sqrt{2k_B T \zeta} d\mathbf{W}_N \quad (1.6)$$

The Rouse model is an example of an ideal chain model where interchain interactions are not taken into account. It also neglects excluded volume within single chains and hydrodynamic interactions. The system of SDEs can be rewritten in terms of independent normal modes (referred to as Rouse modes) which allows for the motion of a chain to be described by a sum of independent random processes. This property allows a number of observables to be determined analytically (*e.g.*, the stress relaxation function, monomer mean-squared displacement and chain end-to-end vector correlation function). A good description of the analytical calculations is presented by Likhtman [32] we briefly review some of these here. These observables are also calculated in our computer simulations and provide a means by which to probe dynamic behaviour.

Stress relaxation function

In the Rouse model the equilibrium stress relaxation function is defined in terms of the Rouse mode relaxation times

$$G(t) = \frac{k_B T c}{(N+1)} \sum_{p=1}^N \exp\left(-\frac{2t}{\tau_p}\right)$$

where the relaxation time of the p -th Rouse mode, τ_p , is given by

$$\tau_p = \frac{\zeta b^2}{12k_B T} \sin^{-2}\left(\frac{\pi p}{2(N+1)}\right)$$

and the concentration c is the number of monomers per unit volume. The longest relaxation time (or Rouse time) is given by

$$\tau_R = \frac{\zeta b^2}{12k_B T} \sin^{-2}\left(\frac{\pi}{2(N+1)}\right) \approx \frac{\zeta b^2 N^2}{3\pi^2 k_B T} \quad (1.7)$$

which is used in characterising the dynamic behaviour of polymers. The last approximation is the most commonly quoted in the literature and is valid for large N

(the error is known to be less than 1% for $N > 8$ [32]). In melts of long polymer chains (where $N > 50$), the relaxation time has been found to follow a $N^{3.4}$ scaling due to inter-chain interactions (or entanglements) rather than the N^2 scaling shown in eq. (1.7). Chains for which these interactions are important are referred to as above entanglement length. We consider entanglement length polymers in section 1.4.5.

Mean squared monomer displacement

The mean squared displacement for a monomer i is given by

$$g_{1,i}(t) = \langle (\mathbf{R}_i(t) - \mathbf{R}_i(0))^2 \rangle.$$

In the Rouse model for long chains the mean squared displacement of the middle monomer shows the following scaling regimes [32]

$$g_{1,mid}(t) = \begin{cases} \frac{6k_B T}{\zeta} t & t < \tau_N \\ 2b^2 \sqrt{\frac{3tk_B T}{\pi\zeta}} & \tau_N < t < \tau_R \\ \frac{6k_B T}{(N+1)\zeta} t & t > \tau_R \end{cases}$$

where τ_N is the fastest relaxation time (which corresponds to monomer relaxation). For $t < \tau_N$ the scaling behaviour corresponds to particle free diffusion where individual monomers are unaware they belong to a chain. During the intermediate time scale $\tau_N < t < \tau_R$ monomers begin to move coherently where the number of monomers moving together increases proportionally with the square root of time and is therefore subdiffusive. In this regime the end monomers diffuse faster than the middle monomers due to lower time-dependent effective friction. The ratio between the mean square displacement of the end and middle monomers has been shown previously to increase from 1 in the ballistic regime to a plateau value around 2

close to the Rouse time τ_R . [33, 34] Finally, when $t > \tau_R$ all monomers move coherently and the motion of chains becomes diffusive with a mean-squared displacement proportional to time.

Chain end-to-end vector correlation function

The end-to-end vector correlation function of a polymer chain, $\Phi(t)$, can also be calculated which allows for comparison with results obtained from dielectric spectroscopy. The end-to-end vector autocorrelation function is given by

$$\Phi(t) = \frac{\langle \mathbf{R}_{ee}(t) \cdot \mathbf{R}_{ee}(0) \rangle}{\langle \mathbf{R}_{ee}^2 \rangle} \quad (1.8)$$

where $\mathbf{R}_{ee}(t)$ is the end-to-end vector of a polymer chain at time t . Unlike the stress relaxation function, $G(t)$ which corresponds to bond orientation relaxation, the end-to-end autocorrelation function corresponds to relaxation on larger spatial scales. The relationship between these two functions then reveals differences between models and materials. In the Rouse model the end-to-end vector correlation function is given by

$$\Phi(t) = \frac{2}{N(N+1)} \sum_{p, \text{odd}} \tan^{-2} \frac{\pi p}{2(N+1)} \exp\left(-\frac{t}{\tau_p}\right).$$

From the above equation we can see the terminal relaxation time of the end-to-end vector correlation function is twice as fast as that of the stress relaxation function for a Rouse chain.

1.4.5 Tube model

Melts or concentrated solutions of long polymer chains above a critical length scale called entanglement length, N_e , show remarkably slow dynamics. This slowdown has

been confirmed in numerous experiments where the terminal relaxation times were found to scale with chain length N as $\tau_d \sim N^{3.4}$ [35] whereas in unentangled chains ($N < N_e$) studied in the previous section the terminal relaxation time scaled with $\tau_R \sim N^2$. This slowdown in dynamics of long chains results from the topological constraints imposed by surrounding chains which strongly suppress their lateral motion. The first model developed which successfully captured the importance of surrounding chains on entangled polymer dynamics was the tube model.

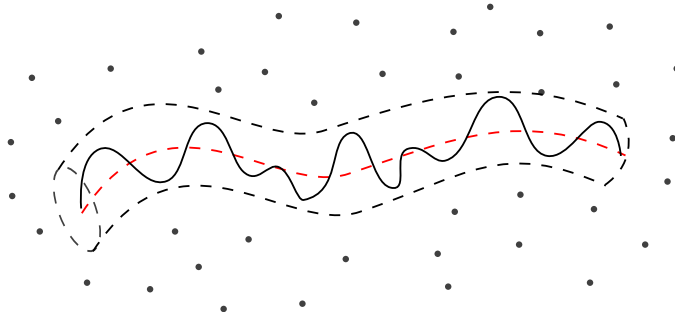


Figure 1.4: A chain in a fixed network of obstacles. The tube is depicted by dashed lines.

In 1971 de Gennes [36] outlined an idea which would ultimately lead to the development of tube theory. By first considering chains in the presence of a fixed network he suggested that an entangled polymer chain experiences snake like diffusion (known as reptation) through a tube formed by the topological constraints imposed by neighbouring chains, see Figure 1.4. This novel idea was later translated into a theory and corresponding constitutive equation by Doi and Edwards [27].

In the tube model the primitive path (red dashed line in Figure 1.4) is the shortest path connecting the two chain ends but maintaining the same topology as the actual chain relative to any obstacles. The primitive path has constant contour length L . As the polymer reptates, the primitive path changes with time due to the creation and destruction of tube segments by the chain ends. This motion is

governed by a one dimensional Rouse motion of the chain inside the tube with a diffusion coefficient, $D_c = k_B T / N \zeta$. Therefore, the “primitive chain” can be thought of as the dynamic equivalent of the primitive path. This is described as $\mathbf{R}(s, t)$ which denotes the primitive path at time t and where s is the contour length measured from the chain end along the tube. It is assumed the conformation of primitive chain becomes Gaussian on large length scale, and so the distance between two points becomes

$$\langle (\mathbf{R}(s, t) - \mathbf{R}(s', t))^2 \rangle = a |s - s'|$$

where a is known as the step length of the primitive chain (or is sometimes referred to as the tube diameter). The mean square end-to-end vector of the primitive chain must be equivalent to the mean square end-to-end vector of the polymer chain, *i.e.*

$$La = Nb^2.$$

Thus, we have only one new parameter a which is related to the network mesh size. The relaxation of chains is then described in terms of the tube survival probability (the fraction of the original tube which remains at time t). The tube survival probability can then be obtained by solving a one-dimensional diffusion equation and is found to be [27]

$$\psi(t) = \sum_{p; \text{odd}} \frac{8}{p^2 \pi^2} \exp(-p^2 t / \tau_d).$$

Here τ_d is known as the reptation time and describes the time taken for the polymer chain to disengage from the tube to which it was initially confined. The reptation time can be written in terms of Rouse model parameters and the tube diameter

$$\tau_d = \frac{\zeta N^3 b^4}{\pi^2 k_B T a^2}.$$

The stress tensor can then be described in terms of chain alignment due to any deformations and the tube survival probability. In the original work by Doi and Edwards in order to make the constitutive equation for the stress tensor more tractable

they assume sections of the chain align independently (this is referred to as the independent alignment approximation (IA)).

For continuous flow histories with both deformation and reptation the stress can be written as an integral equation

$$\sigma_{\alpha\beta} = G_e \int_{-\infty}^t \psi(t-t') \mathbf{Q}_{\alpha\beta}^{IA}(\mathbf{E}(t,t')) dt' \quad (1.9)$$

where

$$\mathbf{Q}_{\alpha\beta}^{IA}(\mathbf{E}(t,t')) = \left\langle \frac{(\mathbf{E} \cdot \mathbf{u})_\alpha (\mathbf{E} \cdot \mathbf{u})_\beta}{|\mathbf{E} \cdot \mathbf{u}|^2} - 1/3\delta_{\alpha\beta} \right\rangle_o$$

the angled brackets $\langle \cdot \rangle_o$ denote an integral over an isotropic distribution of unit vectors \mathbf{u} . The prefactor is given by $G_e = 3k_B T c b^2 / a^2$ and $\mathbf{E}(t,t')$ is the deformation tensor. By using spherical coordinates $(x, y, z) = (r \cos \theta, r \sin \theta \cos \phi, r \sin \theta \sin \phi)$ the integral $\mathbf{Q}_{\alpha\beta}^{IA}(\mathbf{E}(t,t'))$ can be expressed as a surface integral over the unit sphere $\langle \dots \rangle_o = 1/4\pi \int_0^{2\pi} \int_0^\pi (\dots) \sin \theta d\theta d\phi$. Doi and Edwards determined analytic expressions for $\mathbf{Q}_{\alpha\beta}^{IA}(\mathbf{E}(t,t'))$ under both shear and uniaxial extensional flows [37].

The most important mechanism for describing the dynamics of linear polymers is reptation, but a number of other physical processes have also been shown to contribute, including: contour length fluctuations, constraint release and longitudinal relaxation along the tube.

1.5 Theory of associating polymers

The first theories describing associating polymers come from the study of living polymers with the well established Cates theory [38]. Living polymers are linear chains which can break and recombine on experimental timescales. The change in degree of polymerization leads to a situation where the relaxation process involves

cooperation between chain relaxation and the breaking of temporary bonds. In these systems the degree of polymerization changes on experimental timescales. The characteristic timescale of these systems is then given by

$$\tau = (\tau_{rep}\tau_{break})^{1/2}$$

where τ_{rep} is the reptation time and τ_{break} is the expected survival time of a chain before it breaks into two pieces. The characteristic timescale appears deceptively simple, but is derived by considering a relaxation mechanism where a chain must break before combining with a nearby free chain end (one available for bonding).

1.5.1 Sticky Rouse

One of the first theories describing associating unentangled polymers capable of forming networks originates from the work of Rubinstein *et al.* [39, 40]. In these theories associating polymers are studied using scaling theory. The systems are constructed such that each polymer chain has a uniform number of stickers along its backbone, each capable of binary-bonding. In these systems closed stickers act like effective high friction units which dominate the relaxation process. Hence, the relaxation time of the parent chains can be defined in an analogous way to the scaling theory equivalent of the Rouse time ($\tau_R \approx \tau_0 N^2$) by considering only these high friction units. If we regard the monomeric relaxation time τ_0 as the bond lifetime τ_b and the chain length N as the number of closed interchain sticky bonds fp_{inter} , where f is the number of stickers per chain and p_{inter} is the fraction of interchain sticky bonds, we can define the sticky Rouse time as

$$\tau_{Rouse}^{sticky} \approx \tau_b (fp_{inter})^2.$$

The sticky Rouse theory also highlights the need for an effective bond lifetime as while a sticky bond may break at a time of order τ_b , the two stickers will recombine

multiple times before an open sticker (a potential partner) moves near or enters their neighbourhood. The renormalized bond lifetime is therefore defined as the average time from the first moment at which a sticker bonds with one particular partner up to the moment a bond is formed with a new open partner. Therefore, the renormalized bond lifetime is proportional to the reciprocal of the probability for finding a new open sticker in the volume V_{strand} which is explored by a given sticker during its open state

$$\tau_b^* \approx \frac{\tau_b b^3}{\phi_{open} V_{strand}} \quad (1.10)$$

where ϕ_{open} is the volume fraction of open stickers and b is monomer size. The expression for renormalized bond lifetime can then be used to determine the sticky rouse time

$$\tau_{Rouse}^{sticky} \approx \tau_b^* (fp_{inter})^2.$$

This idea of renormalized bond lifetime plays an important role in systems with associating polymers and will be explored further in later chapters.

1.5.2 Sticky Reptation

The sticky reptation model [39] extends the idea of the sticky Rouse model to systems where the parent polymers are above entanglement length. It can be regarded as sticky Rouse motion along the contour of the tube, see Fig 1.4. The sticky reptation time is then given by the sticky Rouse time multiplied by the number of entanglements per chain

$$\tau_{rep}^{sticky} \approx \tau_{Rouse}^{sticky} \frac{N}{N_e} \approx \tau_b^* (fp_{inter})^2 \frac{N}{N_e}.$$

1.5.3 Self-healing

The first theory to deal with the self-healing behaviour of associating polymers was recently proposed by Stukalin *et al.* [41]. The system is modelled using a simplified description of network forming chains. In particular each chain has one end fixed in space and the other has a sticker capable of binary bonding. Using this model they propose two processes for relaxation in the bulk system: a) the anomalous diffusion regime b) the hopping diffusion regime.

In the anomalous diffusion case, when the exploration volume of a given sticker overlaps with the exploration volume of another sticker they form a bond. As a result the concentration of open stickers is approximately given by the inverse of the volume explored as a function of time

$$c_{open}(t) = \frac{1}{V_{explore}(t)} \propto t^{-3/4}.$$

Here we note the volume explored by an open sticker grows slower than linearly with time t . This type of subdiffusive process was originally studied by de Gennes [42] who found for $t < \tau_R$ the scaling behaviour of the root mean squared displacement of a sticker in a Rouse chain is given by $x(t) \sim t^{1/4}$. In this subdiffusive process the number of sites explored is greater than the number of sites present in the region, and therefore the reaction takes place when the volumes explored by the two stickers overlap. This relaxation process occurs with low bonding energies or for long dangling chains.

On the other hand for short dangling chains or higher bonding energies the equilibrium concentration of open stickers can be smaller than one sticker per pervaded volume of a chain. In this case stickers cannot bond through anomalous diffusion. This is where hopping governs the motion of stickers at time-scales longer than the Rouse time of a dangling chain. In the hopping diffusion regime an open sticker

must satisfy two criteria before a bond can form: 1) The open sticker must wait for a previously bonded sticker to disassociate from the network. 2) The open sticker must occupy an overlapping volume with this newly open sticker.

In addition they also studied the self-healing process by considering what happens when bringing together two damaged surfaces. When a material is fractured the damaged surface possesses a structure far from equilibrium (with multiple open stickers), therefore, the waiting time before the two damaged surfaces are reunited, τ_w , plays an important role in determining which mechanism is used for relaxation (*i.e.*, either hopping or anomalous diffusion). The mechanism for relaxation is also dependent on bonding energy which controls the fraction of open stickers in the equilibrium state.

1.6 Network theory

Polymer networks are formed when nearly all chains in a system are cross-linked forming a single percolated structure. These structures exhibit huge deformation elasticity, *e.g.*, consider the reversible deformability of a rubber band. This deformability originates from the entropic elasticity of polymer chains which make up the network. When solvent molecules penetrate these materials they show novel swelling behaviour rather than dissolution, these diluted networks are referred to as cross-linked gels. We discuss two classic models used to understand network elasticity, more advanced models do exist (*e.g.*, the constrained junction model [43]) but these are beyond the scope of this thesis.

1.6.1 Affine network model

The affine network model is the simplest model which captures the idea of rubber elasticity and was originally proposed by Kuhn [44]. In this model the deformation of each network strand is the same as the macroscopic relative deformation imposed on the whole network. Specifically displacement of the mean positions of cross-links or the end-to-end vectors of a chain are transformed affinely.

1.6.2 Phantom network model

The affine network model ignores the fluctuations experienced by cross-links within a network. The first model to account for these fluctuations was proposed by James and Guth [45]. In this model chains of fixed length N are attached to each other at cross-links, and the macroscopic deformation is transmitted to the bulk by chains attached to its surface. They found the mean square fluctuation of the end-to-end vector \mathbf{R} around its average value $\langle \mathbf{R} \rangle$ depends on the cross-link functionality ϕ [46]

$$\langle (\mathbf{R} - \langle \mathbf{R} \rangle)^2 \rangle = \frac{2}{\phi} b^2 N$$

with the magnitude of fluctuations decreasing with functionality. The single-chain description of the phantom network which maps it onto the affine network model was proposed by Rubinstein and Panyukov [47, 48]. In this model chains are connected to the elastic fluctuating background by effective chains (the points of attachment on the elastic fluctuating background deform affinely). The length of these effective chains is determined by first noting the fluctuations experienced by a junction point with functionality f_{phan} , attached to chains of length N are equivalent to those experienced on attachment with an effective chain of length $K = N/f_{phan}$. With this in mind they determined a converging series which gives the length of an effective

chain

$$K = \frac{f_{phan} - 1}{f_{phan} - 2} N$$

in the phantom network model.

1.7 Molecular dynamics

Molecular dynamics (MD) simulations are a numerical method for studying the equilibrium or transport properties of many-body systems. Studied systems can consist of multiple types of particles, each of which has a well-defined set of interactions (these are often considered pair-wise). Molecular dynamics is a term used to describe solution of the classical equations of motion (Newton's equations) for a set of molecules. In many respects these simulations are similar to real experiments [49]: Initially we must prepare the sample. Then the sample is connected to a measuring instrument (*e.g.*, a thermometer), after which the property we are interested in is measured for a certain time interval. As our measurements are subject to statistical noise the accuracy of measurement depends on size of the interval. In molecular dynamics simulations periodic boundary conditions can be used to reduce finite size effects when interested in the properties of bulk systems.

1.7.1 Periodic boundary conditions

In simulations we are usually interested in bulk properties, however, due to the associated computational cost we can only simulate a limited number of molecules (up to a maximum of approximately 10^6 molecules). This then could lead to surface effects, therefore, one often uses periodic boundary conditions [50]. If we start with an initial cubic box of size L in all directions, positioned with corners $x = \pm L/2$,

$y = \pm L/2$ and $z = \pm L/2$. For periodic boundary conditions the cubic simulation box is replicated throughout space to form an infinite lattice with the distance between particles calculated using the minimum image convention

$$\mathbf{r}_{ij}^{min} = (\mathbf{R}_i - \mathbf{R}_j) - L \left[\frac{\mathbf{R}_i - \mathbf{R}_j}{L} \right]$$

where $[\cdot]$ rounds to the nearest whole number. When a molecule moves in the

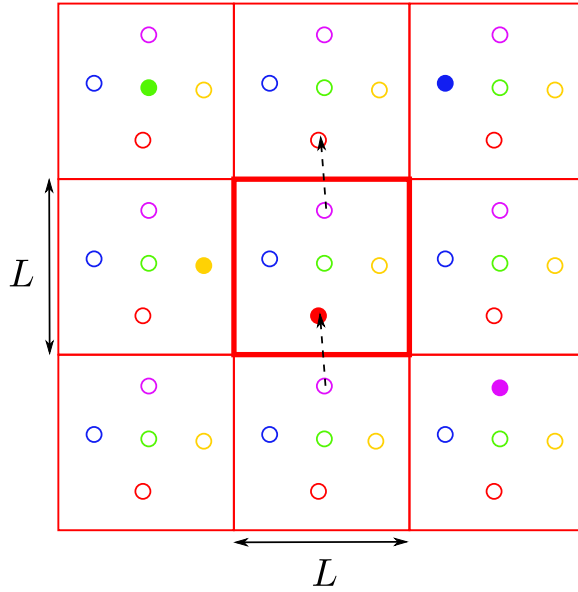


Figure 1.5: Illustration showing 2D periodic boundary conditions.

original box, it's periodic images move in exactly the same way. Thus, when a molecule leaves the central box one of its images will enter through the opposite face. An illustration of periodic boundary conditions in 2D is shown in Figure 1.5. The actual position of the particle is represented by the solid circles and the open circles represent periodic images of particles.

1.7.2 Pair interactions

In our molecular dynamics simulations polymer chains are represented by the bead spring model introduced by Kremer and Grest [51]. In this model the Lennard-Jones (LJ) potential is used to model excluded volume interactions between pairs of particles, which is given by

$$U_{LJ}(r) = 4\epsilon_{LJ} \left[\left(\frac{\sigma_{LJ}}{r} \right)^{12} - \left(\frac{\sigma_{LJ}}{r} \right)^6 \right]$$

where σ_{LJ} is the LJ bead diameter and ϵ_{LJ} defines the depth of the attractive well. The LJ potential acts pairwise between all monomers in a system. For modelling the melt systems, a truncated and shifted version of the LJ potential which neglects short range attraction is often used in simulations. Therefore, all monomers in the system interact pairwise via the purely repulsive Lennard-Jones (LJ) potential

$$U_{LJ}(r) = 4\epsilon_{LJ} \left[\left(\frac{\sigma_{LJ}}{r} \right)^{12} - \left(\frac{\sigma_{LJ}}{r} \right)^6 - \left(\frac{\sigma_{LJ}}{r_c} \right)^{12} + \left(\frac{\sigma_{LJ}}{r_c} \right)^6 \right] \quad (1.11)$$

for $r \leq r_c$, where $r_c = 2^{1/6}\sigma_{LJ}$ is the cut-off radius and $U_{LJ}(r) = 0$ for $r > r_c$. The LJ interaction parameter is chosen to be $\epsilon_{LJ} = 1.0k_B T$ where k_B is the Boltzmann constant and T is the absolute temperature. Each pair of adjacent beads in a chain interact via the finitely extensible non-elastic (FENE) potential

$$U_{FENE}(r) = -\frac{kR_{max}^2}{2} \ln \left[1 - \left(\frac{r}{R_{max}} \right)^2 \right] \quad (1.12)$$

where $R_{max} = 1.5\sigma_{LJ}$ and $k = 30\epsilon_{LJ}/\sigma_{LJ}$. This choice of parameters prevents chains from crossing themselves and others. The FENE potential is harmonic for small r but diverges as $r \rightarrow R_{max}$.

1.7.3 Numerical integration scheme

The equations of motion can be integrated using a number of numerical methods. In this thesis we use the simple Verlet algorithm for equilibrium simulations and the more accurate Gear predictor-corrector method for non-equilibrium molecular dynamics simulations.

Verlet Algorithm

In Molecular Dynamics, one of the most commonly used numerical integration schemes for solving the equations of motion is the Verlet algorithm. This is derived simply by writing two third-order Taylor expansions for the position $\mathbf{r}(t)$, namely

$$\mathbf{r}(t + \Delta t) = \mathbf{r}(t) + \mathbf{v}(t)\Delta t + \frac{1}{2}\mathbf{a}(t)\Delta t^2 + \frac{1}{6}\frac{d^3\mathbf{r}}{dt^3}\Delta t^3 + O(\Delta t^4), \quad (1.13)$$

$$\mathbf{r}(t - \Delta t) = \mathbf{r}(t) - \mathbf{v}(t)\Delta t + \frac{1}{2}\mathbf{a}(t)\Delta t^2 - \frac{1}{6}\frac{d^3\mathbf{r}}{dt^3}\Delta t^3 + O(\Delta t^4), \quad (1.14)$$

where we have written the first derivative of $r(t)$ as $v(t)$ (velocity) and the second derivative of $r(t)$ as $a(t)$ (acceleration). We can now add these two expressions together giving

$$\mathbf{r}(t + \Delta t) = 2\mathbf{r}(t) - \mathbf{r}(t - \Delta t) + \mathbf{a}(t)\Delta t^2 + O(\Delta t^4).$$

Gear predictor-corrector algorithm

The Gear algorithm possesses two stages, an initial prediction stage and a correction step with a force calculation which is used to determine the error in the prediction. We consider the fourth order Gear algorithm and we denote the scaled time derivatives $\mathbf{r} = \mathbf{r}_0$ as $\mathbf{r}_1 = \delta t(d\mathbf{r}_0/dt)$, $\mathbf{r}_2 = \frac{\delta t^2}{2}(d^2\mathbf{r}_0/dt^2)$, $\mathbf{r}_3 = \frac{\delta t^3}{6}(d^3\mathbf{r}_0/dt^3)$. Thus, the

coefficient	value
c_0	251/720
c_1	11/12
c_2	1/3
c_3	1/24

Table 1.1: Fourth order Gear predictor-corrector coefficients.

predictor step can be written in matrix form

$$\begin{pmatrix} \mathbf{r}_0^p(t + \delta t) \\ \mathbf{r}_1^p(t + \delta t) \\ \mathbf{r}_2^p(t + \delta t) \\ \mathbf{r}_3^p(t + \delta t) \end{pmatrix} = \begin{pmatrix} 1 & 1 & 1 & 1 \\ 0 & 1 & 2 & 3 \\ 0 & 0 & 1 & 3 \\ 0 & 0 & 0 & 1 \end{pmatrix} \begin{pmatrix} \mathbf{r}_0(t) \\ \mathbf{r}_1(t) \\ \mathbf{r}_2(t) \\ \mathbf{r}_3(t) \end{pmatrix}$$

The equations of motion enter through the corrector step. Evaluating forces gives the correct second order derivative $\mathbf{r}_2^c(t + \delta t)$, therefore, the error in the prediction can be determined

$$\Delta \mathbf{r}_2(t + \delta t) = \mathbf{r}_2^c(t + \delta t) - \mathbf{r}_2^p(t + \delta t)$$

with this error the corrected values are obtained

$$\begin{pmatrix} \mathbf{r}_0^c(t + \delta t) \\ \mathbf{r}_1^c(t + \delta t) \\ \mathbf{r}_2^c(t + \delta t) \\ \mathbf{r}_3^c(t + \delta t) \end{pmatrix} = \begin{pmatrix} \mathbf{r}_0^p(t + \delta t) \\ \mathbf{r}_1^p(t + \delta t) \\ \mathbf{r}_2^p(t + \delta t) \\ \mathbf{r}_3^p(t + \delta t) \end{pmatrix} + \begin{pmatrix} c_0 \\ c_1 \\ c_2 \\ c_3 \end{pmatrix} \Delta \mathbf{r}_2(t + \delta t)$$

the coefficients c_1, \dots, c_4 were determined by Gear [50] and are highlighted in Table 1.1.

1.8 Monte Carlo methods

Monte Carlo methods are a class of computer algorithms developed at the end of the second world war which allow for deterministic mathematical problems to be treated using a probabilistic analogue which can then be solved using random sampling techniques [50]. In our simulations of supramolecular polymers the formation and breaking of reversible bonds is controlled by the Metropolis Hastings algorithm.

1.8.1 Metropolis Hastings algorithm

In statistical mechanics the equilibrium probability density in the canonical ensemble of a state $\{\mathbf{r}^N\}$ is given by

$$P(\{\mathbf{r}^N\}) = \exp\left(-\frac{U(\{\mathbf{r}^N\})}{k_B T}\right) / \mathbb{Z}$$

where $U(\{\mathbf{r}^N\})$ is the potential energy of the state and \mathbb{Z} is the partition function (*i.e.*, the integral of the equilibrium probability density over all states). While we can determine the energy of a state for a complex system we have no efficient way of calculating the partition function. If we could determine the partition function, simulations of the system would be unnecessary as macroscopic properties (*e.g.*, pressure, energy) could be calculated directly, using theories based on statistical mechanics.

In order to sample configurations from the state space we make use of the detailed balance condition which states that at equilibrium the average number of accepted moves from state \mathbf{o} to any other state \mathbf{n} is exactly equal to the number of reverse moves, *i.e.*, to satisfy the condition

$$P(\mathbf{o})\pi(\mathbf{o} \rightarrow \mathbf{n}) = P(\mathbf{n})\pi(\mathbf{n} \rightarrow \mathbf{o})$$

where π is a transition probability which can take many forms. Given the probability of a trial move $\alpha(\mathbf{o} \rightarrow \mathbf{n})$ from \mathbf{o} to \mathbf{n} and the probability of accepting this move $acc(\mathbf{o} \rightarrow \mathbf{n})$. The transition probability $\pi(\mathbf{o} \rightarrow \mathbf{n})$ becomes

$$\pi(\mathbf{o} \rightarrow \mathbf{n}) = \alpha(\mathbf{o} \rightarrow \mathbf{n})acc(\mathbf{o} \rightarrow \mathbf{n}).$$

In Metropolis' original scheme α is chosen to be symmetric (i.e. $\alpha(\mathbf{o} \rightarrow \mathbf{n}) = \alpha(\mathbf{n} \rightarrow \mathbf{o})$). Therefore, by the detailed balance condition we have

$$P(\mathbf{o})acc(\mathbf{o} \rightarrow \mathbf{n}) = P(\mathbf{n})acc(\mathbf{n} \rightarrow \mathbf{o})$$

and it follows

$$\frac{acc(\mathbf{o} \rightarrow \mathbf{n})}{acc(\mathbf{n} \rightarrow \mathbf{o})} = \frac{P(\mathbf{n})}{P(\mathbf{o})} = \exp\left(\frac{-[U(\mathbf{n}) - U(\mathbf{o})]}{k_B T}\right)$$

The acceptance probability chosen to satisfy this condition by Metropolis was given by

$$acc(\mathbf{o} \rightarrow \mathbf{n}) = \begin{cases} P(\mathbf{n})/P(\mathbf{o}) & \text{if } P(\mathbf{n}) < P(\mathbf{o}) \\ 1 & \text{if } P(\mathbf{n}) \geq P(\mathbf{o}) \end{cases}.$$

1.8.2 Association dynamics

In our simulations chain dynamics are governed by standard Kremer-Grest MD and the formation or breaking of sticky bonds is controlled by the Metropolis-Hastings algorithm. This hybrid approach was originally developed by Huang *et al.* [52, 53] to study living polymers.

When two stickers form a reversible sticky bond, they interact via the bonding potential [54, 55]

$$U_{sb}(r, \varepsilon) = U_{FENE}(r) - U_{FENE}(r_0) - \varepsilon \quad (1.15)$$

where $r_0 \approx 0.97\sigma_{LJ}$ is the equilibrium FENE bond length at the minimum of the combined potential $U_{FENE}(r) + U_{LJ}(r)$. The energy offset $U_{FENE}(r_0) + \varepsilon$ in eq.(1.15)

is introduced to control the lifetime of the sticky bonds and consequently the fraction of associated stickers in the system. Figure 1.6 shows the potential which act

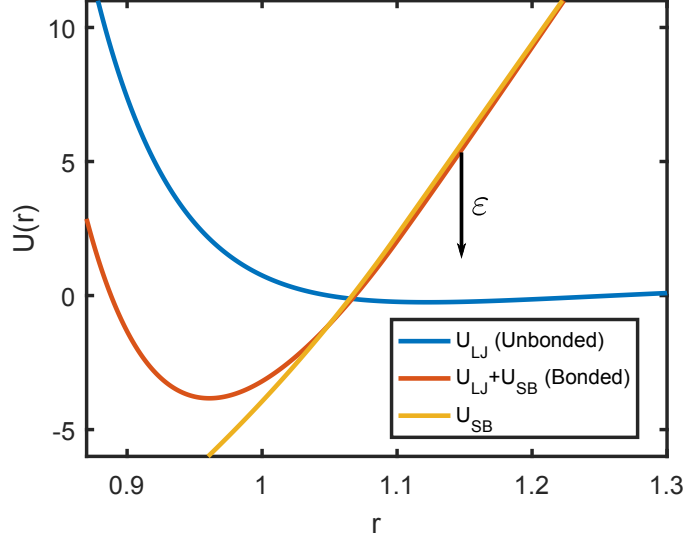


Figure 1.6: A graph showing the potentials experienced by a sticker eq. 1.15

on a bonded sticker, altering ϵ shifts the sticky bond potential in the y -direction increasing the distance at which bonds remain favourable. The sticky bonding energy ϵ is independent of the separation between the two stickers and so does not alter their associating force. The formation and breaking of sticky bonds is controlled by the Metropolis Monte Carlo Algorithm [56] where the energy change due to the formation of a new sticky bond is $\Delta E(r, \epsilon) = U_{sb}(r, \epsilon)$ and the energy change to break an existing bond is $\Delta E(r, \epsilon) = -U_{sb}(r, \epsilon)$. If an MC move causes a reduction in the change of energy $\Delta E(r, \epsilon) \leq 0$ then it is always accepted. On the other hand if $\Delta E(r, \epsilon) > 0$ a move is accepted with probability $\exp[-\Delta E(r, \epsilon)/k_B T]$. At each MC step pairs of stickers are chosen randomly. If the chosen pair is already bonded, an attempt is made to break the bond. Conversely, if the pair is not bonded, an attempt is made to create a sticky bond. Each pair is chosen on average once per MC step. The frequency $f_{MC} = \tau_{LJ}/\tau_{MC}$ at which MC steps occur governs the

reaction kinetics of the stickers. By increasing the MC time step size τ_{MC} the sticky bond relaxation is effectively changed from diffusion-limited to kinetically limited regime, which will consequently alter the dynamic behavior of the system, but not the thermodynamic or static properties. It should be noted that the change of τ_{MC} values will not affect the qualitative results obtained in the equilibrium systems as studied here. Furthermore, Hoy and Fredrickson [55] have shown that small MC time step sizes are needed to reduce systematic errors in calculating dynamic and mechanical properties of reversible associating polymer networks. Stickers are also prevented from bonding with the same partner twice to prohibit the formation of “double” strength sticky bonds. If these double strength bonds were allowed we would expect to only see the bonding of sticker pairs.

Chapter 2

Dynamics in supramolecular polymer networks

2.1 Introduction

In this chapter we study both static and dynamic properties of supramolecular polymers formed from simulations of unentangled telechelic chains under equilibrium conditions using the hybrid MD/MC method outlined in Chapter 1.

Supramolecular polymer systems behave like permanent polymer networks at time scales smaller than the bond lifetime, and as a standard polymer melt or solution when bonding constraints are fully released. The most fascinating properties of supramolecular polymer networks are associated with the relaxation dynamics in between these two time limits.

In associating polymer systems the reversible bonds formed by stickers have been theoretically treated as effective high friction units [57, 58, 59, 60, 61, 62] For

example the sticky Rouse model described in section 1.5.1 relies on this assumption to calculate the characteristic timescale. This model was one of the first models to describe the need for a renormalized bond lifetime. It has also been extended for studying entangled associating polymers see section 1.5.2. In recent years the interest in self-healing materials has led to the development of a scaling theory to describe the self-healing process of unentangled supramolecular polymer networks see section 1.5.3.

If stickers are able to aggregate into large clusters, leading to reversible networks of interconnected micelles, two mechanisms have been proposed to relieve stress, namely polymer chain diffusion [63, 64] and positional rearrangement of micelles [64]. In these systems, the hopping of stickers is assumed to proceed by dissociating from one micellar core and then associating into another. If the distance between aggregates or micelles is much smaller than the chain length, Marrucci *et al.* predicted a power-law dependence of the terminal relaxation time of unentangled telechelic chains on the polymer concentration and molecular weight. [63] For associating polymers with many regularly spaced stickers, Semenov and Rubinstein predicted that the chain relaxation time has a power-law dependence on polymer concentration in the unentangled or weakly entangled regime, but an exponential concentration dependence in the strongly entangled regime. [64] Unlike the pairwise association case [61], the bond lifetime renormalization is considered negligible when the sticker dissociation energy is in the range of $M^{1/2} < \varepsilon/k_B T < M^{4/3}$ with M the average aggregation number of sticker clusters. [64] This is because the aggregates can accommodate a varying number of stickers and the estimated energy change before and after a sticker hopping event is lower than the thermal energy $k_B T$. The terminal stress relaxation time of these networks is determined by the micellar positional rearrangements, which is exponentially longer than the single-chain relaxation time due to high energy barriers. [64]

A number of experiments have been carried out to test the predictions of the above mentioned theoretical models and qualitative agreements have been found on the diffusion and rheological behaviour of certain associating polymer networks.[65, 20, 66, 63] For example, Colby and co-workers have shown that the sticky Rouse model can well describe the linear viscoelasticity of polyester ionomers when using the ionic association lifetime measured in dielectric relaxation spectroscopic responses as model input parameters.[20] But there is still a lack of microscopic evidence to validate the assumptions made in the theoretical models, such as the microscopic description of the sticker hopping process and positional rearrangement of micelles. Computer simulations at the atomistic or fine-grained level can help to provide such microscopic insights which are generally difficult to access in experiments.

Simulation studies on associating polymers have been mostly focused on static properties, in particular the sol-gel transition and the aggregation of associating groups [67, 68, 69, 70, 71, 72, 73, 74, 75, 76]. Much less attention has been paid to the dynamic and rheological properties and their relation to the topological structures and parent chain dynamics. [77, 78, 79, 80] Bedrov *et al.* performed standard molecular dynamics (MD) simulations of solutions of short telechelic polymers where the attractive Lennard-Jones interactions among the end groups lead to the formation of networks of interlinked micelles or end-group clusters. [78] The stress relaxation in the system was described as a two-step process: a first decay due to the translational motion of the end-groups inside their clusters and second by the rapid hopping diffusion of end-groups between neighbouring clusters, which is followed by the terminal relaxation due to cluster disintegration. Hoy and Fredrickson applied hybrid molecular dynamics/Monte Carlo (MD/MC) simulations to study supramolecular networks formed by unentangled associating polymers. [55] In this system multiple stickers are equally spaced along the chain and can only form bi-

nary bonds. The hybrid MD/MC method used by Hoy and Fredrickson uses the sticky bonding potential eq. (1.15) and the Metropolis Hastings algorithm for controlling sticky bond formation and breaking see section 1.8.2. The key difference in our system is the adjustable sticker functionality and we allow sticker pairs to both break and form a sticky bond in the same Monte Carlo step (this is required to satisfy detailed balance). Hoy and Fredrickson study mechanical properties of the system under non-equilibrium condition by using creep and constant volume tension simulations. Simulation results on monomer diffusion, non-equilibrium chemical dynamics and non-linear mechanical properties have been understood in terms of the crossover from diffusion-limited to kinetically limited sticky bond recombination and chain connectivity. In the above-mentioned simulations, the spacers in between the stickers are still relatively short (6 – 15 monomers), which limits the capacity of clearly identifying the contributions from the parent polymer dynamics and its interplay with the sticker hopping process, both playing an important role in theoretical models of associating polymer networks.

In this chapter, we study the dynamics and rheology of supramolecular polymer networks using a model system consisting of unentangled telechelic polymers. The flexible polymer chains are represented by the Kremer-Grest bead-spring model [81] outlined in section 1.7. In this model a finitely-extensible non-linear elastic potential eq. (1.12) is used to represent all polymer backbone bonds and the truncated Lennard-Jones potential eq. (1.11) is applied between all pairs of monomers. The end monomers of chains or stickers can associate with each other to form reversible bonds, also called sticky bonds, with controllable reaction kinetics.[55] The functionality of stickers is set to $f = 3$, meaning that each sticker can maximally associate with two other stickers. This is the minimum functionality required for percolated network formation [82]. Telechelic chains with functionality of $f = 2$ undergo head-to-tail associations, which have been studied in other theoretical and simulation

works. [83, 54, 80, 84] The choice of $f = 3$ leads to systems which are comparable to supramolecular networks constructed by mixtures of associating ditopic (A2) and tritopic (B3) molecules [7, 85, 86]. By making the sticky monomer association directional, this model can also be conveniently applied to study reversible networks formed by $\pi - \pi$ stacking [13, 14] or ureidopyrimidinone (UPy) stacking [87, 88]. More importantly, stickers with finite functionality can form clusters with well-defined size distribution in the equilibrium state, which is essential for providing a clear microscopic picture of the relationship between the dynamics of cross-links and the viscoelastic behaviour in the reversible networks of interconnected clusters or micelles. Our simulations revealed that the dynamics and stress relaxation in such systems are dominated by the partner exchange process of stickers which is facilitated by the repeated dissociation and association of clusters, rather than by the single sticker hopping process which requires a sticker to overcome a high energy barrier when trying to fully detach from its original cluster.

The rest of the chapter is organised as follows. In section 2.2 we describe the polymer chain model and the hybrid MD/MC simulation method used in this study. Simulation results on the static, dynamic and rheological properties of supramolecular systems are presented and discussed in section 2.3, together with some theoretical models developed for describing the dynamic behaviour of reversible polymer networks. The conclusions are drawn in section 2.4.

2.2 Models and Simulation Methods

The parent polymers are represented by the Kremer-Grest bead-spring model see section 1.7.2. [81] Each telechelic chain consists of N monomers with the two end monomers defined as stickers. The stickers are identical to normal monomers except

that they are capable of reversibly associating with one another. The formation and breaking of sticky bonds is controlled by the Metropolis Hastings algorithm described in section 1.8.2. In the system studied each sticker is allowed to associate with a maximum of two other stickers, giving a functionality of $f = 3$. The functionality can be easily adjusted for modelling different polymer systems.

The monomer density in the systems is fixed at $\rho = 0.85/\sigma_{LJ}^3$ where σ_{LJ} is the diameter of the monomers. This choice of ρ has been widely used to simulate polymer melts.[81] For flexible Kremer-Grest chains in the melt condition, the entanglement length is estimated to be in the range $N_e = 50 - 80$. [89, 90, 33] Therefore, we choose to study two polymer chain lengths, $N = 25$ and 45 , in the unentangled regime, bearing in mind that there could occasionally be locked-in entanglements due to the reversible association of the end monomers. As will be seen in the stress modulus calculations, there is no significant contributions from such entanglements. By employing unentangled parent polymer chains we can focus on relating the dynamics of the cross-links to the dynamic and rheological behaviour of the resulting transient networks.

The equations of motion of the monomers are solved numerically using the Verlet algorithm (section 1.7.3) with a MD time step size $\delta t = 0.01\tau_{LJ}$ where the Lennard-Jones time $\tau_{LJ} = \sqrt{m\sigma_{LJ}^2/\epsilon_{LJ}}$. [81, 91, 33] The simulations are carried out in the canonical (NVT) ensemble with periodic boundary conditions applied in all three directions. The stickers are allowed to associate across periodic boundaries.

Most of the simulation data presented in this chapter were generated using $\tau_{MC} = 0.01\tau_{LJ}$ (*i.e.*, one MC step at each MD time step), with some extra runs using $\tau_{MC} = 1.0\tau_{LJ}$ for comparison. As will be shown in next section, the use of smaller τ_{MC} value leads to shorter terminal relaxation times and so enables us to obtain good statistical results with affordable computational efforts.

Each simulation system undergoes two stages of equilibration before any analysis takes place. At first the system is equilibrated as a polymer melt with all stickers treated as normal monomers along the chains. [90, 33] This stage lasts for a period of multiple Rouse times of the unentangled chains. As an example, the Rouse time for the flexible chains of length $N = 25$ as used in our simulations is $\tau_R \approx 923\tau_{LJ}$. In the second stage the hybrid MD/MC simulation are carried out with the sticker association mechanism switched on. This stage is considerably longer than the first one due to the much longer relaxation time of polymer chains in a supramolecular network than in a melt (typically increased by a factor of 5 – 10). Following the equilibration stages the static and dynamic properties of the reversible network are calculated on the fly over an equilibrium run of 10 – 100 terminal relaxation times of the whole system.

The static, dynamic, and rheological properties of the model systems are studied for a range of sticky bonding energy from $\varepsilon = 0$, corresponding to regular polymer melt, up to $\varepsilon = 12k_B T$. As will be shown in the next section, the sol-gel transition of such systems takes place at $\varepsilon \approx 4.3k_B T$, which is consistent with the critical ε value found in simulation systems where sticky monomers interact with the same bonding potential as in eq. (1.15), but follow the binary bonding rule. [55] The simulation box we used contains $N_{ch} = 400$ polymer chains in the case of polymerization $N = 25$. For $N = 45$ there are $N_{ch} = 200$ chains. To improve the statistics, all simulation data on the reversible networks is averaged over at least four independent runs for each set of system parameters. For example if we consider $\varepsilon = 10k_B T$ the stress relaxation and end-to-end vector correlation functions show a relative standard error in the range 1 – 9%. Much larger ensemble averages are taken for the permanent networks generated by preventing the sticky bonds from dissociation, as will be seen in the next section.

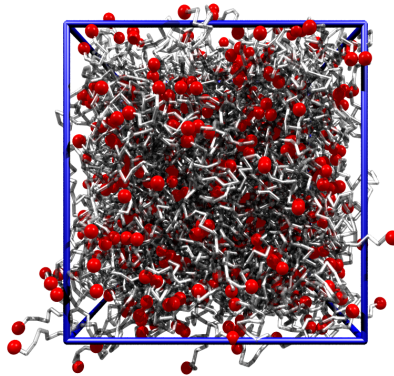


Figure 2.1: Snapshot of a transient network formed by associating telechelic chains of length $N = 25$ and sticky bonding energy $\varepsilon = 10k_B T$. The red spheres represent the stickers at the chain ends.

2.3 Results and Discussions

2.3.1 Static properties: reversible network analysis

Figure 2.1 presents a snapshot of the simulation system consisting of associating telechelic chains of length $N = 25$ and sticky bonding energy $\varepsilon = 10k_B T$. It shows clearly that at high enough bonding energy, the stickers associate into clusters of different sizes which cross link the parent polymer chains into a transient network. The topological structures of the networks can thus be understood from the sticker cluster size distributions.

Sol-gel transition in supramolecular polymer systems

In supramolecular polymer systems, the association of stickers leads to the formation of chain clusters of different sizes. For a system consisting of N_{ch} telechelic chains with sticky end monomers of functionality f , the extent of reaction is measured by

$$p = \frac{N_{bond}}{N_{ch}(f-1)} \quad (2.1)$$

where N_{bond} is the ensemble-averaged total number of sticky bonds formed in the system. The reaction extent p increases with the increase of the sticky bonding energy ε . The sol-gel transition occurs when p exceeds a critical threshold of p_c .

In order to determine if the system is percolated in a given direction we use the method of Koopman and Lowe [92] which tests whether any group of associated chains is connected to its periodic image. We only require the system to be percolated in one direction. This analysis allows us to identify which chains make up the gel and which are part of the sol. The sol-gel transition can be characterized by the weight-averaged cluster size measured in the sol phase [93, 55]

$$N_W^C = \frac{\sum_{j=1}^{N_{ch}} j^2 P_{sol}(j)}{\sum_{j=1}^{N_{ch}} j P_{sol}(j)}. \quad (2.2)$$

where $P_{sol}(j)$ is the probability for a chain to be associated into a finite cluster consisting of j chains. When p approaches p_c , N_W^C diverges in infinite system due to the formation of a percolated network. However, since our simulations can only consider finite N_{ch} , a maximum in $N_W^C(p)$ is expected at the percolation transition.

Figure 2.2 presents the simulation results on N_W^C as a function of the extent of reaction as obtained in hybrid MD/MC simulations using different box sizes. The maximum of N_W^C occurs at $p_c \approx 0.4$, which is in agreement with that found in

systems of binary associations [55]. This p_c value corresponds to a sticker bonding energy $\varepsilon_c \approx 4.3k_B T$. In Figure 2.3 this bonding energy is approximately where the fraction of open stickers becomes less than the fraction of partially- and fully-reacted stickers. Percolated transient networks are formed in the systems with $\varepsilon > \varepsilon_c$.

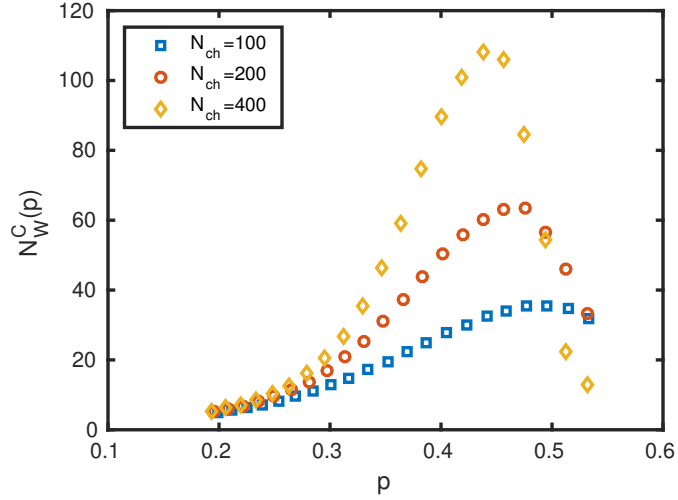


Figure 2.2: Weight-averaged chain cluster size as a function of the extent of reaction p as obtained in supramolecular polymer systems with sticker functionality $f = 3$. The simulations were performed using different box sizes and so different number of parent chains N_{ch} .

Sticker cluster formation

In our model systems each sticker can bond with up to two partners. This allows for three possible bonding states: open with no bonded partner, partially reacted with one bonded partner and fully reacted with two bonded partners. The average fraction of stickers in each state is calculated as a function of the bonding energy ε . The simulation results in Figure 2.3 for the systems with chain length $N = 25$ demonstrate that the fraction of open stickers decreases monotonically with an

increase of ε , while the total fraction of (partially and fully) reacted monomers keeps on increasing and gradually saturates at high ε values. The crossover of these two fraction curves occurs at $\varepsilon \approx 4.3k_B T$ which is very close to the critical bonding energy for the sol-gel transition. The fraction of fully reacted stickers becomes dominant when $\varepsilon > 6k_B T$. At high bonding energies $\varepsilon \geq 10k_B T$, the majority of the stickers are fully reacted and the fraction of open stickers is down to less than 1%. In the sticker hopping picture for binary bonding systems [60, 59, 61, 94, 55], if the fraction of open stickers is low, pairs of associated stickers usually break and recombine many times before finding other open stickers to associate with. This significantly slows down the dynamic relaxation behaviour as recombination with previous partners leaves the network topology unchanged. In the transient networks we studied, the formation of larger sticker clusters can facilitate the partner exchange process as shown in the next section.

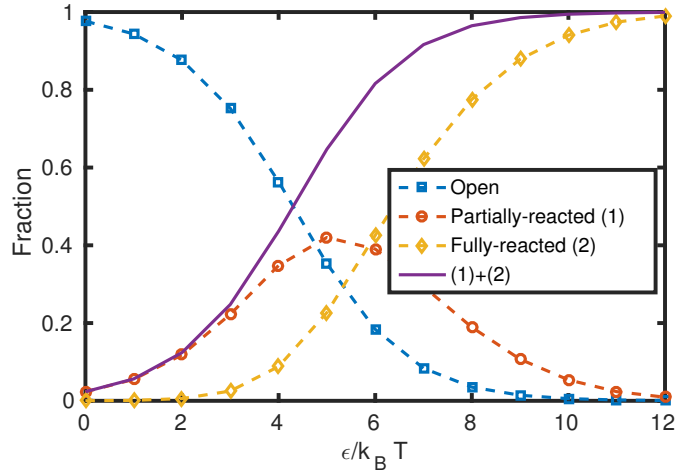


Figure 2.3: Average fractions of stickers that are in open, partially reacted and fully reacted states as a function of sticky bonding energy ε . The chain length is $N = 25$.

Stickers with functionality $f = 3$ (or above) can associate into clusters with various sizes. The cluster size distribution can be described by the probability for

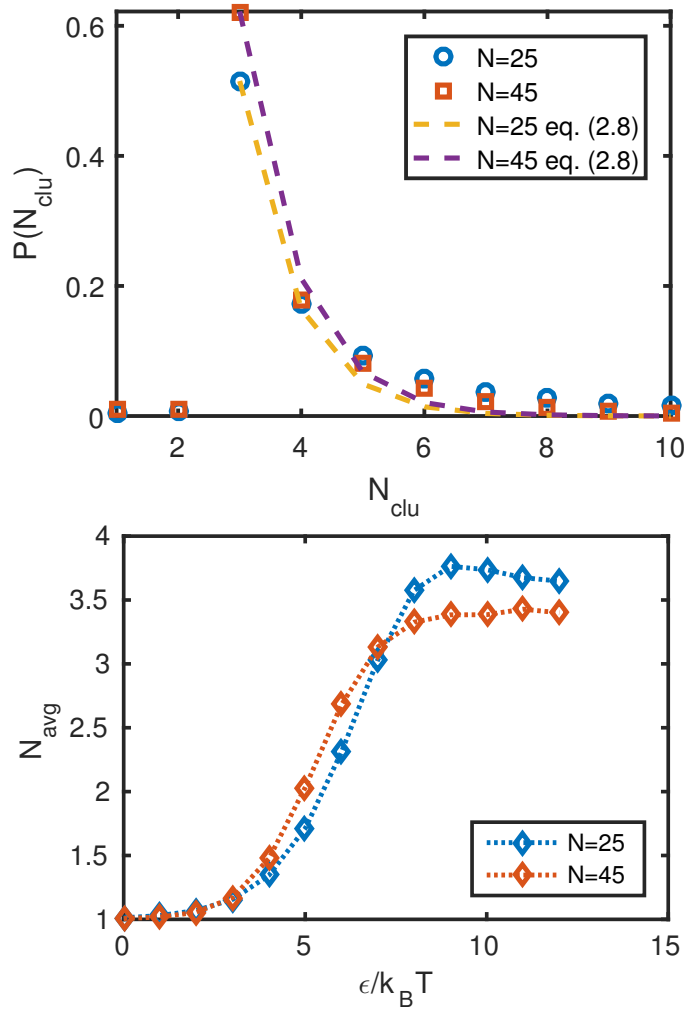


Figure 2.4: (a) Probabilities for finding a sticker in a sticker cluster of size N_{clu} in the systems with sticky bonding energy $\epsilon = 10k_B T$. The dashed curves illustrate the analytical results given by eq. (2.8). (b) Average sticker cluster size as a function of sticky bonding energy.

finding a sticker in a cluster of size N_{clu}

$$P(N_{clu}) = \frac{n_{N_{clu}} N_{clu}}{2N_{ch}} \quad (2.3)$$

where $n_{N_{clu}}$ is the average number of sticker clusters of size N_{clu} and $2N_{ch}$ is the total number of stickers in the system. Simulation results on $P(N_{clu})$ for the two different chain lengths at $\varepsilon = 10k_B T$ are given in Figure 2.4(a). In agreement with the high reaction rate at this bonding energy (Figure 2.3), the majority of the stickers aggregate into clusters with sizes $N_{clu} \geq 3$. The distinct peak at $N_{clu} = 3$ corresponds to the smallest cluster size for which each sticker can be fully reacted and so gain $-\varepsilon$ in association energy. The cluster size distribution is determined by the competition between this energy gain and the entropic penalties due to the loss of sticker translational entropy. In solutions of associating polymers, the formation of sticker clusters or micelles can lead to elastic stretching of the polymer chains, which in turn affects the sizes of stable clusters. But this polymeric effect is negligible in the melt condition because the average end-to-end distance of the polymer chains is nearly constant in the systems with different ε values.

Cluster formation of stickers in the equilibrium state can be theoretically described in a similar way to micelle formation of amphiphilic molecules in dilute solutions. [95] Equilibrium thermodynamics requires the mole fraction, $X_{N_{clu}}$, of stickers associated into clusters of size N_{clu} to satisfy the condition

$$\mu_{N_{clu}}^0 + \frac{k_B T}{N_{clu}} \ln (X_{N_{clu}}/N_{clu}) = const, \quad (2.4)$$

where the chemical potential of a sticker inside a cluster is given by

$$\mu_{N_{clu}}^0 = -\varepsilon + F^{poly}(N_{clu}), \quad N_{clu} \geq 3. \quad (2.5)$$

The second term on the right hand side of eq. (2.5) allows the inclusion of possible (positive) polymeric contributions to the free energy. Since the chemical potential

has a minimum value of $\mu_{M_{clu}}^0 = -\varepsilon$ at the cluster size $M_{clu} = 3$, it is convenient to describe the mole fraction $X_{N_{clu}}$ by [95]

$$\frac{X_{N_{clu}}}{N_{clu}} = \left(\frac{X_{M_{clu}}}{M_{clu}} \exp [M_{clu}(\mu_{M_{clu}}^0 - \mu_{N_{clu}}^0)/k_B T] \right)^{N_{clu}/M_{clu}}, \quad N_{clu} \geq M_{clu} \quad (2.6)$$

In our system of telechelic chains $X_{N_{clu}}$ is related to the sticker density as

$$\sum_{N_{clu}=1}^{\infty} X_{N_{clu}} = \frac{2}{N}. \quad (2.7)$$

Hence, the probability of finding a sticker in a cluster of size N_{clu} is related to $X_{N_{clu}}$ by $P_{clu}(N_{clu}) = X_{N_{clu}} N/2$ where $\sum_{N_{clu}} P_{clu}(N_{clu}) = 1$. If we neglect all the polymeric effects by assuming $F^{poly}(N_{clu}) = 0$, eq. (2.6) can be simplified to

$$P_{clu}(N_{clu} \geq 3) = N_{clu} \left(\frac{2}{N} \right)^{N_{clu}/3-1} \left(\frac{P_{clu}(3)}{3} \right)^{N_{clu}/3}, \quad (2.8)$$

where the only input parameter is $P(N_{clu} = 3)$ whose value can be found in simulations.

As shown in Figure 2.4(a), the predictions of eq. (2.8) are in reasonably good agreement with the simulation data. The relatively faster decay of the theoretical curves can be attributed to the assumption of dilute solution of stickers made in developing eq. (2.6). Since the polymer chain lengths we studied are still relatively short, the small sticker clusters have a fairly high probability to meet each other and associate into larger clusters, leading to a slower decay of $P_{clu}(N_{clu})$ at large N_{clu} values. When the chain length is increased from $N = 25$ to 45, the peak at $P_{clu}(N_{clu} = 3)$ becomes higher and consequently the fraction of larger clusters gets smaller because of the reduced sticker density. The agreement between the theoretical and simulation results also improves.

Simulation results on the average sticker cluster size which is defined as $N_{clu}^{avg} = \sum N_{clu} P(N_{clu})$, are plotted in Figure 2.4(b) as a function of ε . The value of N_{clu}^{avg}

first increases with the sticky bonding energy until $\varepsilon \approx 9k_B T$ and then reaches a plateau, e. g., of $N_{clu}^{avg} \approx 3.6$ for $N = 25$. This is consistent with the results in Figure 2.4(a) that at high ε values more than 50% stickers are in clusters of size 3 because the chemical potential of stickers is minimized at $N_{clu} = 3$ for the functionality of $f = 3$. The average sticker cluster size can be considered as the active functionality of junctions in polymer networks.[96] We find the fraction of fully-reacted stickers at chain length $N = 45$ is higher than $N = 25$ for bonding energies $\varepsilon \geq 4k_B T$ (results not shown). One might expect this to result in an average cluster size larger than $N = 25$, however Figure 2.4(b) only shows an increase for intermediate bonding energies $4k_B T \leq \varepsilon \leq 6k_B T$. At higher bonding energies when the majority of stickers are fully reacted the partner exchange mechanism described in section 2.3.2 becomes dominant allowing for stickers to change their connectivity to the network without complete detachment. This is achieved through the repeated association and disassociation of sticker clusters, therefore, systems with a high sticker density (e.g in the $N = 25$ case) experience such events more rapidly, and so having a higher frequency to associate into larger clusters and consequently causing a net increase in cluster size see Figure 2.4(a). As will be shown in section 2.3.2, the existence of large clusters plays an essential role in determining the terminal relaxation time of the supramolecular systems.

Elastically effective strands

The mechanical strength of a polymer network is determined by the fraction of elastically effective strands. In unentangled networks each effective strand contributes to the rubbery modulus by an order of $k_B T$. [82] Apart from the reversible nature of cross-links, the transient networks formed by associating polymers has similar topological structures to chemically fixed networks and so possess elastically inef-

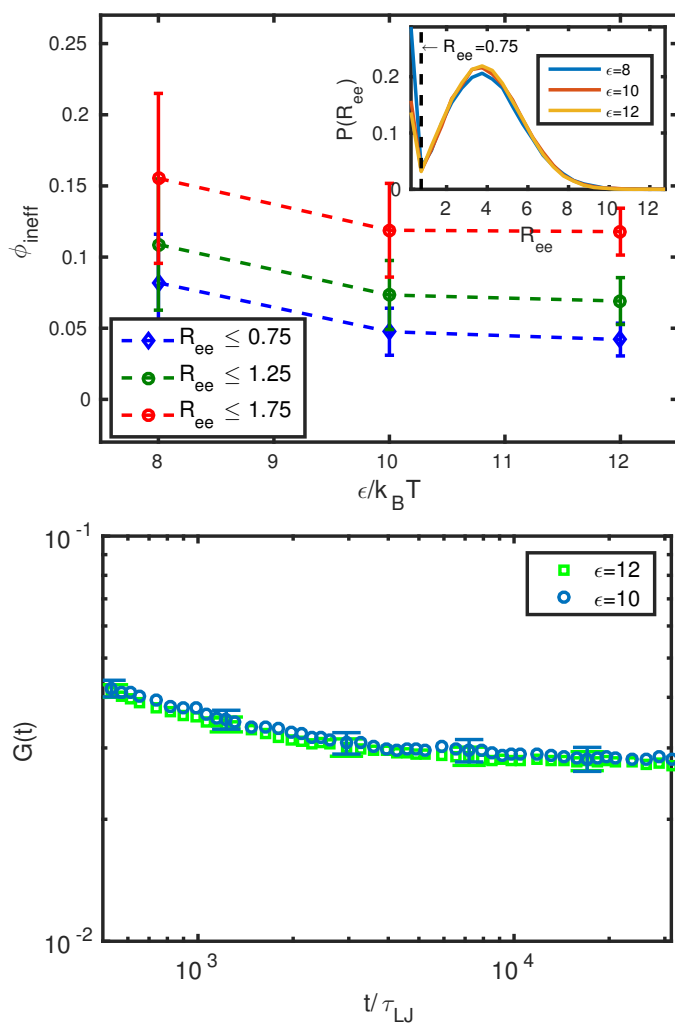


Figure 2.5: (a) Fraction of elastically ineffective strands, ϕ_{ineff} , in the supramolecular networks obtained by using different cutoffs to identify fully contracting chains in the PPA-type analysis. The inset presents the probability distributions of the chain end-to-end distances in the fixed networks with both excluded volume interactions and thermal fluctuations switched off. (b) Direct MD simulation results on the stress relaxation of fixed polymer networks that are generated by fixing the topological structures of transient networks obtained from hybrid MD/MC simulations. All results are averaged over 100 statistically independent network configurations, and the error bars show the standard deviation of the mean. The polymer chain length is $N = 25$.

fective components, such as dangling chains and loops. This can already be seen in Figure 2.3 from the nonzero fraction of open stickers even at the highest bonding energy studied. In addition, some of the partially reacted stickers are involved in the formation of sticker clusters of size two and consequently longer chains or network strands by the linear association of two or more parent polymer chains. This also reduces the modulus of the network.

We investigated the fraction of elastically effective strands in the transient networks using a method inspired by the primitive path analysis (PPA) of entangled polymers.[89] This was done by randomly selecting instantaneous network configurations from the trajectories obtained in well-equilibrated hybrid MD/MC simulations. The topological structures of these networks were fixed by preventing any existing sticky bonds from breaking in addition to stopping the creation of new sticky bonds. The excluded volume interactions among all monomers were then switched off to make the bonds contract and the system temperature was set to zero to remove thermal fluctuations. This results in the collapse of chains not contributing to the plateau modulus. The dangling chains shrink into single points, giving the chain end-to-end distance $R_{ee} = 0$. The chain loops are somewhat different. Even though both ends of the loop belong to the same cluster or cross-link, they may still have a small separation ($R_{ee} \neq 0$) because other stickers in the cluster are subject to tension along the shrunken network strands connected to them. For this reason, we need to introduce a cutoff distance for R_{ee} to identify the ineffective strands.

In Figure 2.5(a) we show the fraction of elastically ineffective chains, ϕ_{ineff} , obtained from the PPA-type analysis of transient networks formed by telechelic polymers of length $N = 25$. The ϕ_{ineff} values decrease with the use of smaller cut-offs and start to converge after $R_{ee} \leq 0.75\sigma_{LJ}$. This is consistent with the probability distributions of the chain end-to-end distances given in the inset of Figure

2.5(a) which show two distinct peaks at higher bonding energies with the minimum between the peaks occurring at $R_{ee} \approx 0.75\sigma_{LJ}$. The peak located at smaller R_{ee} is indicative of chains that have collapsed, while the one at larger R_{ee} represents the chains that contribute to the network elasticity. Therefore, we can reasonably use this minimum location ($0.75\sigma_{LJ}$) between these peaks as an approximation for the cutoff. It follows that there are approximately 5% ineffective strands in the networks formed at sticky bonding energies $\varepsilon \geq 10k_B T$ when the average sticker cluster size nearly saturates, see Figure 2.4. The strongly associated transient networks thus have high elastic efficiency. We note that unlike the PPA method our analysis algorithm does not preserve entanglements between the network strands. The cross-linking of unentangled polymer chains will unavoidably lock in a certain number of entanglements. How such entanglements contribute to the stress relaxation of the reversible networks should be investigated as a function of the parent chain length and sticky bonding energy, which will be left for further study.

To provide a reference for the plateau modulus of the reversible networks, we calculate the stress relaxation function, $G(t)$, of the fixed polymer networks used in Figure 2.5(a) by performing standard MD simulations. The MD results on $G(t)$ are presented in Figure 2.5(b) for network configurations taken from hybrid MD/MC simulations using two different sticky bonding energies $\varepsilon = 10k_B T$ and $12k_B T$. Each curve has been averaged over 100 statistically independent fixed network configurations. As expected, the stress relaxation behaviours of the two sets of fixed networks agree with each other within error bars, confirming the similar topological structures of the reversible networks formed at high enough sticky bonding energies ($\varepsilon \geq 9k_B T$). The initial reduction in both curves is due to the Rouse motion of chains which occurs when $t \ll \tau_R$ and therefore before chains become aware of the constraints imposed by the fixed network.

The corresponding plateau modulus is $G_N \approx 0.028k_B T/\sigma_{LJ}^3$, which is close to the estimation of $G_N = \rho k_B T/N = 0.034k_B T/\sigma_{LJ}^3$ for an ideal polymer network with monomer number density $\rho = 0.85\sigma_{LJ}^3$ and strand length $N = 25$. In the classic phantom network model (section 1.6.2) the plateau modulus can be rewritten in terms of the number density of elastically effective strands. From our PPA-style analysis we can determine the number density of elastically effective strands directly

$$N_{active} = \frac{N_{ch}(1 - \phi_{ineff})}{V},$$

thus the plateau modulus is given by

$$G_N = N_{active}(1 - 2/f)k_B T$$

where f is the cross-link functionality. For $\varepsilon = 10$ if we assume a cross-link functionality $f = 4$, the plateau modulus is approximated as $G_N = 0.0234T/\sigma_{LJ}^3$ which is close to the calculated value.

2.3.2 Dynamic and rheological properties

A key difference of supramolecular polymer networks from polymer melts and permanent or chemical networks is the formation of reversible bonds. This introduces additional timescales into the systems and consequently affects their dynamic and rheological behaviour. We thus start with identifying the timescales characterizing the dynamics of reversible association of stickers and the underlying microscopic pictures, and then relate them to experimentally measurable properties, such as sticky monomer diffusion, stress and chain end-to-end vector relaxation functions.

Timescales characterizing reversible association of stickers

Sticky bonds are formed by physical association of pairs of stickers. Considering the dissociation of sticky bonds as a thermally activated process, their average lifetime, τ_b , is predicted to depend exponentially on the bonding energy ε [55, 94]

$$\tau_b \approx \tau_{MC} \exp(\varepsilon/k_B T), \quad (2.9)$$

where the MC step size τ_{MC} reflects the controllable reaction rates of the stickers in the hybrid MD/MC simulation model. Figure 2.6 presents the simulation data on τ_b for two different chain lengths and $\tau_{MC} = 0.01\tau_{LJ}$, which follows the expected exponential dependence on ε . When increasing τ_{MC} from $0.01\tau_{LJ}$ to $1.0\tau_{LJ}$, the τ_b value was found to increase by a factor of about 100 without altering any static properties of the systems (results not shown). The average sticky bond lifetimes in the systems with longer chains ($N = 45$) are slightly larger than those in the shorter chain systems ($N = 25$). This can be attributed to the higher probability of stickers to form stable clusters (of size $N_{clu} = 3$, see Figure 2.4) in the former systems, which effectively prolongs their average association time.

In the systems with sufficiently high bonding energies ($\varepsilon \geq 6k_B T$) most of the stickers are associated into clusters as shown in Figure 2.3. Following a bond breaking event, the open stickers will most likely recombine with their old partners due to the low density of available opening reaction sites nearby. This breaking and reforming process needs to be repeated many times before a sticker finally combines with new partners without returning to the old ones. It is through such partner exchange events that the topological constraint imposed by a sticker on its parent polymer chain is partly released. Therefore an additional timescale much longer than τ_b is required for describing the dynamic properties of associated polymer systems. [61, 97, 55, 94] In systems where stickers only experience binary bonding,

the renormalized bond lifetime, τ_b^* , was defined as the average time from the first moment that a sticker is bonded with one particular partner up to the moment that a bond is formed with a new open partner (see section 1.5.1). The renormalized bond lifetime in the sticky Rouse model was shown to be dependent on both the concentration of open stickers and the volume that an open sticker can explore. The situation becomes more complicated for systems consisting of stickers with higher functionality ($f \geq 3$) where larger sticker clusters are formed.

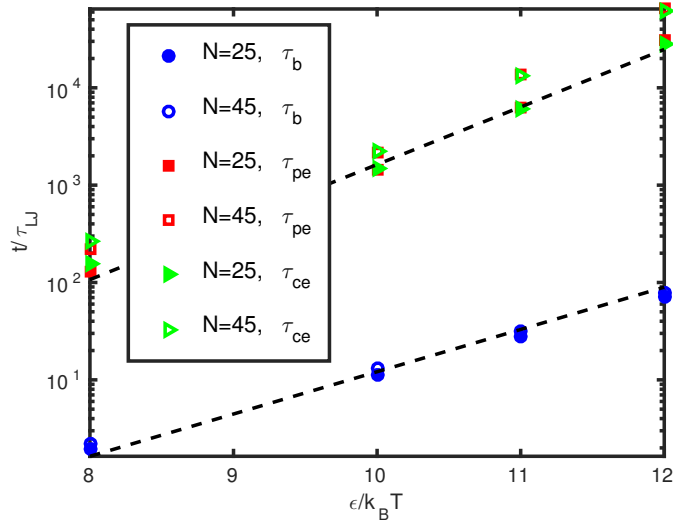


Figure 2.6: Average sticky bond lifetime τ_b , partner exchange time τ_{pe} , and cluster exchange time τ_{ce} with respect to sticky bonding energy ϵ for the systems with two different chain lengths and $\tau_{MC} = 0.01\tau_{LJ}$.

We introduce two timescales for characterizing the dynamic process of releasing topological constraints imposed by associated stickers. The first one is the partner exchange time, τ_{pe} , which is defined as the average time taken for a given sticker from first being bonded with two particular partners until forming bonds with two new partners, as sketched in Figure 2.7(a). For a partner exchange event to take place there is no requirement for both stickers to break at once, instead multiple sticky bond formation and breaking events usually take place before a sticker exchanges its

partners. This definition can be considered as an extension of the renormalized bond lifetime concept from the binary association case ($f = 2$) to systems with sticker functionality $f = 3$. In many supramolecular systems the stickers can associate with more than two partners and the sticker clusters also have a broad size distribution, e. g., see Figure 2.4. A more general definition of the characteristic timescale could be the cluster exchange time, τ_{ce} , which is the time taken for a given sticker from being initially associated with one cluster consisting of three or more stickers until associating with another sticker cluster of size $N_{clu} \geq 3$ which shares no stickers in common with the original cluster. A cluster exchange event can occur in multiple stages with stickers within a cluster changing over time until none match the original. This definition can be easily understood from the hopping picture of a sticker from one sticker cluster or micellar core to another. [63, 64] We note that these timescales are better defined in the strongly associated supramolecular networks than in the systems with low bonding energies. The latter cases are anyhow of little interest, because no transient network is formed and so chain dynamics are only weakly altered by the presence of stickers. The partner exchange time and cluster exchange time can not be directly understood via the proposed expression for the renormalized bond lifetime in the sticky Rouse model eq. (1.10). This is because partially reacted stickers can also form reversible associations, and so must be taken into account in the volume explored by open stickers V_{strand} and concentration of open stickers ϕ_{open} .

Figure 2.7 compares the probability distributions of the partner exchange and cluster exchange times for the system with chain length $N = 25$ and bonding energy $\varepsilon = 10k_B T$. The two distributions agree with each other reasonably well at timescales $t \gg \tau_b$. We note the tails for both distributions can be well approximated by a single exponential. This is expected for the systems with $f = 3$ where more than 50% of the sticker clusters are of size 3. The ensemble-averaged values of τ_{pe}

and τ_{ce} are presented in Figure 2.6 as a function of ε for the two different chain lengths. The two definitions provide nearly identical results within error bars (of symbol size). At small timescales the cluster exchange time has higher probabilities because of the inclusion of events involving partially-reacted stickers. In the partner exchange time we require both stickers to be bonded, while in the cluster exchange time a sticker need only have a single bond attaching it to a cluster. For convenience, we will only use the partner exchange time τ_{pe} to represent these timescales in the remaining sections. These events are studied further in the next section. The simulation data on τ_{pe} and also τ_{ce} can be fitted with an exponential function of the form

$$\tau_{pe,ce} \approx \tau_{MC} \exp(B\varepsilon/k_B T) \quad (2.10)$$

where $B = 1.36 > 1$ indicates that the partner exchange time grows with ε faster than the single exponential function of $\tau_b \sim \exp(\varepsilon/k_B T)$. This is qualitatively consistent with the renormalized bond lifetime $\tau^* \sim \exp(7\varepsilon/6k_B T)$ predicted by Stukalin et al. when studying self-healing behaviour (details of the model studied were described in section 1.5.3).

For a given bonding energy, the values of τ_{pe} and τ_{ce} are up to 2 orders of magnitude larger than the average bond lifetime τ_b , indicating that τ_b is not sufficient for describing the dynamics in supramolecular networks. Our simulation results are thus very different from the theoretical assumption that the bond lifetime renormalization is negligible in systems with micellar core formation, although the sticker bonding energy we studied does not fall exactly into the relevant range of $N_{clu}^{1/2} < \varepsilon/k_B T < N_{clu}^{4/3}$. [64]

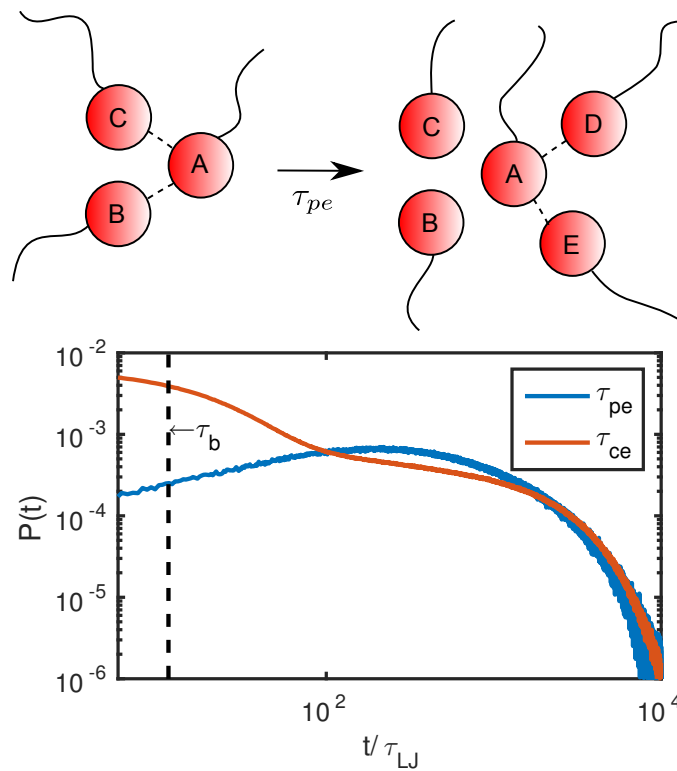


Figure 2.7: (a) Schematic demonstration of a partner exchange event which has a characteristic time τ_{pe} ; (b) Probability distributions of the partner exchange time τ_{pe} and cluster exchange time τ_{ce} for supramolecular systems with chain length $N = 25$ and bonding energy $\varepsilon = 10k_B T$.

Microscopic picture of sticker partner exchange

According to the original sticker hopping picture, a sticker first dissociates from the initial sticker cluster or micellar core and then diffuses as an open sticker until meeting another cluster to associate with. Although the difference in the total bonding energy of the sticker is negligible between the initial and final states, it needs to overcome an energy barrier on the order of $(f - 1)\varepsilon$ to break off all the sticky bonds formed in the initial cluster. In equilibrium systems the probability for such hopping events to happen is exponentially low, and the corresponding time scale would be $\tau_{hop} \sim \exp[(f - 1)\varepsilon/k_B T]$. But the simulation results on τ_{pe} or τ_{ce} in Figure 2.6 grow with the association energy ε much slower than $\exp(2\varepsilon/k_B T)$ for $f = 3$. This implies the existence of other pathways that have much lower energy barriers to allow the stickers to move from one cluster to another.

The sticker clusters in a supramolecular network fluctuate in space just like junction points in a permanent polymer network. Sticky bonds are short lived breaking and recombining many times while two clusters are close to one another, therefore they may associate into a larger cluster at no additional energy cost with the total number of sticky bonds remaining constant between the small clusters and the larger cluster.

The stickers coming from these two different clusters can then easily swap their partners inside the large cluster, because each sticker now has equal probability to associate with any other sticker in the cluster owing to fast bond breaking and reformation events. Since the large cluster is entropically unfavorable and so short-lived, it will break apart into two new clusters which may or may not be of the same size as the two original ones but has a relatively high probabilities to contain different member stickers. It is through this association-dissociation process of sticker clusters

that stickers change their partners. Figure 2.8(a) sketches such a process where two sticker clusters both of size $N_{clu} = 3$ associate into a larger one of size 6, which later breaks into two new clusters to complete a partner exchange event. The cluster association-dissociation pathway thus facilitates changes in the transient network topology without requiring stickers to fully dissociate from the network. In Figure 2.8(a) the total number of sticky bonds remains 6 throughout the process, with sticky bonds frequently breaking and recombining so there is no additional bonding energy cost involved.

On the basis of the microscopic picture in Figure 2.8(a), we perform a detailed analysis of partner exchange events, and correspondingly network topological changes, by studying the variation of sticker cluster size from the perspective of a sticker. Firstly, we define stable sticker clusters as those possessing a lifetime larger than the average bond lifetime, $\Delta t > \tau_b$. Then we look at the transitions through which a sticker initially attached to a stable cluster finally associates with another stable cluster. We require the new cluster to either be of a new size or contain different members from the original cluster. This allows for three possible cases: (1) two clusters combine to form a larger cluster; (2) a smaller cluster breaks off from a larger cluster; (3) a cluster exchanges members with another cluster but remains the same size. The events where two clusters combine together and then separate back into the original ones are not counted, because they do not result in changes in transient network topology. From the number of transitions we can determine a right-stochastic matrix, $M_{i,j}$, which measures the probability that a sticker initially in a cluster of size $N_{clu} = i$ (initial state or i th row in the matrix) transfers into a final cluster of size j (final state or j th column of the matrix). The matrix is described as right-stochastic because we normalize each row such that $\sum_j M_{i,j} = 1$. The matrix is illustrated in Figure 2.8(b) where the color of a block represents the magnitude of the transition probability.

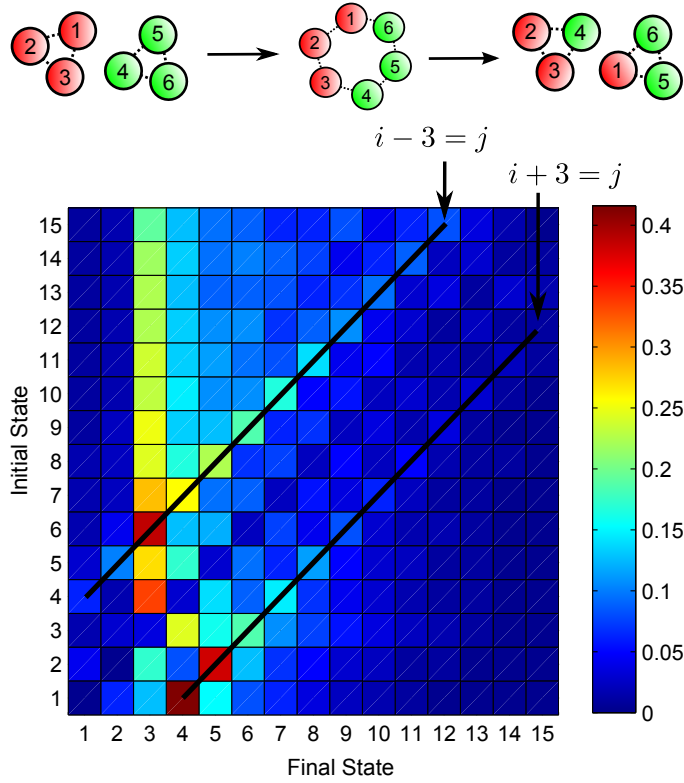


Figure 2.8: (a) Sketch of a partner exchange event via the sticker cluster association-dissociation process. (b) Right-stochastic matrix that measures the probability for a sticker initially in a cluster of size i (i th row) to transfer into a final cluster of size j (j th column) for the system with $\varepsilon = 10k_B T$ and $N = 25$. The two solid lines indicate the high probabilities for the cluster sizes to change by ± 3 stickers.

Figure 2.8(b) shows that for $N_{clu} \leq 3$ the clusters usually attempt to grow in size, e. g., from a cluster of size 2 to that of size 5 with $M_{2,5} = 0.383$ (red block). This is contrasted by a usual decrease in cluster size when $N_{clu} \geq 4$, e. g., from a cluster of size 7 to clusters of sizes 3 and 4 with $M_{7,3} = 0.281$ (orange block) and $M_{7,4} = 0.259$ (yellow block), respectively. It is evident that the most probable pathway for sticker cluster size changes is the addition or subtraction of three stickers, as marked by the two solid lines in Figure 2.8(b). This can be understood by the fact that a group of three associated stickers has the maximum possible translational entropy without compromising bonding energy, as discussed in the next section. On the contrary, the probabilities in the first column of the transition matrix are very low, indicating that it is very unlikely for a single sticker to break off a cluster. This further confirms that the partner exchange events usually take place via the cluster association and dissociation processes, rather than by single sticker hopping. The presence of large sticker clusters thus facilitates the rates of partner exchange and so polymer chain relaxation. In section 3.3.2 we investigate how imposing an upper cap on the sticker cluster size would affect the stress relaxation behaviour of the transient networks. We note that a sticker may need to experience multiple cluster association-dissociation events in order to exchange all of its original partners. This can be seen more clearly in the example sketched in Figure 2.8(a) where stickers 1 and 4 have successfully exchanged both of their partners, while other stickers have only exchanged half of their original partners and so need more cluster association-dissociation events to exchange those which remain.

Mean square displacement of stickers

The effect of varying bonding energy on the mean square displacements (MSD) of stickers, $g_1^{sticker}(t) = \langle (\mathbf{r}^{sticker}(t) - \mathbf{r}^{sticker}(0))^2 \rangle$ where $\mathbf{r}^{sticker}(t)$ is the coordinate

of the sticker bead, is shown in Figure 2.9(a). For comparison we also include the MSD data of chain end monomers in polymer melts ($\varepsilon = 0k_B T$) and of stickers in fixed polymer networks whose configurations were taken from the simulations of supramolecular systems with $\varepsilon = 12k_B T$. Since the chain lengths studied are well below the entanglement length N_e , the monomer mean square displacement in the melt system follows Rouse behaviour which was described in section 1.4.4. In supramolecular systems, the association of stickers significantly slows down their diffusion behaviour. The transition from the subdiffusive to diffusive regime is delayed beyond the partner or cluster exchange time $\tau_{pe,ce}$ ($> \tau_R$). This is in contrast to non-associating unentangled polymers which follow Rouse behaviour where the transition between the subdiffusive and diffusive regime occurs at $t = \tau_R$.

At time scales $t < \tau_{pe}$, the MSD of the stickers is governed by the cluster size distribution. Figure 2.9(b) shows the mean square displacements of sticker clusters of different sizes, $g_1^{N_{clu}}(t)$, for the system with $\varepsilon = 10k_B T$. The MSD of stickers in clusters of size $N_{clu} = 2$ is analogous to that of middle monomers in chains of length $2N$. As expected the growth rates of the g_1^{clu} curves decrease with the increase of N_{clu} . For each given bonding energy, the $g_1^{sticker}$ data in Figure 2.9(a) can be exactly calculated by taking a weighted average of the cluster MSD results by using the cluster size distribution $P_{clu}(N_{clu})$,

$$g_1^{sticker}(t) = \sum_{i=1}^{\infty} P_{clu}(i) g_1^i(t)$$

up to the lifetimes of the related clusters.

The growth rate of $g_1^{sticker}(t)$ decreases with the increase of ε as a consequence of the increased average cluster size. When $\varepsilon \geq 9k_B T$ the average cluster size converges, e. g., to $N_{avg} \approx 3.6$ in systems with chain length $N = 25$. Correspondingly the sticker MSD curves obtained at these high ε values follow a universal behaviour

similar to that resulting from the thermal fluctuations of cross-links in fixed polymer networks (dotted-dashed line) up to the partner exchange time in each case. This indicates that below τ_{pe} the supramolecular systems behave as permanent networks. At larger time scales $t > \tau_{pe}$, the stickers are able to exchange their partners through the cluster association-dissociation processes and so gradually forget their topological constraints. The $g_1^{sticker}(t)$ curves slowly cross over into the diffusive regime. Figure 2.9 also shows that for the bonding energies studied in this thesis ($\varepsilon \leq 12k_B T$), there is still no extended plateau regime in the diffusion curves due to the limited lifetimes of the clusters.

The diffusion coefficients D of the stickers and equivalently of the entire chains in the free diffusion regime are plotted as a function of ε in the inset of Figure 2.9(a). The decrease of the chain diffusivity with increasing sticker association energy has also been observed in experimental measurements of tracer chain diffusion in supramolecular polymer networks with different strength of chain cross-linking.[98, 99] Our simulation data on D show an exponential decay with ε at higher bonding energies. As will be seen below, this is consistent with the exponential dependence of the chain terminal relaxation time τ_d on ε .

Stress and dielectric relaxation

The reversible association of stickers also strongly affects the rheological behaviour of the supramolecular systems. In simulations the stress relaxation function and chain end-to-end vector correlation functions are calculated using eq. (1.1) and eq. (1.8) respectively. Figure 2.10 presents simulation results of the stress relaxation function, $G(t)$, and chain end-to-end vector correlation function or dielectric relaxation function, $\Phi(t)$, for the systems with $N = 25$ and various bonding energies

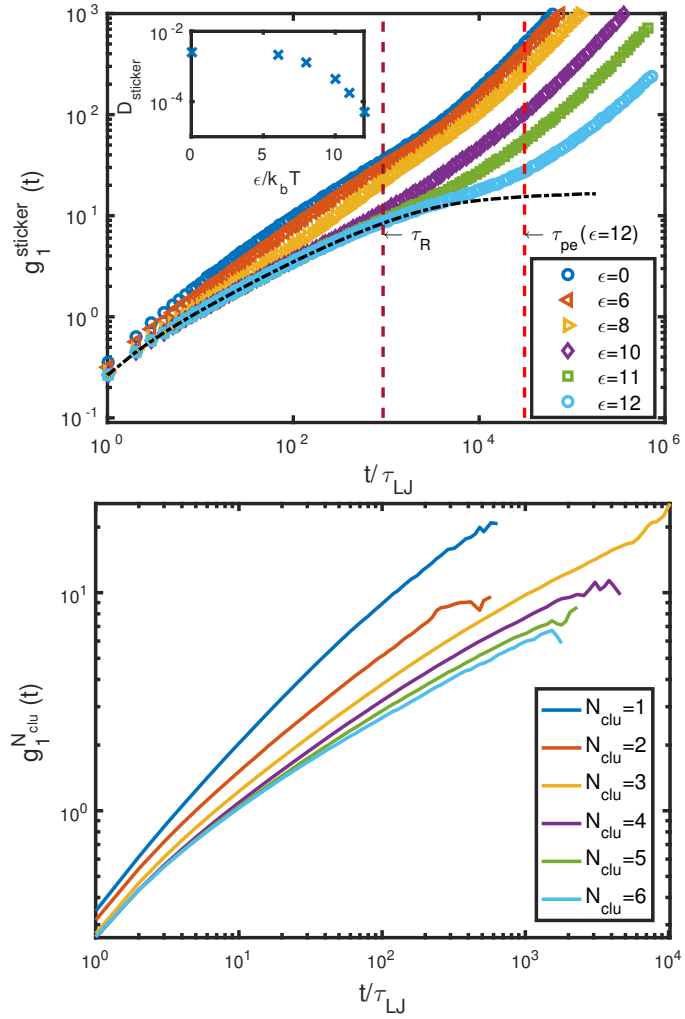


Figure 2.9: (a) Mean-square displacements of stickers in supramolecular systems with different sticky bonding energies ϵ . The black dotted-dashed curve shows results obtained from fixed polymer networks whose configurations were taken from simulations of supramolecular systems with $\epsilon = 12k_B T$. For reference the Rouse time τ_R and the sticker partner exchange time at $\epsilon = 10T$ are given by the two vertical dashed lines on the right. (b) MSD of sticker clusters with different sizes $N_{clu} \leq 6$ at $\epsilon = 10k_B T$. The parent chain length is $N = 25$ in all cases.

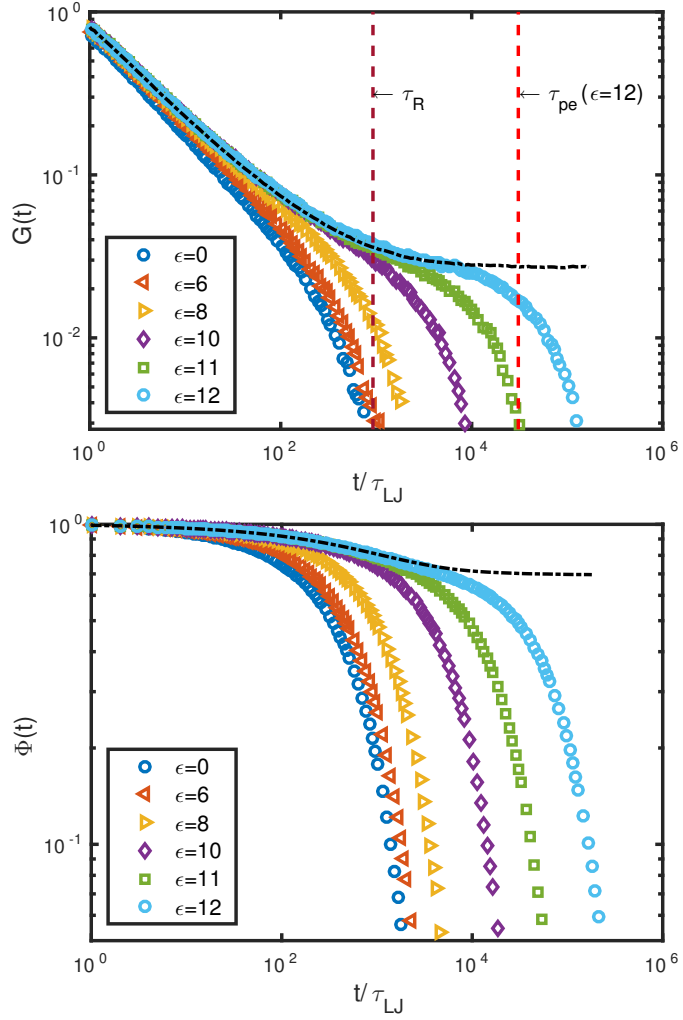


Figure 2.10: Stress relaxation (a) and chain end-to-end vector correlation functions (b) in the systems with $N = 25$ and various bonding energies ε . The dotted-dashed curves present the results obtained from fixed polymer networks whose configurations were taken from simulations of supramolecular systems with $\varepsilon = 12k_B T$.

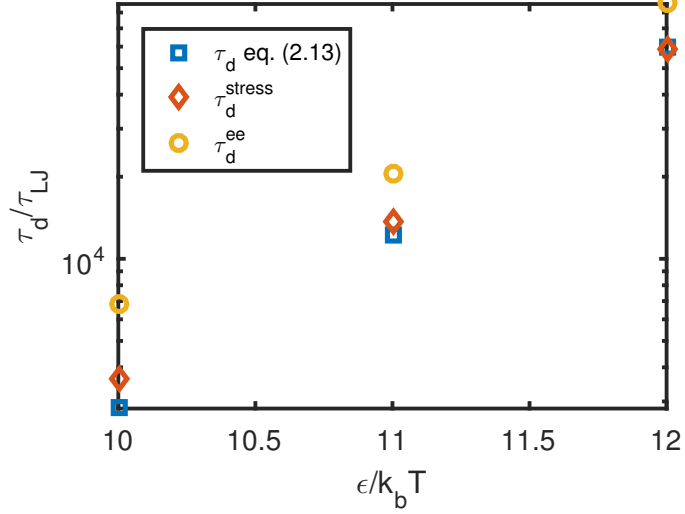


Figure 2.11: Simulation results on the terminal relaxation times of the stress and chain end-to-end vector correlation functions. The terminal relaxation times predicted by eq. (2.12) using simulation data on the sticker partner exchange time and hopping distance are also included.

ε . Results obtained from polymer melts and fixed polymer networks are also included for comparison. All these time correlation functions were calculated on the fly using the multiple-tau correlator method to ensure good statistics. [100] In unentangled melt systems polymer chains can be described by the Rouse model (see section 1.4.4) with stress fully relaxing at $t = \tau_R/2$ (which corresponds to $\varepsilon = 0$ in Figure 2.10a) and the end-to-end vector correlation function relaxing at $t = \tau_R$. On the other hand in supramolecular systems as the bonding energy ε increases, the relaxation behaviour demonstrates a gradual transition from polymer melt-like behaviour to fixed network-like behaviour. In the systems with high enough ε values where $\tau_R < \tau_{pe}$, three distinct relaxation regimes can be clearly identified in the $G(t)$ and $\Phi(t)$ curves: (1) initial Rouse regime at $\tau_0 < t \ll \tau_R$ where the relaxation curves follow universal Rouse-like behaviours, $G(t) \sim t^{-1/2}$ and $\Phi(t) \sim t^{-1/2}$; (2) intermediate rubbery regime at $\tau_R < t < \tau_{pe}$ where the systems show rubber-like

behaviour due to the transient network formation; (3) terminal relaxation regime at $t > \tau_{pe}$ where the sticker partner exchange events lead to the stress and dielectric relaxation. Figure 2.11 shows that at high sticky bonding energy the terminal times, τ_d^{stress} and τ_d^{ee} , of the stress and chain end-to-end vector relaxation functions both grow exponentially with ε . There is roughly a factor of 2 difference between these two terminal times, but subject to rather poor statistics in τ_d^{stress} at high bonding energies. The analogy to Rouse chain behaviour ($\tau_d^{ee} = 2\tau_d^{stress}$) [27] implies that the release of topological constraints by partner exchange events takes place in a random-walk manner, and therefore a theoretical model could be constructed based on this observation.

Earlier we described how the presence of large sticker clusters facilitates the partner exchange events. We now test this effect on the stress relaxation behaviour directly by imposing an upper cap on the maximum size of the clusters, N_{clu}^* , in simulations. Figure 2.12 presents the stress relaxation functions for the systems with two different upper caps, namely $N_{clu}^* = 3$ and 4 respectively, together with that of the regular uncapped systems ($N_{clu}^* = \infty$). The $G(t)$ results show clearly that preventing the sticker clusters from growing in size leads to a much slower stress relaxation behaviour in comparison with the regular supramolecular network we simulated, even though single sticker hopping events are allowed in both cases. Partner exchange events facilitated by sticker cluster dissociation-association processes thus play a dominant role in controlling the dynamic and rheological behaviour of supramolecular networks cross-linked by stickers cluster or micellar cores. In a theoretical work on the dynamics of telechelic ionomers, Leibler *et al.* have also pointed out that the stress relaxation should take place by exchanging pairs of charged chain ends to lower the free energy costs. [101]

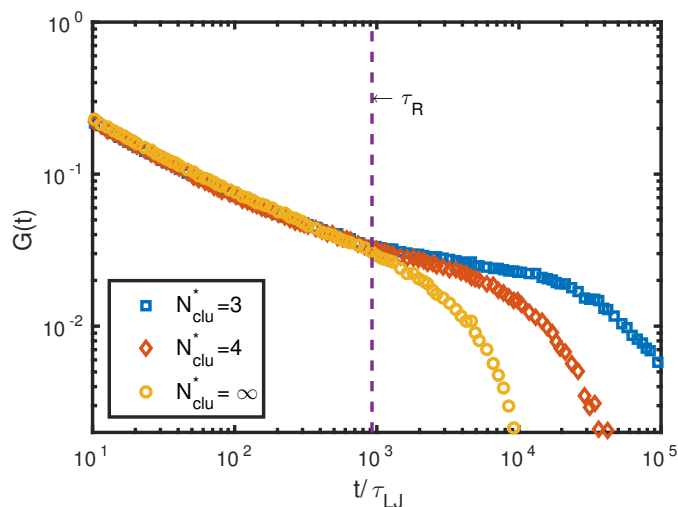


Figure 2.12: Stress relaxation functions of supramolecular systems with and without a upper cap N_{clu}^* for the sticker cluster sizes. The system parameters are $\varepsilon = 10k_B T$ and $N = 25$.

2.3.3 Theoretical models

Phantom chain hopping model

In this section we introduce a simple theoretical model to describe the dynamic behaviour of supramolecular polymer networks formed at high bonding energies ($\varepsilon \geq 9k_B T$) where nearly all stickers have associated into clusters. At time scales $t < \tau_{pe}$, the system behaves like a fixed polymer network and so can be described by the phantom network model where the sticker clusters act as cross-links or junctions. [82] In a phantom network consisting of ideal-chain strands of length N^* and cross-links of functionality f^* , each end monomer of a target network strand is considered to be effectively connected to the elastic non-fluctuating background via a virtual chain of length $N_{eff} = N/(f^* - 2)$. The other end, also called the anchor point, of the virtual chain is fixed in space. For mapping the phantom model to a supramolecular

network formed by bead-spring chains with a broad distribution of sticker cluster sizes, we first choose a strand length N^* and then match the time scales of the two systems by the ratio between the Rouse times of the phantom network strand and the parent polymer chains in the supramolecular system. Following that, the virtual chain length N_{eff} , or equivalently the effective cross-link functionality f^* , is determined by matching the mean square fluctuations of the end-to-end vectors of the network chains in the two different systems.

Unlike a permanent network, the end monomers or stickers of a polymer chain in a supramolecular network can change their topological connection to the network by moving from one sticker cluster or cross-link to another at time scales $t > \tau_{pe}$. The change of topological constraint on the target chain end via partner exchange process can be represented by a hopping of the anchor point of the virtual chain in the phantom model. Figure 2.13 sketches this phantom chain hopping model (PCHM) where a target Rouse chain consisting of N^* beads is end-linked to two other Rouse chains each of N_{eff} beads and anchored in space at the other end. The dynamic behaviour of the system is then controlled by chain fluctuations and anchor point hopping.

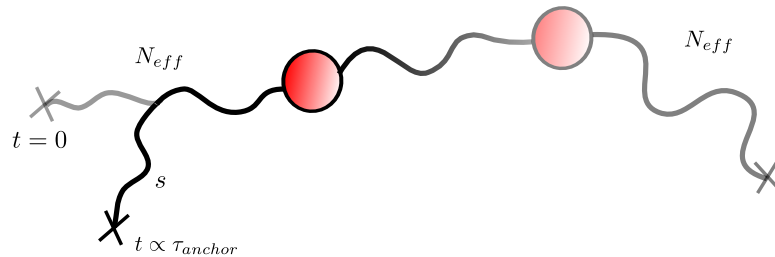


Figure 2.13: Sketch of the phantom hopping model. The red circles represent the stickers at the ends of the target chain.

The motion of all beads apart from the two anchored beads is governed by eq. (1.5). The phantom chain hopping model can then be solved numerically to provide

dynamic relaxation functions of the target polymer. Considering the broad distribution of the partner exchange times as shown in Figure 2.7(b), each anchor point is assigned a lifetime t_{life}^* randomly taken from a simple exponential distribution

$$P(t_{life}^*) = P_0 \exp(-t_{life}^*/\tau_{an}), \quad (2.11)$$

where P_0 is a normalization constant and τ_{an} is the average anchor point lifetime whose value can be varied to reflect the dependence of the partner exchange time τ_{pe} on the bonding energy. For a given ε value, we set $\tau_{an} = \tau_{pe}(\tau_R^*/\tau_R)$ where τ_R^* and τ_R are the Rouse times of the target phantom network strand and the polymer chains in the supramolecular systems, respectively.

After t_{life} the anchored bead performs a random hopping to a nearby position. The hopping process is carried out by eliminating a chain segment consisting of $s(\leq N_{eff})$ beads from the anchored end of the virtual chain and then regenerating it by a s -step random walk of step size b , as sketched in Figure 2.13. The position of the regenerated end monomer is taken as the new anchor point which is assigned a new lifetime from the distribution $P(t_{life})$. The resulting anchor point hopping distance follows the Gaussian distribution of the end-to-end distance of an ideal chain with $2s$ bonds and so has the mean value of $a_{an} = (2s)^{1/2}b$. In this algorithm, the impact of the abrupt hopping of the anchor point propagates to the related end monomer or sticker of the target chain through Rouse fluctuations of the virtual chain. Therefore, the sticker can adapt to its new equilibrium position in the transient network smoothly, analogous to the partner exchange events in real supramolecular systems. The average hopping distance of the anchor point and correspondingly the number of hopping events needed for a target chain to fully relax can be tuned by changing the segment length s . The terminal relaxation of the target chain depends on both the mean anchor point lifetime τ_{an} and the mean hopping distance a_{an} . These essentially capture the effect of increasing the bonding

energy and the sticker density as observed in the hybrid MD/MC simulations.

The system parameters of the phantom chain hopping model are set up as follows. For convenience, we choose the number of beads in the target phantom chain same as that of the parent chains in the modeled supramolecular systems, i. e, $N^* = N$. To find the virtual chain length N_{eff} or the effective cross-link functionality f^* , we recall from section 1.6.2 that in the phantom network model the mean square fluctuation of the end-to-end vector around its average value is given by $\langle (\mathbf{R}_{ee} - \langle \mathbf{R}_{ee} \rangle)^2 \rangle = 2N^*b^2/f^*$. [102] Figure 2.10 (b) shows that the end-to-end vector correlation function $\Phi(t)$ of the polymer chains with $N = 25$ is relaxed by about 30% in the fixed supramolecular polymer networks. One can thus deduce the effective cross-link functionality by the relation of $2/f^* \approx 0.3$, which gives $f^* = 7$. This f^* value is somewhat larger than the average sticker cluster size $N_{clu}^{avg} \approx 3.6$ found in the supramolecular networks. But as shown in Figure 2.14 (a), the resulting virtual chain length of $N_{eff} = 5$ provides a very good prediction of the permanent phantom network model for the chain end-to-end vector correlation function in the fixed supramolecular networks. As mentioned above, the average lifetimes of the anchor points τ_{an} are determined directly from the sticker partner exchange times τ_{pe} obtained in the hybrid MD/MC simulations at different bonding energies ε .

Figure 2.14 presents the numerical results of the PCHM on the chain end-to-end vector correlation functions $\Phi(t)$ and the end-monomer or sticker mean square displacements $g_1^{sticker}(t)$ of the target chains, together with the MD/MC simulation data on supramolecular networks with $N = 25$. At each ε value the two sets of data show reasonably good agreement in both the Rouse and rubbery (plateau) relaxation regimes without requiring any extra tuning parameters. Further agreement in the terminal relaxation regime after τ_{an} or τ_{pe} is achieved by choosing proper hopping distance a_{an} or s . For example, a value of $s = 4$ has been used for modeling the

supramolecular systems with $N = 25$ and $\varepsilon = 10k_B T$.

Discrete model of sticker diffusion

In supramolecular networks formed by associating telechelic chains, the topological constraints on the polymer chain ends are released in a step-by-step manner by sticker partner exchange events. The terminal relaxation time of the system can thus be estimated as the time taken for a sticker to diffuse a distance comparable to the size of its parent chain,

$$\tau_d \approx \frac{Nb^2}{a_{pe}^2} \tau_{pe}, \quad (2.12)$$

where a_{pe} is the average distance that a sticker diffuses after one partner exchange event with the characteristic time τ_{pe} . Eq. (2.12) takes a similar form as the free path (FP) model proposed by Marrucci *et al.* for equilibrium conditions [63], but the microscopic origins of the time and length scales of the discrete diffusion steps are very different from their model assumption.

In hybrid MD/MC simulations, we define a_{pe} as the separation between the mean positions of the initial and final sticker clusters that a sticker is associated with before and after a successful partner exchange event. The value of a_{pe} is found to increase with the sticky bonding energy ε even while the average size of clusters converges (Figure 2.4(b)). This implies that the sticker diffusion distance is determined by not only the average distance between sticker clusters, but also the lifetime of clusters. As the bonding energy increases, a cluster is able to explore a larger volume before the bond breakage permits its association with another cluster to facilitate sticker partner exchange. Figure 2.11 compares the predictions of eq. (2.12) obtained by using the simulation values of a_{pe} and τ_{pe} with the terminal times of the stress relaxation and chain end-to-end vector correlation functions of the supramolecular

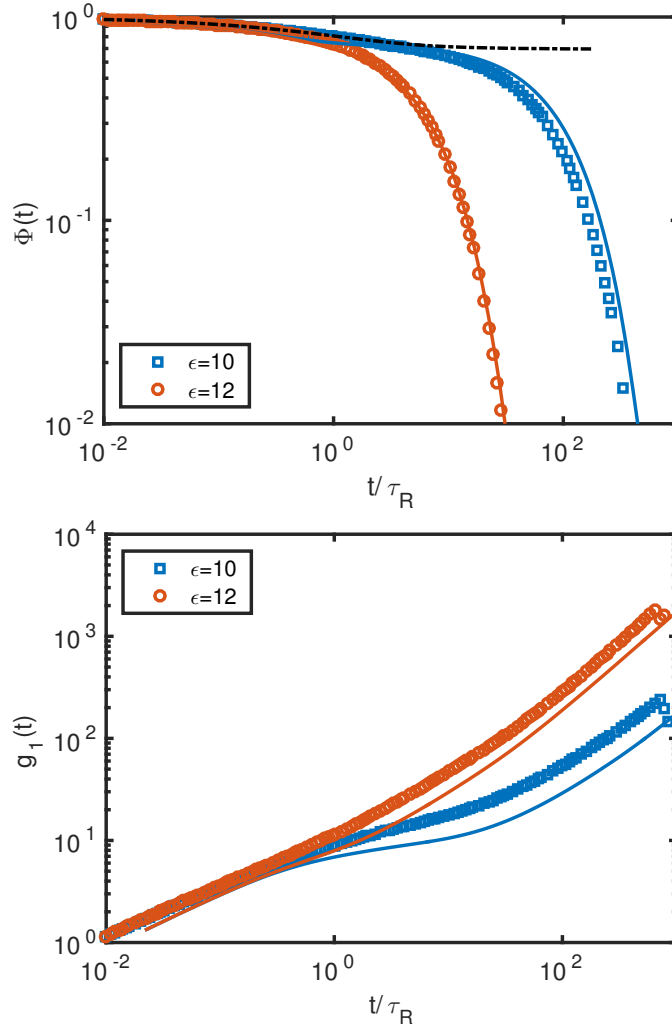


Figure 2.14: Simulation results of the phantom chain hopping model on the end-to-end vector correlation function $\Phi(t)$ (a) and the sticker mean square displacement (b) of the target chains. The symbols are the results obtained from hybrid MD/MC simulations of supramolecular networks with polymer chain length $N = 25$ at various bonding energies ϵ . The simulation times in both the PCHM and supramolecular systems have been rescaled by the Rouse times of the corresponding polymer chains. The dotted-dashed line in (a) presents the $\Phi(t)$ data of the fixed polymer network same as in Figure 2.10(b).

networks formed at high ε values. They show qualitatively good agreement. But it should be noted that the statistics of the a_{pe} and τ_{pe} values as well as the terminal times τ_d^{stress} and τ_d^{ee} are getting worse with increasing bonding energy because the simulation runs can only last 15 – 200 terminal relaxation times depending on ε .

We note that the sticker diffusion step size a_{pe} used in eq. (2.12) is different from the anchor point hopping distance a_{an} defined in the phantom chain hopping model. But the random walk feature of the chain end diffusion can be well correlated to the Rouse-like relationship between the terminal times of the stress and chain end-to-end vector relaxation functions, namely $\tau_d^{ee} \approx 2\tau_d^{stress}$. The PCH model has the advantage of being able to predict the entire relaxation functions over eq. (2.12) that only gives the terminal times.

2.4 Conclusions

Hybrid molecular dynamics/Monte Carlo simulations have been performed to study the static, dynamic and rheological properties of supramolecular systems consisting of unentangled telechelic chains with end sticky monomers. The choice of functionality $f = 3$ allows each sticker to form reversible bonds with two other stickers, which is the minimum requirement for network formation. The sol-gel transition occurs at a critical sticky bonding energy of $\varepsilon \approx 4.3k_B T$ when the fraction of reacted stickers overtakes that of the unreacted ones. At sufficiently high bonding energies ($\varepsilon \geq 10k_B T$), the majority of stickers are fully reacted and less than one percent of stickers remain open. The distribution of the sticker cluster sizes can be well described by a theoretical model analogous to that used to predict micellar size distribution in dilute solutions of amphiphilic molecules. The proportion of elastically inefficient strands in the strongly associated supramolecular networks is found

to be less than 5%.

The dynamic and rheological behaviour of the strongly associated supramolecular networks are shown to be dominated by the partner exchange events in which the stickers exchange their associated partners, and so release the imposed topological constraints, through the disassociation-association processes of the sticker clusters. This is in contrast to the traditional picture of single sticker hopping where a sticker needs to first pull out of a cluster by breaking all existing sticky bonds, which is energetically unfavorable. Our study indicates that the system can relax without waiting for the chain ends to completely disassociate from the network. The presence of large sticker clusters can actually increase the chain relaxation rate. Preventing the sticker clusters from associating into larger ones will significantly slow down the stress relaxation.

Two characteristic time scales, namely the partner exchange time τ_{pe} and cluster exchange time τ_{ce} , are introduced to measure the dynamics of supramolecular networks formed at high sticky bonding energies. These time scales are up to two orders of magnitude larger than the average sticky bond lifetime τ_b . Three distinctive regimes can be identified in the stress and end-to-end vector relaxation functions, *i.e.*, an initial Rouse regime at time scales $\tau_0 < t \ll \tau_R$, an intermediate rubbery or plateau regime at $\tau_R < t < \tau_{pe}$ and a terminal relaxation regime at $t > \tau_{pe}$. A phantom chain hopping model is developed based on the microscopic picture of the sticker partner exchange process. Numerical predictions of this model on the sticker mean square displacement and chain end-to-end vector correlation functions are in reasonably good agreement with the hybrid MD/MC simulation results. Furthermore, the terminal relaxation time of a supramolecular network can be estimated as the time taken for a sticker to diffuse a distance comparable to the size of its parent chain. The time and length scales of the discrete steps of the chain-end diffusion are

determined by the sticker partner exchange events.

Chapter 3

Non-linear rheology of supramolecular polymer melts

3.1 Introduction

In this chapter we study the non-linear rheology of polymers which can form reversible associations under both planar extensional flow and shear flow. These systems are modelled using the hybrid MD/MC method described in section 1.8.2. Each chain possesses stickers at chains ends which can reversibly associate with up to two other stickers.

The two main types of flows used to characterise the viscoelastic properties of liquids are known as shear and extensional flows. The latter encompasses irrotational geometries including: uniaxial extension, biaxial extension and planar extension. In this thesis we focus on shear flow and planar extensional flow in a canonical ensemble (*i.e.* a system with fixed volume). Figure 3.1 illustrates the evolution of an initial

volume under the application of shear flow (a) and planar extensional flow (b). The

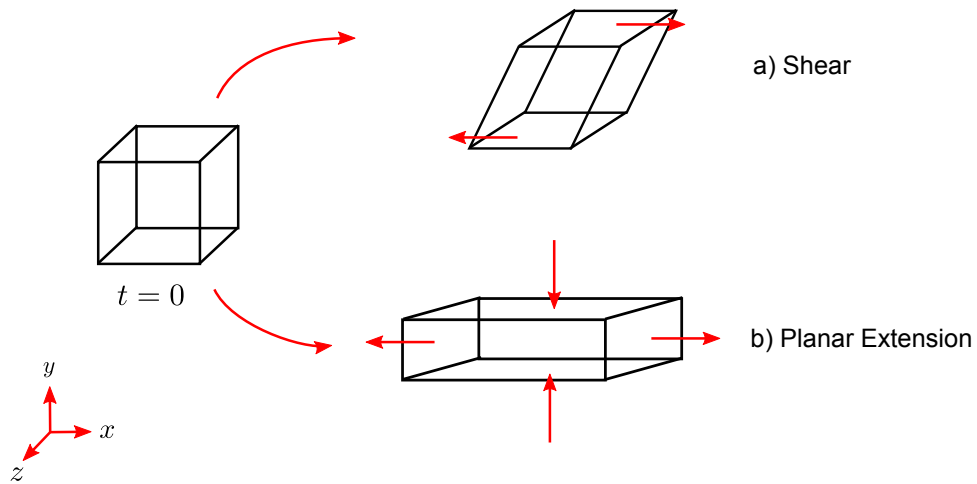


Figure 3.1: Illustration showing the deformation of a volume under the application of shear and planar extension.

first use of extensional viscosity, under a different name is attributed to Trouton [103]. He outlined the relationship between shear viscosity and what he called the “coefficient of viscous traction”. Trouton determined a ratio of three between the extensional and shear viscosities of a Newtonian fluid (now known as the Trouton ratio). For the planar extension which we will be studying here the Trouton ratio is four [29].

The difficulty in characterising extensional viscosities is highlighted in a review by James and Walters [104]. In this paper the authors collate experimental results on the extensional viscosity of the same polymer liquid using different experimental techniques (*e.g.*, spinline rheometer, contraction flow, filament stretching). Each technique produced different flow histories, which gives rise to inconsistent results when comparing transient extensional viscosities as a function of strain rate, see Figure 3.2. For this reason the authors went on to suggest that results should be viewed in terms of the total strain for consistency.

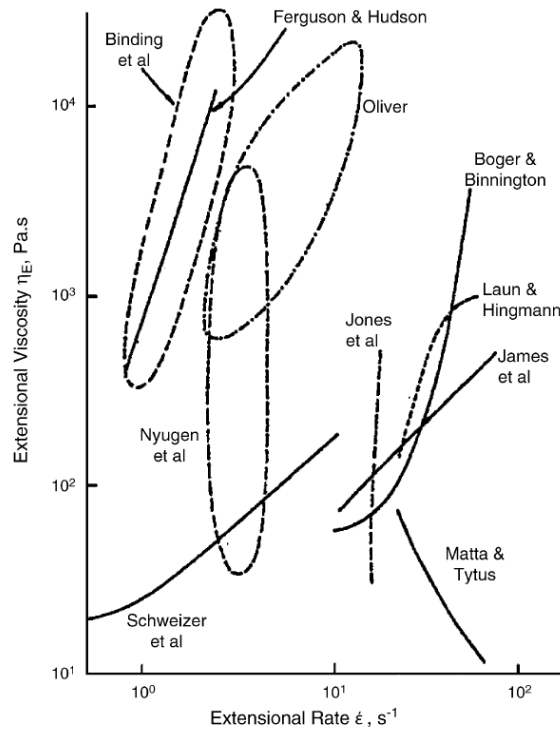


Figure 3.2: The “M1” muddle described by James and Walters (1993). Shows the difference in extensional viscosity calculated for a single material using different experimental techniques.

3.1.1 Supramolecular polymers

Supramolecular polymers have been shown to exhibit either shear thickening [105, 106] or shear thinning behaviour. In some cases both types of behaviour have been seen in the same system when probed under different experimental conditions [107].

Shear thinning describes the process by which the viscosity decreases when increasing shear rate. In supramolecular polymer networks shear thinning is often attributed to the shear induced rupture of sticky bonds. Chains detach from the network once the tension supported by the chain exceeds some critical threshold

determined by the strength of the sticky bonds [108]. If the chains can reach this critical value before they naturally detach due to thermal fluctuations, this will result in an overall reduction in bond lifetime. Shear banding in transient polymer networks has also been shown to cause shear thinning on macroscopic scales. An inhomogeneous flow profile forms which is caused by fractures in brittle materials. These fractures lead to the presence of concentration gradients in the sheared material [109].

Shear thickening on the other hand describes the process by which the viscosity of a material increases with shear rate. There are two main mechanisms which have been proposed to explain shear thickening behaviour:

1. Non-Gaussian stretching of polymer chains: when a polymer chain is stretched under shear, the stress along the polymer chain will increase exponentially with strain [48]. This mechanism for shear thickening was first proposed by Marrucci *et al.* [110].
2. Network reorganisation or structure formation under shear: the application of shear can lead to an increase in the number of active strands in the transient network [105].

Literature tends to focus on the network reorganisation or structure formation explanation. For example in systems of hydrophobically modified ethoxylate-urethane (HEUR) polymers chains can form into micelles or flower-like structures. In these systems an increase in the number of active strands is described in terms of an increase in the ratio of chains bridging micelles to looping chains [111]. As a result many theoretical approaches focus on models with populations of active (bridging) and inactive (dangling or looping) strands [106, 112]. Two characteristic rates

then define the transition between these two states: from active to inactive (usually termed the destruction rate) and inactive to active (the creation rate). These rates are linked to the bond lifetime, τ_b , and the time a sticker spends detached from the network, τ_{open} . Shear thickening is usually observed in systems with slower cross-linking kinetics [113]. That is in systems with a low destruction rate or long-lived active strands. In some studies like the Brownian dynamics simulations of Hernández *et al.* [112] a variable is introduced to artificially reduce the destruction rate. Concentration has also been shown to play an important role in shear thickening [111]. If the concentration is low, an increase in the number of inactive strands is seen with far fewer chains forming bridges between micelles. Therefore, reducing the concentration decreases the creation rate. Under shear (see Figure 3.1), as the deformation rate increases, detached stickers have an increased probability of collision due to the differential velocity in the y -direction [106]. This results in an increase in the creation rate or decrease in τ_{open} . The increase in creation rate due to a deformation leads to a net increase in the number of active strands which increases the stress held by the system (i.e., an additional $k_B T$ per chain) and consequently results in shear thickening. The conversion of intrachain bonds to interchain bonds was suggested by Witten *et al.* [114] as another mechanism to facilitate structure formation (in systems where multiple stickers are placed along the polymer backbone).

To our knowledge very few simulations have been carried out to study the non-linear rheology of supramolecular polymers. The Brownian dynamics simulations reviewed above represent polymer chains using only dumbbells and so disregard the contributions of polymer dynamics. One example of a full chain simulation comes from Li *et al.* [80] who present non-equilibrium molecular dynamics simulations of supramolecular polymers under steady shear flow. In these simulations, short linear chains capable of reversible head-to-tail association are studied. Chains of

this kind can not produce a 3D network structure, instead behaving more like living polymers. In their shear simulations they find increasing association energy results in a higher shear viscosity. These simulations also demonstrate shear thinning behaviour. Another example of non-linear rheology simulations comes from the work of Hoy and Fredrickson [79] discussed in section 2.1, which contains results from creep experiments, but not steady shear flow or steady extensional flow which are studied here.

3.2 Time-dependent rheology

Viscosity describes the resistance of a material to a gradual deformation by shear stress. The viscosity in the linear regime is given by

$$\eta(t) = \int_0^t G(t') dt'$$

where $G(t)$ is the stress autocorrelation function, this will be calculated as additional validation of our non-equilibrium procedure.

In our simulations we consider only start-up flow, therefore, the shear rate $\dot{\gamma}$ and extension rate $\dot{\epsilon}$ are independent of time. Under shear flow the stress components σ_{yz} and σ_{xz} vanish identically by symmetry, therefore, the relevant stress components are the shear stress σ_{xy} , and the normal stresses $N_1 = \sigma_{xx} - \sigma_{yy}$, and $N_2 = \sigma_{yy} - \sigma_{zz}$. The shear viscosity η as a function of time (also known as the shear stress growth coefficient) is then given by the shear stress divided by the shear rate $\dot{\gamma}$,

$$\eta(t) = \frac{\sigma_{xy}(t)}{\dot{\gamma}}. \quad (3.1)$$

The first normal stress growth coefficient is then given by

$$\Psi_1(t) = \frac{N_1(t)}{\dot{\gamma}^2} \quad (3.2)$$

and similarly the second normal stress growth coefficient is

$$\Psi_2(t) = \frac{N_2(t)}{\dot{\gamma}^2}.$$

In the linear regime the transient first normal stress coefficient is related to the stress autocorrelation function such that

$$\Psi_1(t) = 2 \int_0^t t' G(t') dt'. \quad (3.3)$$

For planar extensional flow the off-diagonal components of the stress vanish, and there are then two extensional viscosities, firstly

$$\eta_E(t) = \frac{\sigma_{xx}(t) - \sigma_{yy}(t)}{4\dot{\epsilon}} \quad (3.4)$$

where the four in the denominator accounts for the Trouton ratio which allows for comparison between shear and planar extensional flows [29]. This viscosity describes the tensile stress required to stretch the material in the x -direction. The second viscosity is known as the "cross viscosity"

$$\eta_c(t) = \frac{\sigma_{zz}(t) - \sigma_{yy}(t)}{2\dot{\epsilon}} \quad (3.5)$$

which denotes the tensile stress required to prevent deformation in the neutral direction (z -direction). This second viscosity has only been measured rarely with one example coming from Wagner *et al.* [115] who compared the results from a number of constitutive models to experimental results from linear and long-chain branched polyolefin melts.

3.3 Equations of motion

The first methods for non-equilibrium molecular dynamics involved using solid-wall boundaries to drive flow, these methods however are not efficient if one is interested

in bulk properties far away from the boundary surface.

For studying bulk properties there are two methods for applying flows in simulations: 1) The first involves modifying the periodic boundaries conditions to simulate systems far from equilibrium. 2) The second method involves applying a synthetic field which allows for the required streaming velocity profile to be maintained indefinitely. The first approach using only modified boundaries requires longer simulation times for the translation of atoms between boundaries to communicate throughout the fluid, and has been shown to be insufficient in driving the most general time perturbations [50]. For this reason homogeneous non-equilibrium molecular dynamics (NEMD) algorithms which make use of an artificial field have been proposed, the most commonly used is the SLLOD equations of motion which were initially proposed by Evans and Morris [116]

$$\dot{\mathbf{r}}_i = \frac{\mathbf{p}_i}{m_i} + \mathbf{r}_i \cdot \nabla \mathbf{u} \quad (3.6)$$

$$\dot{\mathbf{p}}_i = \mathbf{F}_i - \mathbf{p}_i \cdot \nabla \mathbf{u} \quad (3.7)$$

where \mathbf{F}_i is the sum of all interatomic forces (*i.e.*, when modelling polymer chains the non-bonded Lennard-Jones and bonded FENE forces) acting on an atom i and peculiar velocity, \mathbf{p}_i , and the gradient of the streaming velocity, $\nabla \mathbf{u}$. Here m_i denotes the mass of atom i . This set of equations is described as the atomic version of SLLOD, with the deformation applied to each particle in the system. An alternative “molecular” approach to SLLOD has also been developed which applies the deformation to the centre of mass of each molecule. These two versions exhibit differences in the initial transient phase, but reach equivalent steady states. In our simulations we use the atomic version as this will produce more accurate trajectories for all atoms within a chain rather than just the polymer as a whole. In order to calculate the bulk properties the SLLOD equations of motion must be used with periodic boundary conditions which do not interfere with the particle trajectories. There-

fore, the choice of periodic boundary conditions is dependent on the flow profile. As was discussed in section 3.1.1 the inhomogeneous flow profile caused by shear banding may result in the shear thinning of supramolecular polymer systems. The use of an artificial field via the SLLOD equations of motion prevents shear banding as particles experience a predetermined velocity profile. Therefore, the role of this mechanism in shear thinning can not be studied in our simulations. Shear banding has been explored in simulations by using dissipative particle dynamics [117] a technique which allows for the study of time and space scales much larger than those which can be studied in MD.

3.4 Thermostat

In NEMD simulations using SLLOD we use the Gaussian thermostat, which has been shown to be effective in maintaining temperature in both planar extensional flow and shear flow [118]. For this thermostat an additional term is added to the equation for peculiar velocity eq. (3.7)

$$\dot{\mathbf{p}}_i = \mathbf{F}_i - \mathbf{p}_i \cdot \nabla \mathbf{u} - \zeta_\alpha \mathbf{p}_i$$

where ζ_α is known as the Gaussian multiplier and is given by

$$\zeta_\alpha = \frac{\sum_i \mathbf{p}_i \cdot (\mathbf{F}_i - \mathbf{p}_i \cdot \nabla \mathbf{u})}{\sum_i \mathbf{p}_i^2}.$$

However, it was shown by Todd and Daivis [118] that after long times the temperature will tend to drift when using the Gaussian thermostat. This numerical drift is caused by truncation errors. A simple solution for this problem was suggested by Baranyai *et al.* [119] and involves the addition of a proportional feedback term to counteract the drift. In simulations of the SLLOD equations of motion, Todd and Daivis [120] applied this technique to the thermostat by modifying the Gaussian

multiplier ζ_α . This is achieved by adding a small perturbation which is proportional to the difference between the desired temperature and the actual kinetic temperature obtained by summing momenta. Thus, the thermostat multiplier can be rewritten as

$$\zeta_{new} = \zeta_\alpha + \zeta_0 \left[\frac{\sum_i \frac{\mathbf{p}_i^2}{m_i} - 3Nk_B T}{3Nk_B T} \right]$$

where ζ_0 is a weighting term and T is the desired temperature. The weighting term ζ_0 is selected such that it is large enough to correct for numerical drift, but not so large that the equations of motion become stiff. They suggest typical values for the weighting term are in the range 0.1 – 10. We select a weighting term of $\zeta_0 = 10$ which we find results in a temperature ratio of approximately one between the actual temperature and the desired temperature.

3.4.1 Simulation parameters

In simulations of non-equilibrium behaviour of supramolecular networks, we study parent chains of length $N = 45$ and each simulation box contains $N_{ch} = 400$ chains. We also use slower reaction kinetics, specifically maintaining $\tau_{LJ} = \tau_{MC}$. The polymer density is set to $\rho = 0.85/\sigma_{LJ}$ which has been widely used to study melt systems. Unless stated otherwise a time-step of $\delta t = 0.005\tau_{LJ}$ has been used in simulations. For some faster shear or elongation rates the time-step will need to be decreased, but the kinetic rate will remain fixed so that results are comparable.

3.5 Shear flow

The first type of deformation we considered is shear flow or planar Couette flow (PCF), in which the fluid flows in the x -direction with velocity gradient $\dot{\gamma}$ in the y -direction. Therefore, the strain rate tensor can be written as

$$\nabla \mathbf{u} = \begin{pmatrix} 0 & 0 & 0 \\ \dot{\gamma} & 0 & 0 \\ 0 & 0 & 0 \end{pmatrix}. \quad (3.8)$$

Accordingly, the SLLOD equations of motion in the x -direction become

$$\begin{aligned} \dot{r}_{ix} &= \frac{p_{ix}}{m_i} + \dot{\gamma} r_{iy} \\ \dot{p}_{ix} &= f_{ix} - \dot{\gamma} p_{iy}. \end{aligned}$$

With the equations of motion in all other directions unchanged from equilibrium simulations.

For shear flow the Lees-Edwards periodic boundary conditions can be used [121]. These periodic boundary conditions are illustrated in two dimensions in Figure 3.3, in which periodic images above the central simulation cell slide with velocity $+\dot{\gamma}L$, while images below it slide with velocity $-\dot{\gamma}L$. If a monomer passes through the top or bottom interface its x -position must be adjusted by $\pm\dot{\gamma}Lt$. An alternative approach for periodic boundary conditions in shear flow is the Lagrangian-Rhomboid method [50], which involves the deformation of an initial rectangular simulation box in line with the shear strain, followed by remapping to the initial simulation box when the shear strain $\dot{\gamma}t$ is a multiple of box length, L . This alternative approach is equivalent to Lees-Edwards boundary conditions. Therefore, we use the easier to implement Lees-Edwards periodic boundary conditions in simulations of shear flow. In shear flow simulations the length of the simulation box in the x -direction is usually

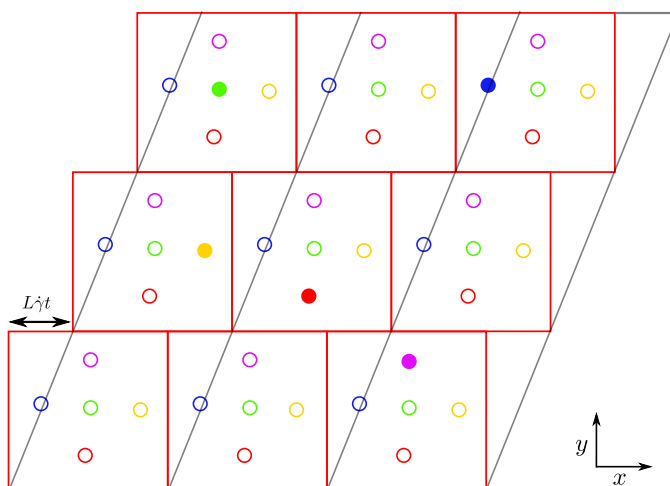


Figure 3.3: Illustration of the Lees-Edwards sliding brick periodic boundary conditions for planar Couette flow. The grey lines show the equivalent simulation box for Lagrangian-Rhomboid periodic boundaries.

set to be twice the box length in the y and z directions. This is to ensure elongated chains do not interact with their own images through the periodic boundaries [122].

3.6 Extensional flow

The other type of flows considered in experiments are extensional flows. There are three main types of extensional flows, namely: uniaxial, biaxial and planar extension.

For planar extensional flow (PEF) the strain rate tensor is given by

$$\nabla \mathbf{u} = \begin{pmatrix} \dot{\epsilon} & 0 & 0 \\ 0 & -\dot{\epsilon} & 0 \\ 0 & 0 & 0 \end{pmatrix}.$$

Hence, the SLLOD equations of motion become

$$\begin{aligned}\dot{r}_{ix} &= \frac{p_{ix}}{m_i} + \dot{\epsilon}r_{ix} \\ \dot{r}_{iy} &= \frac{p_{iy}}{m_i} - \dot{\epsilon}r_{iy} \\ \dot{p}_{ix} &= f_{ix} - \dot{\epsilon}p_{ix} \\ \dot{p}_{iy} &= f_{iy} + \dot{\epsilon}p_{iy}.\end{aligned}$$

The equation of motion in the z -direction is unchanged from equilibrium simulations.

These flows can be difficult to simulate, as suitable periodic boundary conditions are required which are compatible with the flow geometry *i.e.*, which allow one or more directions of the simulation box to contract with time. If we deform the box in line with the flow, the simulation will be forced to stop when the width of the simulation box in the contracting direction(s) reaches twice the radius of interactions between particles since the minimum image convention is violated. This limits the length of time that the simulations are able to run, ultimately preventing the simulation from reaching steady state.

3.6.1 KR boundary conditions

To overcome the above mentioned problem, Kraynik and Reinelt proposed a method in 1992 [123] to allow time unrestricted simulations of planar elongational flows of spatially periodic lattices, this method was later applied to molecular dynamics simulations by Todd and Daivis [124]. The KR boundary conditions consist of rotating a square lattice to a special angle and performing elongation with respect to the original lattice. Thus, it has been shown that after some strain period ϵ_p known as the Hencky strain the lattice can be reproduced onto the original lattice. A simple illustrative simulation of these boundary conditions for randomly positioned

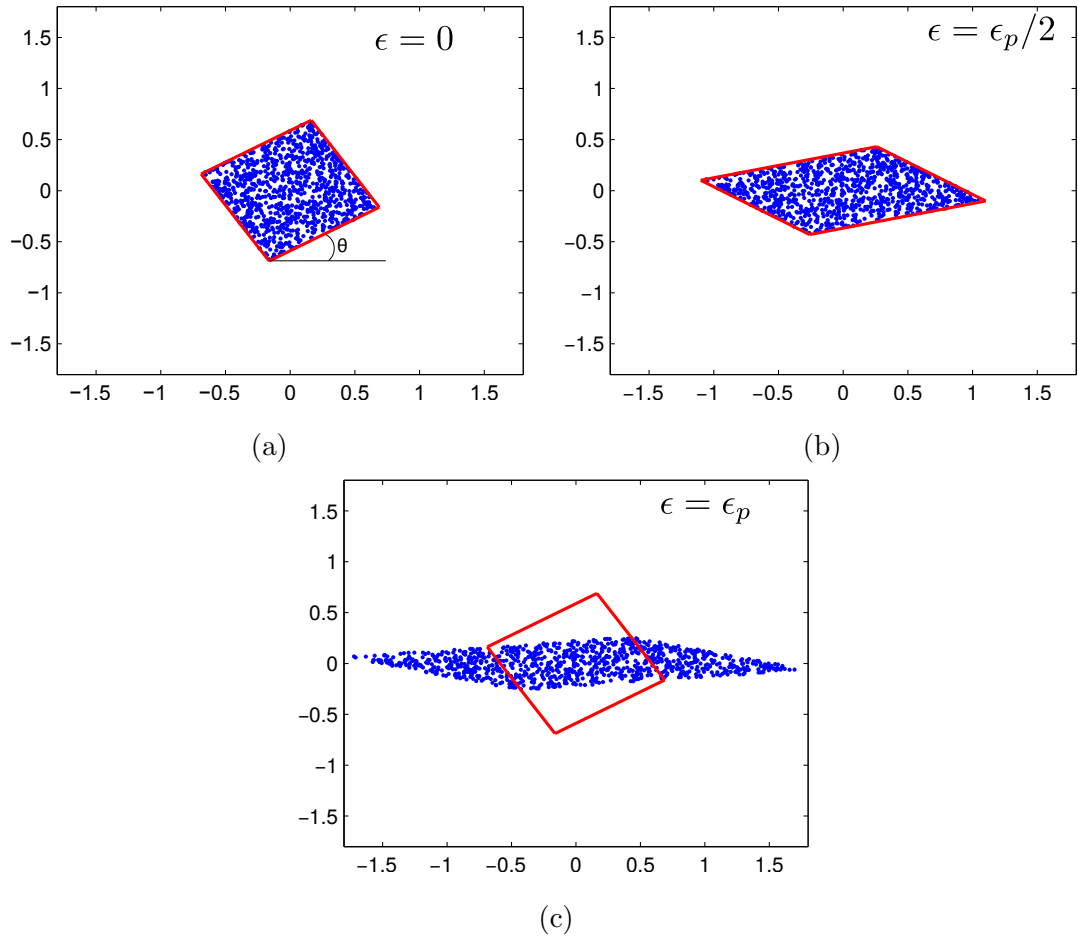


Figure 3.4: Evolution of randomly positioned particles via the Kraynik-Reinelt (KR) lattice under planar extensional flow as a function of time. Only the x - and y -axis vary with time. At $\epsilon = \epsilon_p$ the lattice reproduces itself, and the particles are shown before the positions are folded back (c).

particles being displaced with an appropriate flow ($\dot{\epsilon}$ in the x -direction and $-\dot{\epsilon}$ in the y -direction) is shown in Figure 3.4. The initial image shows the undeformed unit cell aligned to an angle θ between the x -axis and the axis of expansion (Figure 3.4a), and the final image shows the fully transformed unit cell before it is mapped back to the initial unit cell Figure in 3.4c.

In the algorithm outlined by Todd and Daivis [124] one must initially determine the “magic” angle, θ , describing the angle that the box is initially rotated in the xy -plane and the Hencky strain, ϵ_p , at which the deformed box is mapped to the original. These are calculated as follows:

1. Choose any integer k , such that $k = 3, 4, 5, \dots$
2. Defining λ_p as $\lambda_p = \exp(\epsilon_p)$, we have

$$\lambda_p = \frac{k \pm \sqrt{k^2 - 4}}{2}$$

which in turn gives us the value of ϵ_p . Hence, as $\epsilon_p = \dot{\epsilon}\tau_p$ where $\dot{\epsilon}$ is the extension rate, we can determine the strain period τ_p .

3. For the chosen value of k , choose a positive integer N_{11} , then solve for N_{12} using the following expression

$$N_{12} = -\sqrt{N_{11}(k - N_{11}) - 1}.$$

4. If and only if N_{12} is an integer then a solution has been found, and the “magic” angle θ is determined as

$$\theta = \tan^{-1} \left(\frac{N_{11} - \lambda_p}{N_{12}} \right).$$

We use the typical values of $\theta \approx 31.7^\circ$, and $\epsilon_p \approx 0.9624$ which correspond to $k = 3$, $N_{11} = 2$ and $N_{12} = -1$. This selection guarantees that the system

remains spatially and temporally periodic at times $t = n\tau_p$ where n is an integer.

From the above we can determine the basis vectors for the simulation cell as a function of time, namely

$$L_1(t) = (e^{\dot{\epsilon}t} \cos \theta, e^{-\dot{\epsilon}t} \sin \theta)$$

and

$$L_2(t) = (-e^{\dot{\epsilon}t} \sin \theta, e^{-\dot{\epsilon}t} \cos \theta).$$

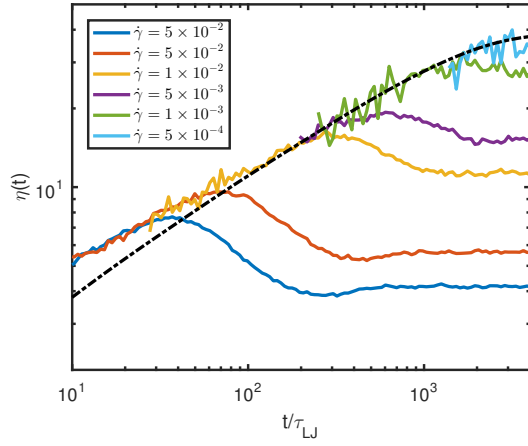
3.7 Results

In addition to the supramolecular system we also run simulations of a melt system with analogous parameters without stickers. This will allow us to investigate the differences in material properties which arise from the introduction of reversible associations. All non-equilibrium viscosity curves are averaged over six statistically independent simulations.

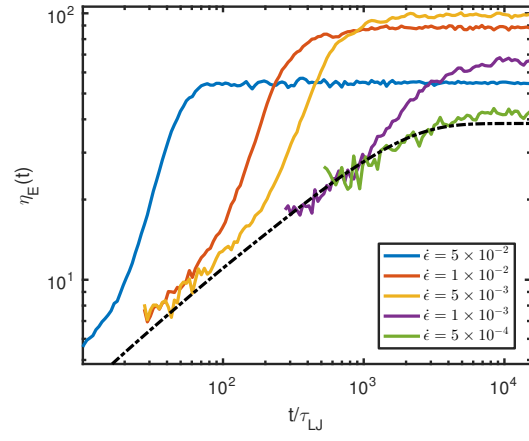
3.7.1 Viscosity

Monodisperse polymer melt system

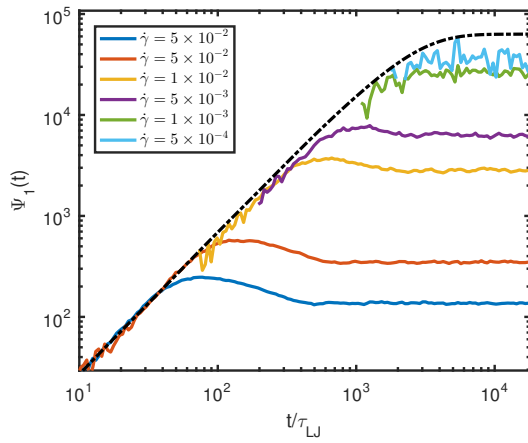
We firstly look at results obtained from a melt system without stickers (equivalent to $\varepsilon = 0k_B T$). Under start-up of shear flow the viscosity as a function of time (eq. (3.1)) is shown in Figure 3.5a for a number of shear rates, $\dot{\gamma}$.



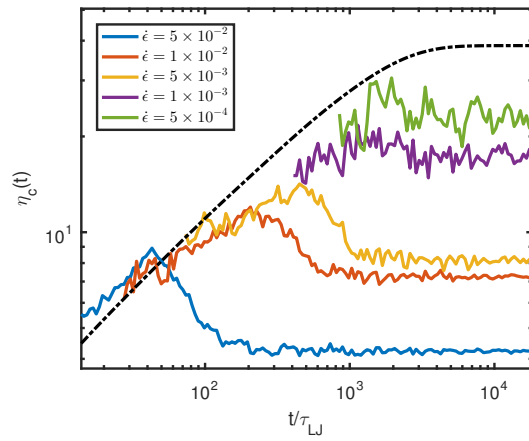
(a) Shear viscosity



(b) Planar extensional viscosity



(c) First normal stress growth coefficient



(d) Extensional cross viscosity

Figure 3.5: Simulations results for a melt system without stickers for a number of shear and extension rates. The black dot-dashed line highlights the linear viscosity curve calculated from the equilibrium stress autocorrelation function.

At small strains shear viscosity curves for all applied shear rates are expected to superimpose with the linear viscoelastic behaviour. In the simulation results we present the linear viscosity curve is calculated by first fitting Maxwell Modes using Reptate [125] to the stress relaxation function, then the resulting function is numerically integrated. The error present in the initial behaviour is due to the fitting. The terminal stress relaxation time τ_d of a monodisperse melt system with chain length $N = 45$ is approximately $1.21 \times 10^3 \tau_{LJ}$ at equilibrium. If the shear rate $\dot{\gamma}$ is larger than the reciprocal of the terminal time τ_d of the system, the viscosity $\eta(t)$ passes through a maximum and then decreases until it reaches the steady-state. In start-up shear the stress overshoot in entangled monodisperse polymer systems for rates $1/\tau_d < \dot{\gamma} < 1/\tau_R$ is thought to be caused by changing tube segment orientation [122]. On the other hand for rates larger than $1/\tau_R$ chain stretching is thought to cause the stress overshoot. The chain stretching and segment orientation mechanisms are also both present in unentangled monodisperse melt systems. The first normal stress growth coefficient is shown in Figure 3.5c. For small strains all curves collapse onto the linear first normal stress growth curve given by eq. (3.3). The overshoot in the first normal stress growth coefficient appears at high shear rates.

We now look at planar elongational flow of a melt system in the absence of stickers. The extensional viscosity as a function of time (eq. (3.4)) is shown in Figure 3.5b for a number of extension rates, $\dot{\epsilon}$. For small strains the linear viscoelastic regime differs only by the Trouton ratio (four in PEF). For higher extension rates the extensional viscosity rises above the linear viscoelastic regime, this is known as extensional thickening.

The results for extensional cross viscosity shows analogous behaviour to the shear viscosity. The curves superimpose for small strains and the cross viscosity

passes through a maximum and then decreases until it reaches the steady-state if the extension rate $\dot{\epsilon}$ is higher than the reciprocal of the terminal time τ_d of the system.

Supramolecular polymer system

We now look at the systems with the addition of stickers at chain ends each capable of reversibly associating with up to two partners. Simulations are carried out with a sticky bond association energy of $\varepsilon = 10k_B T$. In our study of the equilibrium dynamics of supramolecular polymers we showed the existence of a transient network for this and higher bonding energies. Hence, we would expect an increase in viscosity as the presence of temporary network junctions should make the material more resistant to deformation.

Figure 3.6a shows the viscosity as a function of time for a number of shear rates, $\dot{\gamma}$. We find a large increase in viscosity for all shear rates, $\dot{\gamma}$. Again if the shear rate $\dot{\gamma}$ is higher than the reciprocal of the terminal time τ_d of the system, the viscosity $\eta(t)$ passes through a maximum and then decreases until it reaches the steady-state. The terminal time τ_d of a supramolecular polymer system with bonding energy $\varepsilon = 10k_B T$ and chain length $N = 45$ is approximately $2.46 \times 10^5 \tau_{LJ}$ at equilibrium. The magnitude of the maximum or overshoot is much larger than the equilibrium case and more importantly for higher shear rates the overshoot reaches a viscosity higher than the linear viscosity curve, demonstrating shear hardening in supramolecular networks. This increase in viscosity above the linear viscosity curve is due to non-Gaussian stretching which occurs for shear rates higher than the reciprocal of the bond lifetime, τ_b . For lower rates chains have time to rearrange themselves within the transient network preventing the onset of stretching. This is

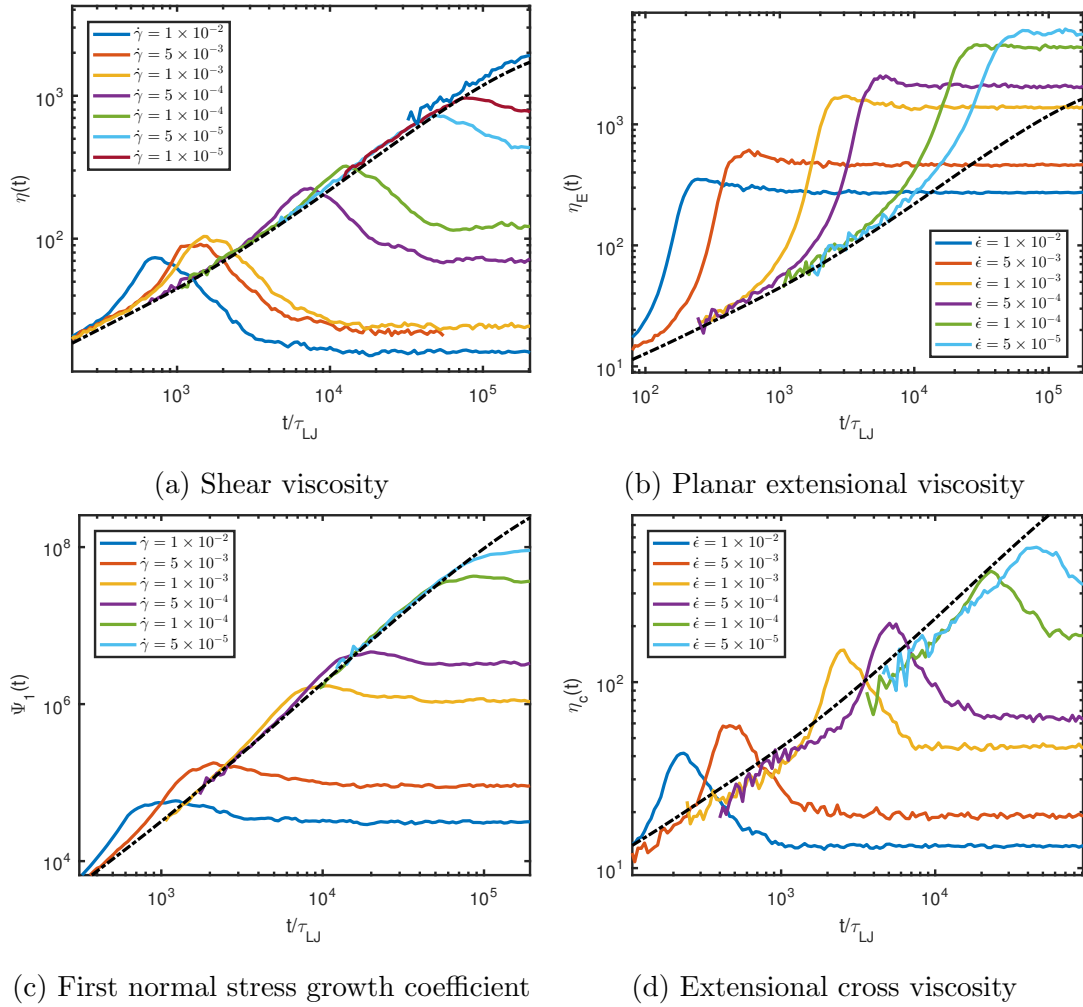


Figure 3.6: Simulation results for the supramolecular system with bonding energy $\varepsilon = 10$ for a number of shear and extension rates. The black dot-dashed line highlights the linear viscosity curve calculated from the equilibrium stress autocorrelation function.

discussed further in the section 3.7.2. If we look at the first normal stress growth coefficient given by eq. (3.2) in Figure 3.6c we again see signs of shear hardening at higher shear rates.

The extensional viscosity Figure 3.6b shows an increase in the magnitude of extensional thickening compared with the melt system and the introduction of a small overshoot for higher deformation rates just before the steady state is reached. The terminal time τ_d increases dramatically with the introduction of stickers so it becomes too computationally expensive to simulate extension rates which are small enough to see a reduction in extensional thickening. This extreme extensional thickening has also been observed in experiments [126].

The extensional cross viscosity Figure 3.6d is again found to produce qualitatively similar results to those obtained in shear with higher rates, leading to an overshoot much larger than the linear viscosity curve.

Marrucci *et al.* [110] were the first to explore the role of non-Gaussian chain stretching and shear thickening. In the system they studied stickers can quickly rejoin the network once detached, allowing chain stretching to persist when a sticker is free. This was guaranteed by assuming the spacing between aggregates was much smaller than the equilibrium chain size. In this theory chains were said to become fully stretched at a shear rate $\dot{\gamma} \approx N^{1/2}/\tau$ where τ is the effective relaxation time of a chain. If we assume this picture is valid then in our system the proposed shear rate for maximum stretching is approximately $\dot{\gamma} \approx 2.72 \times 10^{-5}/\tau_{LJ}$. Fig 3.6a however shows no obvious signs of chain stretching for rates lower than $\dot{\gamma} \approx 1e - 4/\tau_{LJ}$.

The important deformation rates should be related to key material timescales, these are τ_d , τ_R , τ_{pe} and τ_b . If we consider these in terms of deformation rates we

have

$$\frac{1}{\tau_d} < \frac{1}{\tau_{pe}} < \frac{1}{\tau_b}.$$

As discussed in Chapter 2 sticky bonds frequently break, which facilitates the exchange of partners. Under deformation when a sticky bond breaks the elastic energy built up by chain stretching is released. This results in fewer recombination events as is highlighted by the decrease in partner exchange time with increasing deformation rate (studied in section 3.7.3). Therefore, for the effects of stretching to be apparent a chain must remain associated to the network at both ends. Therefore, chain stretching should occur for shear rates $\dot{\gamma}_{stretch}$ such that

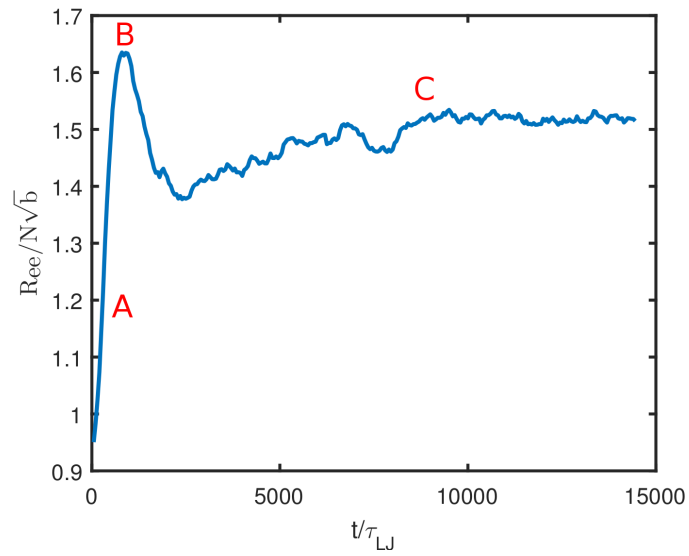
$$\dot{\gamma}_{stretch} > \frac{1}{\tau_b}$$

where τ_b is the equilibrium bond lifetime. For such rates the stretching will lead to an increased overall viscosity and an increase in the overshoot above even the linear viscosity curve.

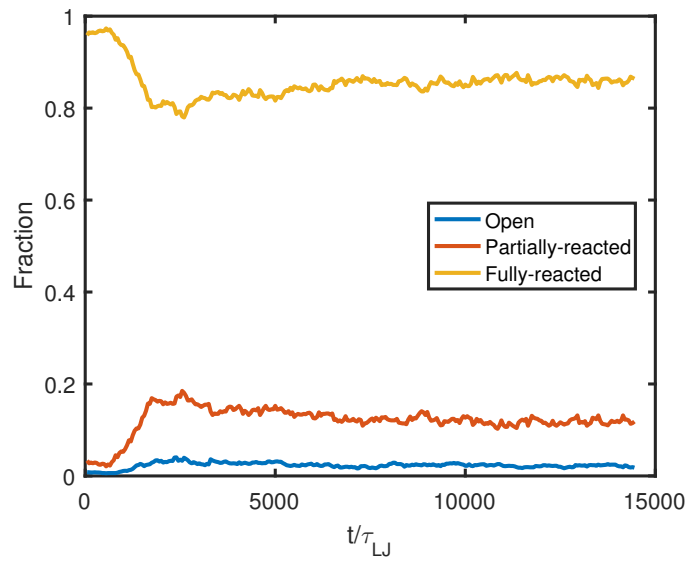
3.7.2 Chain stretching and network structure

Viscosity can be increased above the linear viscoelastic behaviour by either chain stretching or network reorganisation. To study the shear hardening behaviour observed in Figure 3.6a we can look at the number of sticky bonds and the mean end-to-end distance as a function of time. This will allow us to identify whether this hardening is caused by structural changes or chain stretching.

We can study chain stretching by looking at the average end-to-end distance R_{ee} of polymer chains as a function of time, see Figure 3.7a. This shows how the end-to-end distance varies with time at $\dot{\gamma} = 5 \times 10^{-3}/\tau_{LJ}$. The results are averaged over three statistically independent simulations. Initially a sharp increase to over



(a) Instantaneous end-to-end vector.



(b) Instantaneous sticky bond fraction.

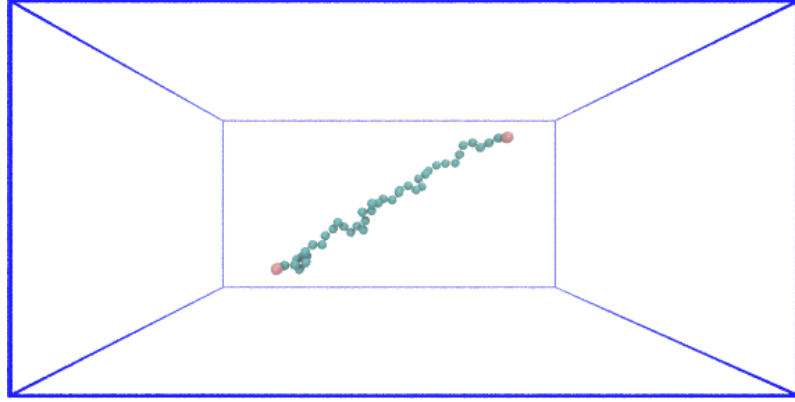
Figure 3.7: The end-to-end vector and the fraction of open, partially- and fully-reacted stickers as a function of time.

1.6 times the equilibrium end-to-end distance is experienced, followed by a sharp drop and eventually reaching an equilibrium value of approximately 1.5 times.

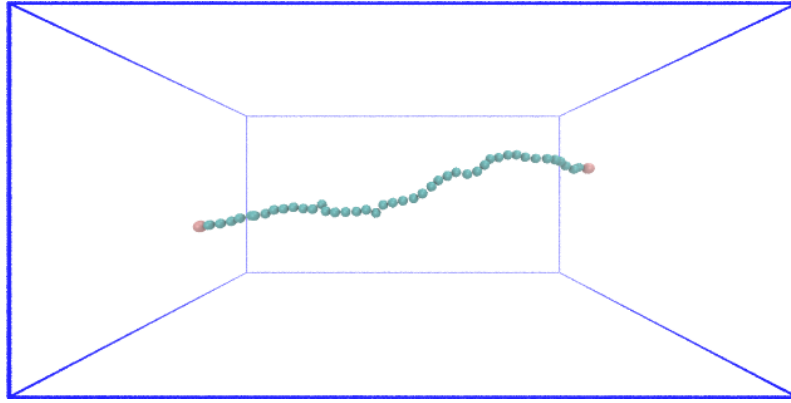
Stretching of chains can occur for shear rates higher than the reciprocal of the equilibrium sticky bond lifetime, τ_b . This stretching leads to shear hardening, as shown in Figure 3.6a.

We can examine the evolution of chains with time by considering chain conformations during key times: initial behaviour (A), overshoot (B) and the steady-state (C). The three regimes are labelled in terms of chain stretching in Figure 3.7a and Figure 3.8 shows the conformation of a single chain at these key times under shear flow with a deformation rate $\dot{\gamma} = 5 \times 10^{-3}/\tau_{LJ}$.

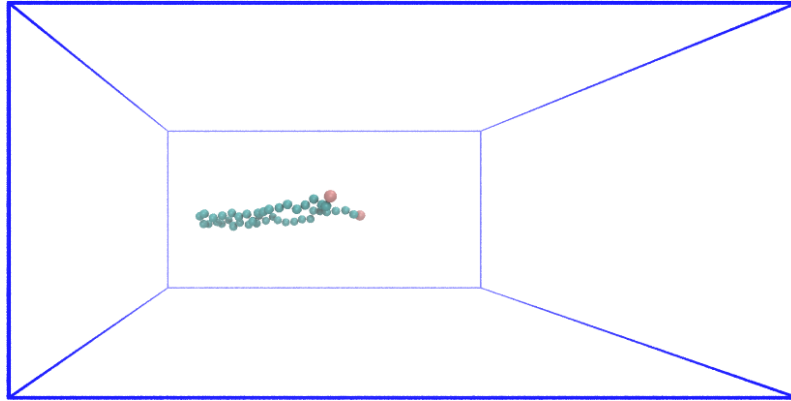
Initially when the deformation is applied, the chain begins to align in the direction of flow. Figure 3.8a shows the initial behaviour (A) taken at $t = 350\tau_{LJ}$. As the flow continues the chain starts to stretch which leads to a large overshoot (B) around $t = 2050\tau_{LJ}$, see Figure 3.8b. As the elastic energy due to stretching increases, so does the likelihood for the sticky bonds to break. Following a breaking event the stickers will quickly reattach to the network, but owing to the relatively high restoring force stored in the stretched chains they will be less likely to combine with their previous partners (which is reflected by the decrease in partner exchange time which will be seen in section 3.7.3). The chain conformation in the steady-state (C) at time $t = 14450\tau_{LJ}$ is shown in Figure 3.8c. In this snapshot the chain has folded back on itself, nearly forming a loop (an elastically ineffective structure). Under simple shear flow the magnitude of elongational and rotational components are equal. In this case it has been suggested polymers will not attain a stable strongly stretched state in steady shear. Instead the end-to-end vector tumbling of the molecules occurs as the stretched state is destabilized by the rotational component of shear flow. Evidence for polymer chain tumbling under shear has been provided by fascinating



(a) Initial transient behaviour $t = 350\tau_{LJ}$.



(b) Overshoot $t = 2050\tau_{LJ}$.



(c) Steady state $t = 14450\tau_{LJ}$

Figure 3.8: Evolution of a chain configuration (taken from a simulation of $N = 45$, $N_{ch} = 400$ and $\varepsilon = 10k_B T$) with shear rate $\dot{\gamma} = 5 \times 10^{-3}/\tau_{LJ}$.

experiments of single-chain polymer dynamics [127]. In the supramolecular system studied chains are attached to a transient network via chain ends which counters the rotational effects allowing for a far greater degree of stretching. The degree of shear hardening depends on how much stretching chains have experienced before they detach from the network. The increase in elastic energy due to chain stretching must remain below the association energy for the sticky bonds to persist.

Figure 3.7b shows how the fraction of open, partially- and fully-reacted stickers changes as a function of time. Initially the equilibrium system contains a large fraction of fully-reacted stickers, following the overshoot this decreases by approximately 20% with the majority of these stickers being converted to partially reacted stickers. As partially-reacted stickers denote the formation of long linear chains or network strands of length $2N$ or greater, each of these strands contributes only one $k_B T$ to the energy (regardless of length). This leads to an effective reduction in the number of active strands. These longer strands are also able to sustain a larger degree of stretching.

3.7.3 Steady state properties

Figure 3.9 shows the steady state viscosity under extensional and shear flow for either case (with or without stickers), we see no evidence for shear thickening in these systems, with only trivial shear thinning behaviour apparent. This shear thinning could be attributed to the reduction in the fraction of active strands as mentioned above. Figure 3.9 also highlights the huge increase in viscosity due to the introduction of stickers (up to two orders of magnitude at low deformation rates) in supramolecular networks from polymer melts.

We now consider some dynamic properties which show deformation rate depen-

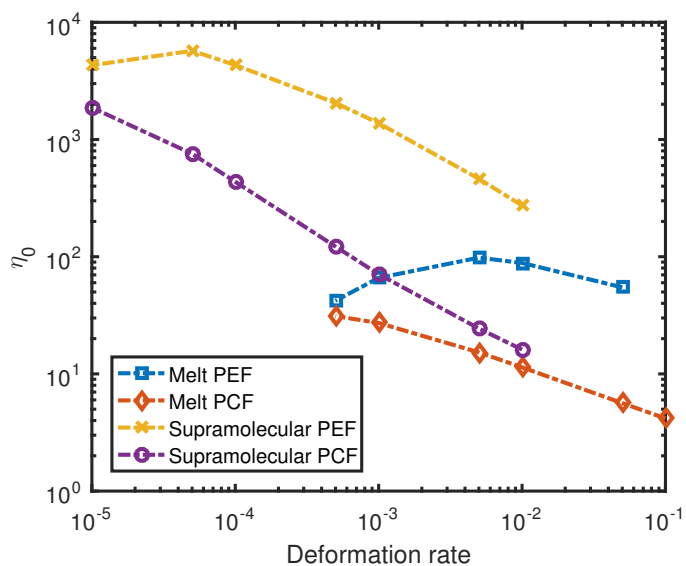


Figure 3.9: Comparison of steady state viscosity with and without stickers present.

dence. An example of one such characteristic in supramolecular polymer systems is the sticky bond lifetime, τ_b , and the partner exchange time, τ_{pe} . The change in these two timescales is presented as a function of deformation rate for both shear and extension flow in Figure 3.10c and Figure 3.10d in steady-state respectively. We observe a small change in the bond lifetime with deformation rate under shear flow. A much larger drop is seen under extension, but to compare these two results we should take into account the Trouton ratio. Specifically under extension the highest rates are equivalent to shear rates which are well above the reciprocal of the sticky bond lifetime, which explains this huge reduction in sticky bond lifetime. Under shear the partner exchange time declines by one order of magnitude for the rates considered while for the extension rates a reduction of almost three orders of magnitude is seen. Again the rates under extension are equivalent to much higher shear rates.

When the shear rate increases the polymer chains experience a greater degree of stretching before sticky bonds break. Following a breaking event the prior stretching

leads to a restoring force pulling the constituent stickers away from one another which causes a reduction in the number of recombination events needed before a sticker can forget its previous partners. This ultimately leads to a reduction in the partner exchange time such that $\tau_{pe} \rightarrow \tau_b$ as shear rate increases.

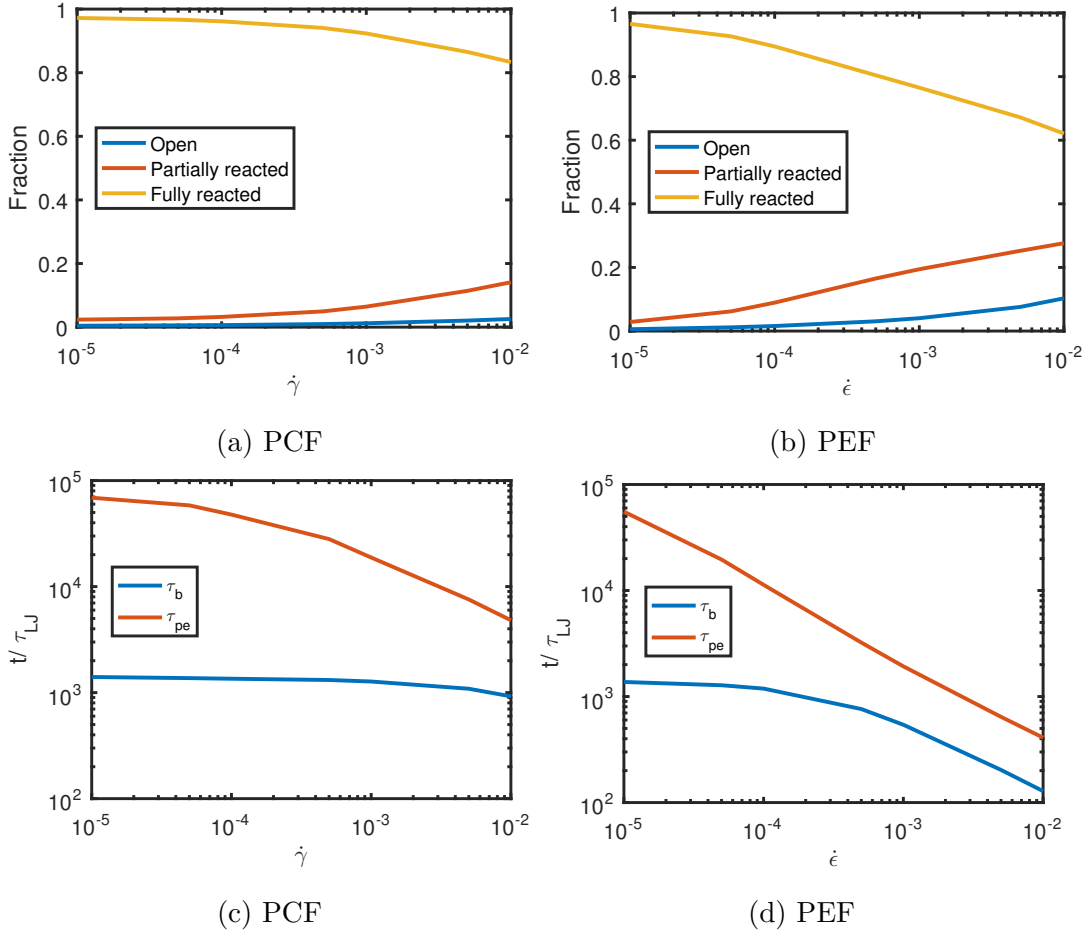


Figure 3.10: (a)-(b) The change in fraction of open, partially- and fully-reacted stickers as a function of deformation rate. (c)-(d) The change in bond lifetime and partner exchange time as a function of deformation rate.

One structural property which we can study is the fraction of open, partially- and fully-reacted stickers as a function of deformation rate, Figure 3.10a-b. Under shear as the deformation rate increases we see an almost 20% reduction in the fraction

of fully-reacted stickers, while a sizeable increase is seen in the number of partially-reacted stickers (15%), and a small increase in the fraction of open stickers (5%). Looking at the fraction of open, partially- and fully-reacted under planar extension, Figure 3.10b we see a much larger decrease of approximately 40% in the fraction of fully-reacted stickers, with an accompanying large increase in partially-reacted stickers.

3.8 Conclusions

We have studied the rheological properties of supramolecular polymers under both shear and extensional flow. The formation of a transient network leads to a large increase in viscosity. In comparison with the polymer melt counterpart we find shear hardening behaviour at higher deformation rates (namely where $\dot{\gamma} > 1/\tau_b$) in the start-up of flow which we conclude is caused by the non-Gaussian stretching of network strands. By studying the change in the end-to-end distance as a function of time we find chains stretch up to 1.6 times their equilibrium length. In the system studied we find no evidence of shear thickening in the steady-state viscosity either via chain stretching or structure formation. In fact the fraction of fully-reacted stickers is reduced by over 20% under shear and nearly 40% under extension. The majority of these fully-reacted stickers are converted to partially-reacted stickers following the stress overshoot. The increased number of partially reacted stickers is indicative of associated linear chains or strands and will cause a reduction in the overall viscosity due to a decrease in number of effectively active strands.

From our equilibrium simulations the small fraction of open or partially-reacted stickers found at higher bonding energies suggests little structure formation is possible. In both experiments and theory the most commonly proposed mechanism for

shear thickening is the conversion of dangling chains to active chains.

The average bond lifetime and partner exchange time are both found to decrease with higher deformation rates. These rate dependent changes are thought to result from the presence of stretching at faster deformation rates which increases the probability for sticky bonds to break. This effect is more pronounced under extensional flow.

Chapter 4

Extensional rheology of entangled polymer melts

4.1 Introduction

In this chapter we carry out molecular dynamics simulations of entangled monodisperse linear chains under planar extension. In order to model systems with multiple entanglements we develop a GPU based simulation protocol to efficiently simulate these large systems. The chain length is chosen to allow for comparison with results obtained from the uniaxial extensional rheology experiments of Nielsen *et al.* [128].

The most successful model for studying entangled polymers is the Doi-Edwards (DE) tube model (section 1.4.5). In this model the effects of topological constraints due to neighbouring chains can be approximated using a mean field tube representation. For start-up planar extension, the deformation tensor $\mathbf{E}(t, t')$ in the DE tube

model is given by

$$\mathbf{E}(t, t') = \begin{pmatrix} \lambda_{t,t'} & 0 & 0 \\ 0 & \lambda_{t,t'}^{-1} & 0 \\ 0 & 0 & 1 \end{pmatrix}$$

where $\lambda_{t,t'} = \exp(\dot{\epsilon}(t)(t - t'))$ and

$$\dot{\epsilon}(t) = \begin{cases} 0 & \text{if } t < 0 \\ \dot{\epsilon} & \text{if } t \geq 0 \end{cases}$$

Therefore, the transient viscosity for some extension rate $\dot{\epsilon}$ can be calculated using eq. 1.9 which makes use of the independent alignment approximation

$$\eta(t) = \frac{G_e}{4\dot{\epsilon}} \int_{-\infty}^t \psi(t - t') [\mathbf{Q}_{xx}^{IA}(\mathbf{E}(t, t')) - \mathbf{Q}_{yy}^{IA}(\mathbf{E}(t, t'))] dt' \quad (4.1)$$

where

$$\begin{aligned} \mathbf{Q}_{xx}^{IA}(\mathbf{E}(t, t')) - \mathbf{Q}_{yy}^{IA}(\mathbf{E}(t, t')) = \\ \frac{1}{4\pi} \int_0^{2\pi} \int_0^\pi \frac{\lambda_{t,t'}^2 \cos^2 \theta \sin \theta - \lambda_{t,t'}^{-2} \sin^3 \theta \cos^2 \phi}{\lambda_{t,t'}^2 \cos^2 \theta + \lambda_{t,t'}^{-2} \sin^2 \theta \cos^2 \phi + \sin^2 \theta \sin^2 \phi} d\theta d\phi. \end{aligned}$$

We solve this integral equation numerically using MATLAB for comparison with results obtained in our molecular dynamics simulations.

In recent uniaxial extension experiments, Bach *et al.* [129] found that for extension rates greater than the reciprocal of entanglement time, τ_e , the steady state extensional viscosity follows the scaling law $\eta \sim (\dot{\epsilon}\tau_d)^{-1/2}$. These experimental results indicate a failure of the DE tube theory when considering chains under uniaxial extension. For extension rates greater than the reciprocal of entanglement time, τ_e , the model predicts a scaling of the form $\eta \sim (\dot{\epsilon}\tau_d)^{-1}$. Consequently the DE tube theory fails to describe the extensional thickening behaviour which has been seen in many experiments [115, 128].

Further developments of tube theory have sought to include a strain-dependent tube diameter [130] where polymer chains stretch because of an increasing restriction of lateral motion due to deformation. This affine chain stretch was found to quantitatively describe the onset of strain hardening but gives no information about the steady state (an appropriate bound for the strain hardening was not determined). Marrucci *et al.* [131] found that this can be remedied by accounting for the confinement pressure exerted by chains trapped within tubes (increases in radial pressure balance the tube diameter reduction). This idea was later incorporated into a constitutive model by Wagner and colleagues [132] through the introduction of a new chain-length dependent function, the tube diameter relaxation time. This was shown to provide good agreement with experimental results.

The experiments of Nielsen *et al.* [128] provide transient viscosity results for uniaxial extension of monodisperse polystyrene obtained using a filament stretching rheometer. We compare the extensional thickening behaviour observed in these experiments with our simulations of planar extension using the method described in Chapter 3.

The difference between results from the various types of extensional flows has been poorly studied. However, Meissner *et al.* [133] have found that for equivalent deformation rates $\dot{\epsilon}$ the steady-state stress values are ordered as follows

$$\sigma_{uniaxial} > \sigma_{planar} > \sigma_{equibiaxial}.$$

This ordering is also supported by the experiments of Wagner *et al.* [115] who calculate the transient extensional viscosity of long-chain branched polyolefin melts under three types of flow: uniaxial, equibiaxial and planar. In addition, comparisons of the transient viscosity in the DE tube theory with experimental results were presented in the same work, showing the absence of strain hardening in the theory.

4.2 System mapping and linear viscosity

To simulate these entangled polymer systems we must first determine the lengths of the bead-spring chains to be used in order to appropriately model the polymers studied in these experiments. Secondly, we need to map the time-scale used in our coarse grained MD simulations for comparison with experiments.

In the experiments of Nielsen *et al.* [128] the monodisperse linear polystyrenes have molecular weights, $Mw = 52kg/mole$, $103kg/mole$ and $200kg/mole$. Polystyrene has an entanglement molecular weight of $M_e^{exp} = 13.3kg/mole$ [134], therefore, the mapping coefficient between polystyrene molecular weight in the experiments and the number of beads in the simulations is

$$\frac{M_e^{exp}}{N_e} = \frac{13.3}{60} = 0.2217kg/mole$$

where we have taken the entanglement length $N_e \sim 60$ for the Kremer-Grest bead-spring model [135, 136]. The mapping coefficient tells us that in order to match the number of entanglements in experiments we need to simulate chains of length $N = 235, 465$ and 902 , respectively. Due to the high computational cost we only consider the shortest polymer chain which represents a molecular weight of $Mw = 52kg/mole$ (or $N = 235$) which we will refer to as PS50K.

In order to map the time-scales used in experiments we must compute the viscosity in the linear regime. As we are considering relatively long chains this becomes computationally expensive for standard CPU based simulations. For this reason we make use of HOOMD-blue, a MD simulation package from the University of Michigan which can be used to run MD simulations on NVIDIA CUDA powered GPUs. This is used in conjunction with the in-house simulation code (the generic polymer simulator) for analysing particle trajectories. Since the stress relaxation function is usually very noisy and so expensive to calculate we instead use the orientation

relaxation function which has been shown in experiments to be proportional to the stress relaxation function. This property is known as the stress-optical law. The orientation relaxation function is given by

$$S(t) = \frac{N}{k_B T} \left\langle \frac{1}{N^2} \sum_{j=1}^{N_{ch}} O_j^{\alpha\beta}(t) \sum_{j=1}^{N_{ch}} O_j^{\alpha\beta}(0) \right\rangle \quad (4.2)$$

where

$$O_j^{\alpha\beta}(t) = \sum_{i=1}^{N-1} \mathbf{u}_{ij}^\alpha(t) \mathbf{u}_{ij}^\beta(t)$$

is the orientation tensor of the chain j and $\mathbf{u}_{ij} = \frac{\mathbf{R}_{i+1,j} - \mathbf{R}_{i,j}}{|\mathbf{R}_{i+1,j} - \mathbf{R}_{i,j}|}$ is the unit bond vector. The stress relaxation function can then be approximated as

$$G(t) = \frac{1}{\beta} S(t)$$

where the constant $\beta = 0.0886$ has been found to collapse the stress and orientation relaxation functions for linear polymer melts represented by the Kremer-Grest model [137]. In this work we use the orientation relaxation function for a single chain (averaged over all chains in a system) to approximate the orientation tensor for the whole system, eq. 4.2, without calculating the cross-correlation contributions. The orientation tensor is given by

$$S(t) = \frac{A(t)}{1 - \kappa(t)}$$

where $A(t)$ is the averaged orientation relaxation function for a single chain. The coupling parameter $\kappa(t)$ was determined by Cao [138] as

$$\kappa(t) = 0.265 + 0.113 \log_{10}(t) - 0.0101 \log_{10}(t^2).$$

The quality of this approximation is shown in Figure 4.1 and is compared with the stress relaxation function, $G(t)$, calculated in a CPU MD simulation running on 8 processors. This approach gives us an accurate approximation for the stress

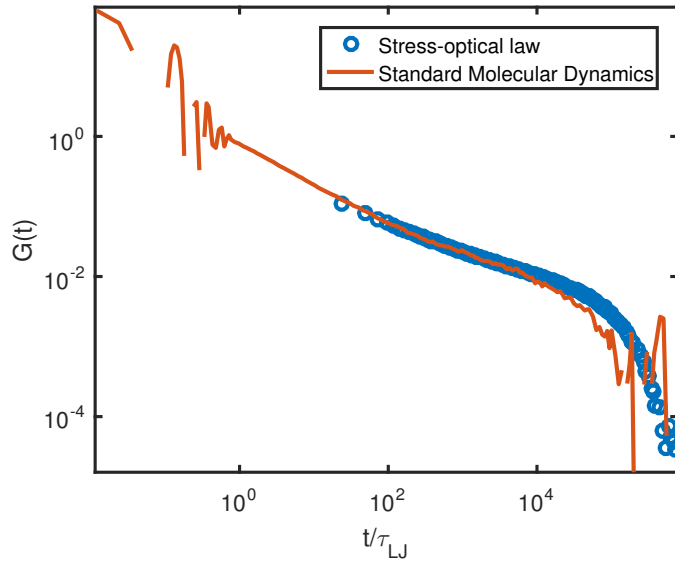


Figure 4.1: Application of the orientation relaxation function to approximate the stress relaxation function following the stress-optical law.

relaxation function when time $t > 100\tau_{LJ}$. The standard CPU MD simulation has been running for over two weeks but still has rather poor statistics at longer times, while via the HOOMD approach using the stress-optical law we have been able to obtain a usable form of the stress relaxation function in a few days. We then determine the Maxwell modes of the stress relaxation function using RepTate [125], which provides us the loss and storage moduli for comparison with those obtained in experiments. As the orientation correlation function only provides an accurate estimate for $t > 100\tau_{LJ}$ the moduli determined for high frequencies are also inaccurate. This allows us to determine the time shift factor required to map molecular dynamics simulation time scales to those in experiments, see Figure 4.2. For $N = 235$ we find a shift factor of 2.05×10^4 in the x-direction when compared with the PS50K data. As we are comparing two different types of flow, namely the experimental uniaxial extension results of Hassager *et al.* [128] with simulations of planar extension, we do not attempt to map the deformation rates directly and instead consider a range

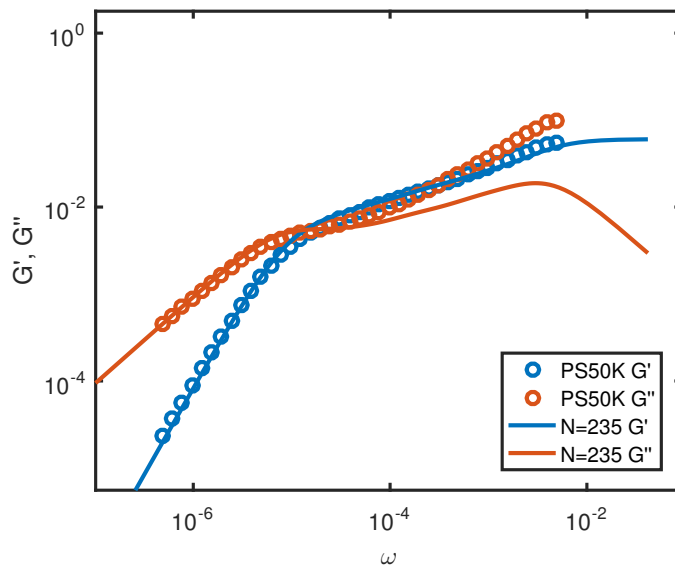


Figure 4.2: Mapping of MD simulations using $N = 235$ using an approximation of the stress relaxation function derived via the stress-optical law to the experimental PS50K data. The time shift factor used in the mapping is 2.05×10^4 .

of Deborah numbers, where the Deborah number is a dimensionless number given by $De = \dot{\epsilon}\tau_d$ which is used in rheology to characterise flow behaviour. If we recall $\dot{\epsilon} = 1/\tau$ where τ is the characteristic time-scale of the flow, then the Deborah number describes the degree to which the elastic (if $\tau \ll \tau_d$) or viscous effects dominate (if $\tau \gg \tau_d$).

For chain lengths far above entanglement lengths we are unable to efficiently probe the transient viscosity using our CPU based simulation protocol (as was used in section 3). For this reason we implement a GPU accelerated version which calculates the transient stress tensor in a far more efficient way.

4.3 GPU simulations

4.3.1 Motivation

In recent years the capabilities of GPUs have been widely used in scientific computing. Generally these devices are designed for an astonishing number of floating point operations per second (FLOPS). The most costly part of a molecular dynamics simulation is calculation of the forces. Thankfully this is an operation which can be effectively computed in parallel with little overhead.

While a number of molecular dynamics packages already exist which take advantage of these devices (*e.g.* LAMMPS, HOOMD-blue), we instead choose to write our own in order to simulate systems using the KR planar extension boundary conditions [123]. This implementation is written using NVIDIA CUDA and will run on NVIDIA K10 GPU accelerators. Each K10 consists of two devices which together are capable of 4.58 trillion FLOPS.

4.3.2 Hardware

Before we go into details regarding our implementation, it's worth reviewing some of the hardware details in NVIDIA GPUs as these will help guide the programming design choices.

Each GPU device contains a specialised processor and its own RAM. The device is connected to a CPU host which again contains a processor and RAM. GPUs are regarded as secondary computation devices: functions known as kernels can be executed on the GPU, but a function running on the GPU can not execute another

kernel, therefore, the CPU must guide the computation. There is a large overhead associated with the transfer of data to and from the device so generally the system is initialized and copied from the host to the device at start-up and subsequently results are intermittently (when we wish to save them) copied from the device to the host.

One device in a K10 GPU accelerator contains a processor with 8 streaming multiprocessors each with 192 cores for arithmetic operations. The most basic unit of computation on a NVIDIA GPU is known as a thread. Each streaming multiprocessor will schedule 32 threads into a group known as a warp and 64 warps are scheduled per streaming multiprocessor at a time. In total four warps can be executed concurrently on a single streaming multiprocessor, therefore, 1024 threads can run at one time on a device.

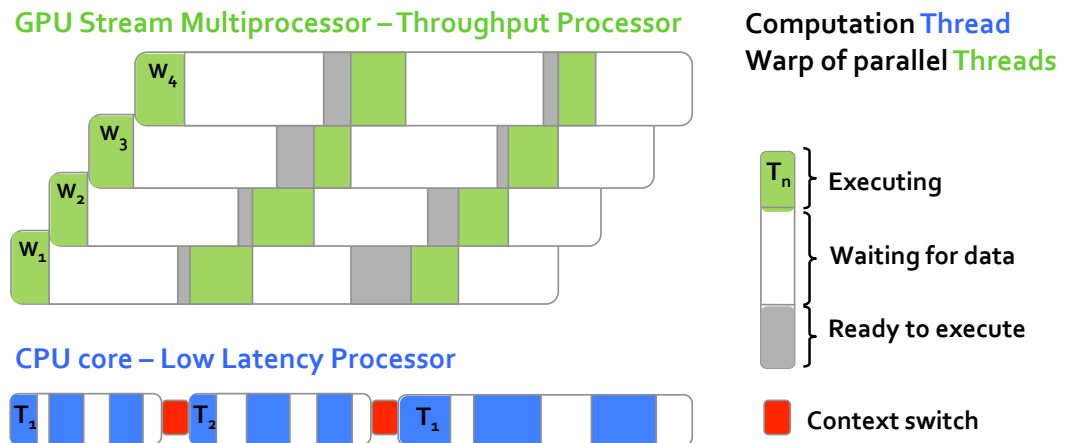


Figure 4.3: Illustration highlighting the difference in execution between GPUs and CPUs. This picture was adapted from a talk presented by James Balfour.

GPUs and CPUs are two fundamentally different approaches to computing, on CPUs a large L1 cache is used to hide latency, while on GPUs the large number

of concurrent threads is leveraged to hide latency. This difference is illustrated in Figure 4.3. The large number of concurrent threads allow for constant execution when viewed across threads (hiding the latency of slow memory reads). To improve GPU memory reads there are a few types of available memory on the device which can be used for specific purposes. The most basic is the global memory which is direct use of the device memory. The second is known as constant memory which resides in device memory but with a cache to speed up reads. This kind of memory will not change over the course of a kernel execution. The third is texture memory which is effectively global memory but with an associated cache for speeding up reads. Texture memory is optimized for spatial locality (and can be used to optimize random reads). Finally, each streaming multiprocessor has a small amount of shared memory which resides on the processor (*i.e.* is very fast) and can be used by resident threads. This can be used for inter-thread communication or as another cache.

4.3.3 Implementation

General considerations

All computations are performed on the GPU with initial particle positions and velocities copied to device memory on start-up. Where possible each computation is carried out as one particle per thread (in the hope of minimising the amount of memory reads per thread while giving each thread enough work).

The implementation of the equations of motion is unchanged from the CPU simulation (we use the Gear-predictor corrector algorithm described in section 1.7.3). This is used in conjunction with a cell list and neighbour list for working out non-bonded interactions. The size of cells in the x -direction needs to be multiplied by

$\sqrt{10}$ in order to ensure all interacting particles in this direction are contained within adjacent cells [139]. When calculating bonded and non-bonded forces the array of particle positions is bound to a texture in order to take advantage of the cache. This cache is designed to speed up spatially local reads, therefore, we can make use of a space filling curve as was first proposed by Anderson *et al.* [140] to order the particle array to increase the cache hit rate. Space filling curves allow one to represent ND data in $1D$ but still preserving spatial locality (e.g. particles close to one another in $3D$ will be remain close in the $1D$ representation). For simplicity

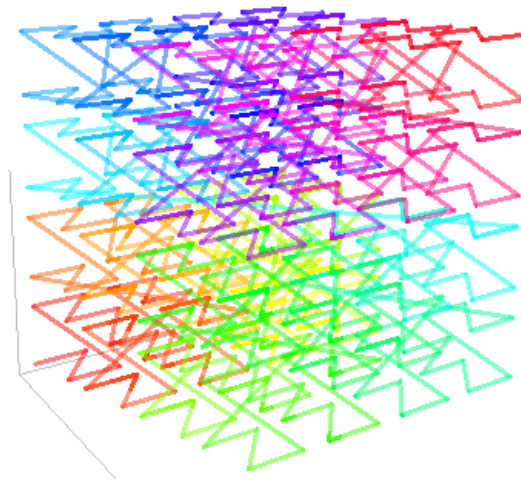


Figure 4.4: Illustration showing Z-order curve iterations in $3D$. This image was created using Mathematica by Robert Dickau (2008).

and speed we opt to do this via a 3D Z-order curve, an illustration of the ordering is shown in Fig 4.4. The Z-order curve is described in terms of Morton codes [141]. The code for a given particle is generated when the system is aligned to the x -axis. Each position has its coordinate normalized such that $r_i \in [0, 1]$ where $i = x, y, z$. Then the Morton code for a point is generated by expanding the binary fixed-point representation of a coordinate by inserting two “gaps” after each bit. Next the bits

of all three coordinates are interleaved to form a single binary number.

Upon sorting these Morton codes an order of the particles will be obtained in terms of the Z-order space filling curve. The Morton codes are sorted using the NVIDIA thrust library. The particles are then reordered in terms of these ordered Morton codes. This is done every one hundred time-steps, where the choice of frequency is a compromise between the added overhead of reordering particles and the speed up due to an improved number of texture cache hits. This approach provides an approximately 10-15% increase in overall performance (with a more substantial speed up for larger systems).

Floating point precision

In the most commonly available GPU devices floating point operations greatly outperform double precision operations. This gives rise to concerns regarding the accuracy of GPU based simulations. The most important problem with floating point arithmetic is that summation is not associative, therefore, the order in which values are summed can lead to differences. For this reason a number of methods for compensated sums exist e.g. Kahan summation [142].

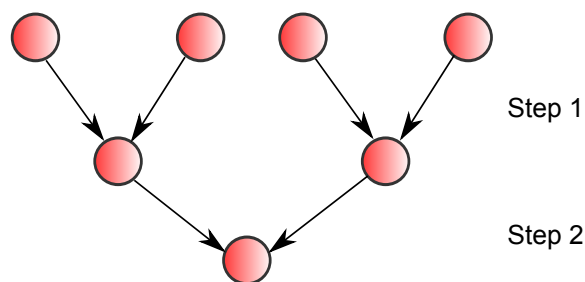


Figure 4.5: The steps of a parallel reduction operation on four elements.

A common approach to reduce the error in accumulation is to sum components

of similar sizes. Thankfully this is exactly what is done when carrying out a summation via a parallel reduction (as is the preferred method for carrying out pairwise operations on GPU hardware). An illustration of this process is shown in Figure 4.5. In a reduction, elements are reduced pairwise on a single thread with each step operating on a pair generated from the previous step (or the initial values).

The most notable accumulation problem in our simulations occurs in the calculation of transient stress. For accuracy this is calculated using logarithmic binning. That is given some quantity $A(t)$ we wish to calculate, the time intervals are defined such that $t_0 = D$ and $t_i = DM^i$ where i is an integer greater than zero. The constant D is the initial time and M is a multiplication factor. In our simulations $D = \delta t$ is taken as the starting time and $M = 1.1$. Then the average at some time interval $t_i \rightarrow t_{i+1}$ of the quantity $A(t)$ is given by

$$A(t_i) = \frac{1}{t_{i+1} - t_i} \int_{t_i}^{t_{i+1}} A(t') dt'.$$

The interval size which is averaged over grows as the simulation progresses. The transient stress tensor is thus given by

$$\sigma_{\alpha\beta}(t_i) = \frac{1}{t_{i+1} - t_i} \int_{t_i}^{t_{i+1}} \sigma_{\alpha\beta}(t') dt'.$$

Each integral is calculated discretely as a summation. If the running total is stored as a floating point it will eventually fail, because as the simulation progresses the time interval grows substantially. Eventually adding values which are significantly smaller than the running total will no longer have any affect on the stored value. This can be fixed simply by making use of a double for storing the running sum which is calculated via a reduction each time step (this small change equates to only seven double precision operations every time-step) without affecting the overall simulation speed.

The only other quantity which is summed over all particles per time-step is the Gaussian multiplier as this plays a crucial role in maintaining stability within the simulation. We go one step further to improve accuracy and use a double-single precision approach *i.e.* two floating points are used to store a more accurate representation of a variable. Double-single precision floating point numbers have been used more extensively in the study of glassy dynamics via the molecular dynamics simulations [143].

4.4 Results

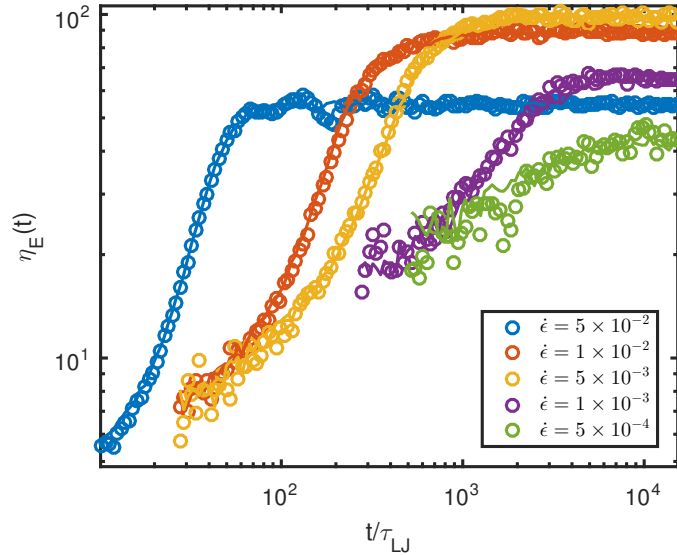


Figure 4.6: Comparison of transient viscosity results obtained from GPU (symbols) and CPU (lines) simulations.

Firstly to test our implementation we simulate a polymer melt system with chain length $N = 45$, time step $\delta t = 0.004\tau_{LJ}$ and $N_{ch} = 400$. The transient viscosity is calculated using eq. 3.4. Figure 4.6 shows these test results which are compared with those obtained from our CPU implementation in section 3. The GPU results

are denoted by symbols and the CPU results are shown as lines. We find very good agreement between the two implementations. For this system our GPU code achieves approximately 820 time steps per second. The comparable CPU based code manages approximately 60-80 time steps per second on a single CPU (an Intel Core i5). A performance increase of over 10 times. However, as mentioned previously the slowest part of a GPU simulation is reading from global memory, therefore, our choice of the Gear predictor-corrector algorithm which uses a staggering eighteen variables per particle for storage of the velocity, position and their derivatives plays a large role in reducing the performance. Even so the GPU version dramatically outperforms our CPU implementation with simulations which could take months being completed in a number of days.

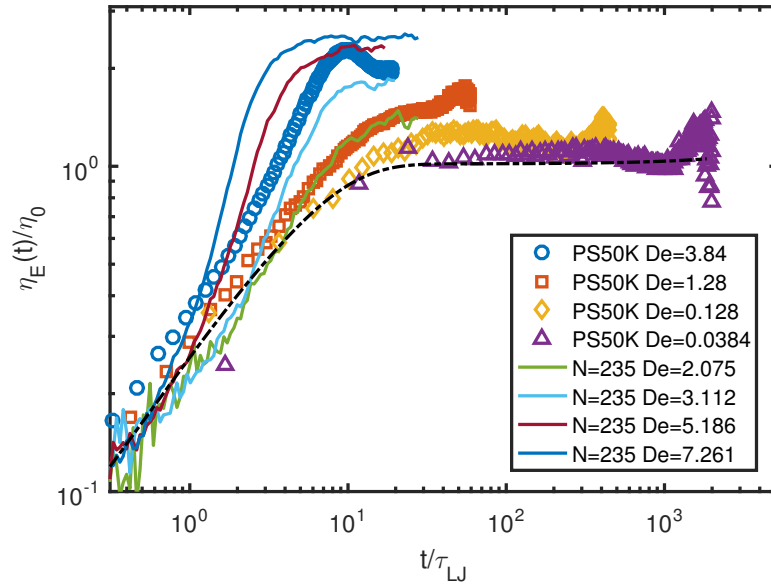


Figure 4.7: Comparison of transient viscosity results obtained from GPU simulations of planar extension of $N = 235$ and experiments of uniaxial extension of PS50K.

We now consider simulation results for chains of length $N = 235$. These chains possess the same number of entanglements as PS50K. Each simulation box con-

tains $N_{ch} = 150$ chains and the results are averaged over two statistically independent runs. The time-step used in these simulations is $\delta t = 0.005\tau_{LJ}$. These non-equilibrium simulations are started using saved configurations from an equilibrium simulation carried out using HOOMD-blue (which has run for approximately $104\tau_d$). The experimental results correspond to extension rates $\dot{\epsilon} = 0.3s^{-1}, 0.1s^{-1}, 0.01s^{-1}$ and $0.003s^{-1}$. The terminal relaxation time of PS50K is $\tau_d = 12.8s$ which has been determined from linear rheology experiments.

Figure 4.7 shows results for Deborah rates $0 < De < 10$ alongside the experimental results. The time scales for simulation results have been scaled appropriately using the time shift factor determined previously and the viscosities, η , have been normalised by the steady state viscosity from the linear regime (shown by the dashed curve). We find that for small Deborah numbers we have reached the limiting steady-state viscosity η_0 .

The similarity between the linear rheology curve and the slowest rate in experiments $\epsilon = 0.003s^{-1}$ or $De = 0.00384$ demonstrates the validity of this mapping. The results show qualitatively similar behaviour with the slowest rates following the linear viscosity curve. For intermediate rates $1 < De < 10$ the steady state extensional viscosity rises above η_0 . In simulations the maximum steady-state viscosity seen is approximately $2.5\eta_0$ for a Deborah number of $De = 7.261$. The experimental results show a maximum of $2\eta_0$ at a Deborah number of $De = 3.84$ which represents the highest rate that can be tested for this material due to an upper limit on extension rate to avoid dissipative heating in the filament stretching rheometer. In contrast molecular dynamics simulations of smaller Deborah numbers (or slower extension rates) are problematic as these lead to a larger degree of error as seen in Figure 4.6 and take considerably longer to reach steady state. A comparison of the steady state viscosities, $\bar{\eta}$, for various Deborah numbers is shown in Figure 4.8. In our simula-

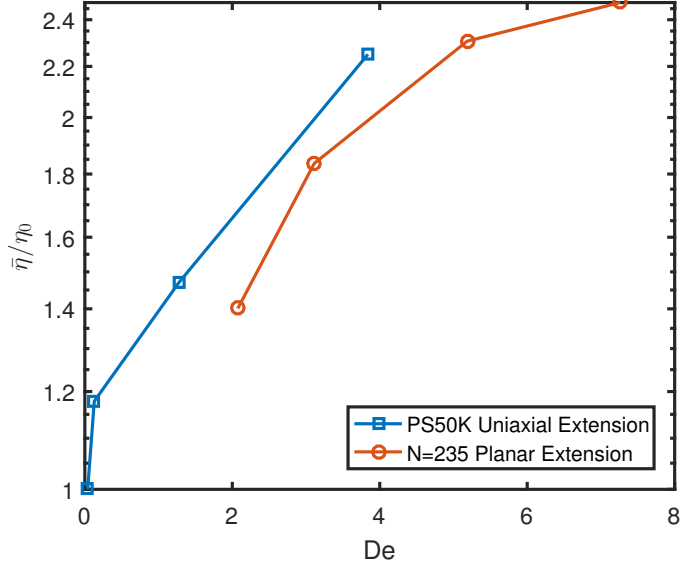


Figure 4.8: Comparison of steady state viscosity results obtained from GPU simulations of planar extension of polymer melts with chain length $N = 235$ and experiments of uniaxial extension of PS50K.

tions of planar extension we observe analogous extensional thickening to that seen in experiments of uniaxial extension but at higher Deborah numbers. When using the same deformation rate, the steady-state viscosity obtained in uniaxial extension is found to be higher than that in planar extension, which is in agreement with the observations of Meissner *et al.* [133].

We now consider the scaling behaviour for extension rates greater than the reciprocal of entanglement time, τ_e . In the experiments of Bach *et al.* [129] the steady state extensional viscosity was found to follow the scaling law $\eta \sim (\dot{\epsilon}\tau_d)^{-1/2}$. In order to see how this scaling differs under planar extension we must run a number of high extension rates. The transient viscosity curves obtained from these simulations are shown in Figure 4.9. Figure 4.10 compares the steady state viscosities, $\bar{\eta}$, with predictions from the DE tube model obtained by numerically solving eq. 4.1. As

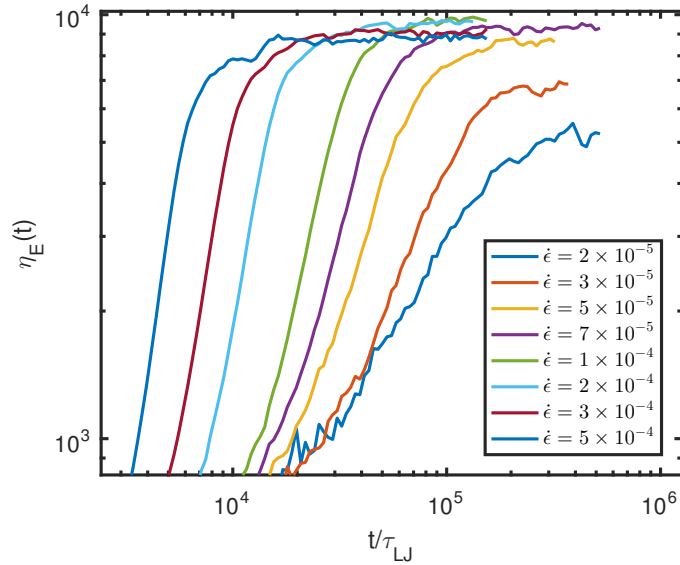


Figure 4.9: Transient viscosity for a large number of extension rates with $N = 235$.

expected the DE tube theory does not predict the extensional thickening behaviour. Due to the limited number of simulation results for extension rates greater than the reciprocal of entanglement time we are unable to draw any concrete conclusions regarding the scaling behaviour at this stage. Using our current simulation protocol we are unable to test higher extension rates. In experiments one surface of the sample is often in contact with the atmosphere which maintains the sample in an Isothermal-isobaric or NpT (constant pressure) ensemble. In molecular dynamics simulations it is customary to use a canonical or NVT (constant volume) ensemble as is the case in all simulations carried out in this thesis. Federico and Todd [144] have shown that using a canonical ensemble at very high extension rates in simulations leads to large deviations in results compared with an Isothermal-isobaric ensemble.

By considering a larger number of extension rates for $N = 235$ we find the maximum viscosity at approximately $De = 10.373$, where it reaches $2.585\eta_0$. The value of η_0 has been calculated accounting for the Trouton ratio.

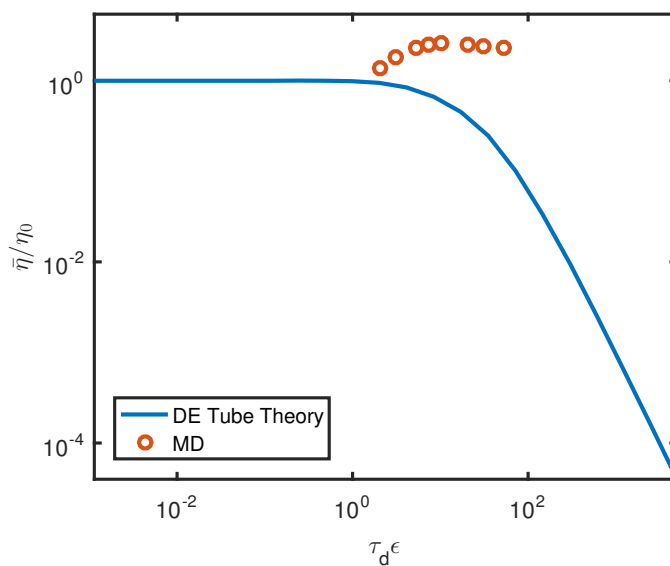


Figure 4.10: Comparison of steady state viscosities, $\bar{\eta}$, for a number of extension rates, $\dot{\epsilon}$, between molecular dynamics simulations and the Doi-Edwards tube theory.

4.5 Conclusions

We have simulated mildly entangled polymer chains under planar extensional flow. This has been proved to be computationally expensive for CPU simulations, so we opt to write new code which takes advantage of the promising performance benefits shown by GPUs in scientific computing. This approach leads to huge performance gains, and we find the results produced using floating point precision in good agreement with simulations carried out on CPUs which use double precision. By modelling polymer chains with the same number of entanglements as PS50K we find an increase in the magnitude of the steady-state viscosity which is comparable with the increase shown by Nielsen and coworkers [128]. We find for low extension rates the viscosity curves and linear viscosity curve superimpose. As the extension rate increases the extensional viscosity rises above the linear viscosity curve (extensional thickening), demonstrating behaviour consistent with experimental observations but

not predicted by the DE tube theory.

For reaching the same extensional viscosities the extension rates required in our planar extension simulations are higher than those used in the uniaxial extension experiments. We are unable to determine how the steady state viscosity scales with Deborah number for extension rates higher than the reciprocal of entanglement time for the chain length studied in this chapter but the GPU method developed here for simulating these systems can readily be applied to longer chain lengths to test this scaling.

Chapter 5

Conclusions

5.1 Conclusions

In this thesis we discussed three main topics: the dynamic behaviour of supramolecular polymer melts, non-linear rheology of supramolecular polymer melts and the extensional rheology of entangled linear polymer melts.

We first present hybrid molecular dynamics/Monte Carlo simulations of supramolecular networks formed by unentangled telechelic chains with sticky end monomers (or stickers). The functionality of the stickers is chosen to be $f = 3$, meaning that each sticker can maximally associate with two other stickers. This is the minimum functionality required for percolated network formation, but allows us to study supramolecular polymer networks that are cross-linked by reversible sticker clusters or micellar cores with well defined size distributions.

We investigated the kinetics of sticker association, the topological structure and the resulting dynamic and rheological behavior of the supramolecular systems as a

function of the sticker bonding energy and the parent polymer chain length. Our simulations revealed that the sol-gel transition occurs at a critical sticky bonding energy around $4.3k_B T$ when the fraction of reacted stickers overtakes that of the open stickers. At sufficiently high bonding energies ($\geq 10k_B T$), the majority of the stickers are fully reacted and less than one percent of stickers remain open. We developed a chain shrinking algorithm to detect the proportion of elastically inefficient strands and found that in the strongly associated supramolecular networks this is less than 5%.

The dynamic and rheological behavior of the strongly associated supramolecular networks were shown to be dominated by a partner exchange mechanism in which the stickers exchange their associated partners, and so release the imposed topological constraints, through the disassociation-association processes of the sticker clusters. This is in contrast to the traditional picture of single sticker hopping where a sticker needs to first pull out of a cluster by breaking all existing sticky bonds, which is energetically unfavourable. Our study indicates that the system can relax without waiting for the chain ends to completely disassociate from the network. We found the presence of large sticker clusters can actually increase the rate at which chains relax.

Two new characteristic time scales, namely the partner exchange time and cluster exchange time are introduced to measure the dynamics of supramolecular networks formed at high sticky bonding energies. These time scales are up to two orders of magnitude larger than the average sticky bond lifetime. Three distinctive regimes can be identified in the stress and end-to-end vector relaxation functions, i. e., an initial Rouse regime, an intermediate rubbery or plateau regime and a terminal relaxation regime. A phantom chain hopping model is proposed based on the microscopic picture of sticker partner exchange process. Numerical predictions of

this model on the sticker mean square displacements and chain end-to-end vector correlation functions are in reasonably good agreement with the hybrid MD/MC simulation results.

These supramolecular networks were then studied under both shear and planar extensional flows. We found the transient networks formed at high bonding energy results in a large increase in viscosity when compared with polymer melts. At deformation rates larger than the reciprocal of the bond lifetime, the sticky bonds do not have enough time to disassociate by thermal fluctuations, the parent polymer chains experience non-Gaussian stretching during the start-up flow, leading to strain hardening. We find chains stretch up to 1.6 times their equilibrium length. During the deformation a change in structure is observed with an overall reduction in the number of fully reacted stickers (between 20 – 40% depending on the type of deformation). This structural change leads to an overall reduction in the number of active strands and therefore results in shear thinning behaviour in steady-state. In these simulations a decrease in both bond lifetime and partner exchange time is seen with increasing shear rate.

Finally, we carried out planar extension simulations of mildly entangled polymer chains. In order to model these systems efficiently using molecular dynamics we developed a GPU based simulation method which was found to be approximately 10 times faster than a CPU approach. The chain length modelled was chosen to allow for comparison with data from uniaxial extension experiments. At low extension rates the viscosity differ from the linear viscosity curve by only the Trouton ratio. But when the extension rate increases extensional thickening was observed. For completeness these results were compared with the Doi-Edwards tube theory which predicts an absence of thickening behaviour. The increase in the steady-state viscosity above the linear viscosity curve were comparable with the experimental

results.

5.2 Future Work

Use the hybrid MD/MC simulation method to study various supramolecular systems, such as binary association systems and networks formed by bridged micellar cores both in equilibrium and under flows. Examine correspondence with existing and if needed develop, new theoretical models on supramolecular polymers.

Perform more detailed analysis of the entangled polymers under extensional flow, comparing simulation results with experimental measurements and theoretical predictions [145, 146] for achieving a better microscopic understanding of non-linear rheology of entangled polymers.

Bibliography

- [1] Wayne Hayes and Barnaby W Greenland, editors. *Healable Polymer Systems*. RSC Polymer Chemistry Series. The Royal Society of Chemistry, 2013.
- [2] Marek W. Urban. *Self-Healing Polymers. From Principles to Applications*. Edited by Wolfgang H. Binder., volume 53. WILEY-VCH Verlag, 2014.
- [3] Tom F. A. de Greef and E. W. Meijer. Materials Science - Supramolecular Polymers. *Nature*, 453(7192):171–173, MAY 8 2008.
- [4] Sebastian Seiffert and Joris Sprakel. Physical chemistry of supramolecular polymer networks. *Chem. Soc. Rev.*, 41:909–930, 2012.
- [5] Michael J. Serpe and Stephen L. Craig. Physical organic chemistry of supramolecular Polymers. *Langmuir*, 23(4):1626–1634, FEB 13 2007.
- [6] Jay A. Syrett, C. Remzi Becer, and David M. Haddleton. Self-healing and self-mendable polymers. *Polym. Chem.*, 1:978–987, 2010.
- [7] Philippe Cordier, François Tournilhac, Corinne Soulié-Ziakovic, and Ludwik Leibler. Self-healing and thermoreversible rubber from supramolecular assembly. *Nature*, 451(7181):977–980, 2008.
- [8] RP Sijbesma, FH Beijer, L Brunsveld, BJB Folmer, JHKK Hirschberg, RFM Lange, JKL Lowe, and EW Meijer. Reversible Polymers formed from

- self-complementary monomers using quadruple hydrogen bonding. *Science*, 278(5343):1601–1604, NOV 28 1997.
- [9] Jean-Luc Wietor, D. J. M. van Beek, Gerrit W. Peters, Eduardo Mendes, and Rint P. Sijbesmat. Effects of Branching and Crystallization on Rheology of Polycaprolactone Supramolecular Polymers with Ureidopyrimidinone End Groups. *Macromolecules*, 44(5):1211–1219, MAR 8 2011.
- [10] Christopher L. Lewis, Kathleen Stewart, and Mitchell Anthamatten. The Influence of Hydrogen Bonding Side-Groups on Viscoelastic Behavior of Linear and Network Polymers. *Macromolecules*, 47(2):729–740, JAN 28 2014.
- [11] Jiahui Li, James A. Viveros, Michelle H. Wrue, and Mitchell Anthamatten. Shape-memory effects in Polymer networks containing reversibly associating side-groups. *Advanced Materials*, 19(19):2851+, OCT 5 2007.
- [12] Kathleen E. Feldman, Matthew J. Kade, E. W. Meijer, Craig J. Hawker, and Edward J. Kramer. Model Transient Networks from Strongly Hydrogen-Bonded Polymers. *Macromolecules*, 42(22):9072–9081, NOV 24 2009.
- [13] Stefano Burattini, Howard M. Colquhoun, Justin D. Fox, Donia Friedmann, Barnaby W. Greenland, Peter J. F. Harris, Wayne Hayes, Michael E. Mackay, and Stuart J. Rowan. A self-repairing, supramolecular Polymer system: healability as a consequence of donor-acceptor pi-pi stacking interactions. *Chemical Communications*, (44):6717–6719, 2009.
- [14] Stefano Burattini, Barnaby W. Greenland, Daniel H. Merino, Wengui Weng, Jonathan Seppala, Howard M. Colquhoun, Wayne Hayes, Michael E. Mackay, Ian W. Hamley, and Stuart J. Rowan. A healable supramolecular polymer blend based on aromatic $\pi - \pi$ stacking and Hydrogen-Bonding interactions. *Journal of the American Chemical Society*, 132(34):12051–12058, 2010.

- [15] WC Yount, DM Loveless, and SL Craig. Strong means slow: Dynamic contributions to the bulk mechanical properties of supramolecular networks. *Angewandte Chemie-International Edition*, 44(18):2746–2748, 2005.
- [16] WC Yount, DM Loveless, and SL Craig. Small-molecule dynamics and mechanisms underlying the macroscopic mechanical properties of coordinatively cross-linked Polymer networks. *Journal of the American Chemical Society*, 127(41):14488–14496, OCT 19 2005.
- [17] DM Loveless, SL Jeon, and SL Craig. Rational control of viscoelastic properties in multicomponent associative Polymer networks. *Macromolecules*, 38(24):10171–10177, NOV 29 2005.
- [18] Hadi Goldansaz, Dietmar Auhl, Bart Goderis, Quentin Voleppe, Charles-Andr Fustin, Jean-Franois Gohy, Christian Bailly, and Evelyne van Ruymbeke. Transient metallosupramolecular networks built from entangled melts of poly(ethylene oxide). *Macromolecules*, 48(11):3746–3755, 2015.
- [19] A. Eisenberg, B. Hird, and R. B. Moore. A new multiplet-cluster model for the morphology of random ionomers. *Macromolecules*, 23(18):4098–4107, SEP 3 1990.
- [20] Quan Chen, Gregory J. Tudryn, and Ralph H. Colby. Ionomer dynamics and the sticky Rouse model. *Journal of Rheology*, 57(5):1441–1462, SEP 2013.
- [21] Quan Chen, Hanqing Masser, Huai-Suen Shiau, Siwei Liang, James Runt, Paul C. Painter, and Ralph H. Colby. Linear Viscoelasticity and Fourier Transform Infrared Spectroscopy of Polyether-Ester-Sulfonate CoPolymer Ionomers. *Macromolecules*, 47(11):3635–3644, JUN 10 2014.

- [22] Russell J. Varley and Sybrand van der Zwaag. Towards an understanding of thermally activated self-healing of an ionomer system during ballistic penetration. *Acta Materialia*, 56(19):5737–5750, NOV 2008.
- [23] C. E. Williams, T. P. Russell, R. Jerome, and J. Horrion. Ionic aggregation in model ionomers. *Macromolecules*, 19(11):2877–2884, NOV 1986.
- [24] M Muller, A Dardin, U Seidel, V Balsamo, B Ivan, HW Spiess, and R Stadler. Junction dynamics in telechelic hydrogen bonded polyisobutylene networks. *Macromolecules*, 29(7):2577–2583, MAR 25 1996.
- [25] M Rubinstein and AV Dobrynin. Solutions of associative Polymers. *Trends In Polymer Science*, 5(6):181–186, JUN 1997.
- [26] K Yamauchi, JR Lizotte, and TE Long. Thermoreversible poly(alkyl acrylates) consisting of self-complementary multiple hydrogen bonding. *Macromolecules*, 36(4):1083–1088, FEB 25 2003.
- [27] M. Doi and S. F. Edwards. *The Theory of Polymer Dynamics*. Oxford University Press, USA, November 1986.
- [28] Jorge Ramirez, Sathish K. Sukumaran, Bart Vorselaars, and Alexei E. Likhtman. Efficient on the fly calculation of time correlation functions in computer simulations. *The Journal of Chemical Physics*, 133(15), 2010.
- [29] Christopher J.S. Petrie. Extensional viscosity: A critical discussion. *Journal of Non-Newtonian Fluid Mechanics*, 137(13):15 – 23, 2006. Extensional FlowWorkshop on Extensional Flows.
- [30] Robert Brown. A brief account of microscopical observations made in the months of June, July and August, 1827, on the particles contained in the

pollen of plants; and on the general existence of active molecules in organic and inorganic bodies. 1828.

- [31] Prince E. Rouse. A theory of the linear viscoelastic properties of dilute solutions of coiling polymers. *The Journal of Chemical Physics*, 21(7), 1953.
- [32] A.E. Likhtman. 1.06 - viscoelasticity and molecular rheology. In Krzysztof Matyjaszewski/Martin Mller, editor, *Polymer Science: A Comprehensive Reference*, pages 133 – 179. Elsevier, Amsterdam, 2012.
- [33] Zuowei Wang, Alexei E. Likhtman, and Ronald G. Larson. Segmental Dynamics in Entangled Linear Polymer Melts. *Macromolecules*, 45(8):3557–3570, APR 24 2012.
- [34] T. Kreer, J. Baschnagel, M. Muller, and K. Binder. Monte carlo simulation of long chain polymer melts: Crossover from rouse to reptation dynamics. *Macromolecules*, 34(4):1105–1117, 2001.
- [35] Michael Rubinstein and Ralph Colby. *Polymer Physics*. Oxford University Press, 2003.
- [36] P. G. de Gennes. Reptation of a polymer chain in the presence of fixed obstacles. *The Journal of Chemical Physics*, 55(2), 1971.
- [37] Masao Doi and S. F. Edwards. Dynamics of concentrated polymer systems. part 1.-brownian motion in the equilibrium state. *J. Chem. Soc., Faraday Trans. 2*, 74:1789–1801, 1978.
- [38] M. E. Cates. Reptation of living polymers: dynamics of entangled polymers in the presence of reversible chain-scission reactions. *Macromolecules*, 20(9):2289–2296, 1987.

- [39] Michael Rubinstein and Alexander N. Semenov. Dynamics of entangled solutions of associating polymers. *Macromolecules*, 34(4):1058–1068, 2001.
- [40] Ludwik Leibler, Michael Rubinstein, and Ralph H. Colby. Dynamics of reversible networks. *Macromolecules*, 24(16):4701–4707, 1991.
- [41] Evgeny B. Stukalin, Li-Heng Cai, N. Arun Kumar, Ludwik Leibler, and Michael Rubinstein. Self-healing of unentangled polymer networks with reversible bonds. *Macromolecules*, 46(18):7525–7541, 2013.
- [42] P. G. de Gennes. Kinetics of diffusioncontrolled processes in dense polymer systems. i. nonentangled regimes. *The Journal of Chemical Physics*, 76(6), 1982.
- [43] Paul J Flory. Jabtonna conference on polymer networks molecular theory of rubber elasticity. *Polymer*, 20(11):1317 – 1320, 1979.
- [44] Werner Kuhn. Beziehungen zwischen molekülgröße, statistischer molekülgestalt und elastischen eigenschaften hochpolymerer stoffe. *Kolloid-Zeitschrift*, 76(3):258–271, 1936.
- [45] Hubert M. James. Statistical properties of networks of flexible chains. *The Journal of Chemical Physics*, 15(9):651–668, 1947.
- [46] Michael Rubinstein* and Sergei Panyukov. Elasticity of polymer networks. *Macromolecules*, 35(17):6670–6686, 2002.
- [47] Michael Rubinstein* and Sergei Panyukov. Nonaffine deformation and elasticity of polymer networks. *Macromolecules*, 30(25):8036–8044, 1997.
- [48] Michael Rubinstein and Ralph H. Colby. *Polymer physics*. Oxford university press, New York, 2003. Reimpression : 2004.

- [49] Daan Frenkel and Berend Smit. *Understanding Molecular Simulation: From Algorithms to Applications*, volume 1 of *Computational Science Series*. Academic Press, San Diego, second edition, 2002.
- [50] M. P. Allen and D. J. Tildesley. *Computer Simulation of Liquids (Oxford Science Publications)*. Oxford science publications. Oxford University Press, reprint edition, 1989.
- [51] Kurt Kremer and Gary S. Grest. Dynamics of entangled linear polymer melts: A molecular-dynamics simulation. *The Journal of Chemical Physics*, 92(8):5057–5086, 1990.
- [52] C.-C. Huang, H. Xu, and J.-P. Ryckaert. Kinetics and dynamic properties of equilibrium polymers. *The Journal of Chemical Physics*, 125(9):094901, 2006.
- [53] C.-C. Huang, H. Xu, F. Crevel, J. Wittmer, and J.-P. Ryckaert. Reaction kinetics of coarse-grained equilibrium polymers: A brownian dynamics study. In Mauro Ferrario, Giovanni Ciccotti, and Kurt Binder, editors, *Computer Simulations in Condensed Matter Systems: From Materials to Chemical Biology Volume 2*, volume 704 of *Lecture Notes in Physics*, pages 379–418. Springer Berlin Heidelberg, 2006.
- [54] C. C. Huang, H. Xu, and J. P. Ryckaert. Kinetics and dynamic properties of equilibrium polymers. *J. Chem. Phys.*, 125(9):094901, 2006.
- [55] Robert S. Hoy and Glenn H. Fredrickson. Thermoreversible associating polymer networks. i. interplay of thermodynamics, chemical kinetics, and polymer physics. *The Journal of Chemical Physics*, 131(22):224902, 2009.
- [56] Daan Frenkel and Berend Smit. *Understanding Molecular Simulation: From Algorithms to Applications*. Computational Science Series. Academic Press, San Diego, second edition, 2002.

- [57] L. G. Baxandall. Dynamics of reversibly cross-linked chains. *Macromolecules*, 22(4):1982–1988, 1989.
- [58] Alexander N. Semenov and Michael Rubinstein. Thermoreversible gelations in solutions of associative polymers. *Macromolecules*, 31:1373–1385, 1998.
- [59] Michael Rubinstein and Alexander N. Semenov. Thermoreversible gelations in solutions of associative polymers. 2. linear dynamics. *Macromolecules*, 31(4):1386–1397, 1998.
- [60] L. Leibler, M. Rubinstein, and R. H. Colby. Dynamics of reversible networks. *Macromolecules*, 24(16):4701–4707, AUG 5 1991.
- [61] M. Rubinstein and A. N. Semenov. Dynamics of entangled solutions of associating Polymers. *Macromolecules*, 34(4):1058–1068, FEB 13 2001.
- [62] Mostafa Ahmadi, Laurence G. D. Hawke, Hadi Goldansaz, and Evelyne van Ruymbeke. Dynamics of entangled linear supramolecular chains with sticky side groups: Influence of hindered fluctuations. *Macromolecules*, 48(19):7300–7310, 2015.
- [63] G. Marrucci, S. Bhargava, and S. L. Cooper. Models of shear-thickening behavior in physically cross-linked networks. *Macromolecules*, 26(24):6483–6488, NOV 22 1993.
- [64] A. N. Semenov and M. Rubinstein. Dynamics of entangled associating polymers with large aggregates. *Macromolecules*, 35(12):4821–4837, 2002.
- [65] RH Colby, X Zheng, MH Rafailovich, J Sokolov, DG Peiffer, SA Schwarz, Y Strzhemechny, and D Nguyen. Dynamics of lightly sulfonated polystyrene ionomers. *Physical Review Letters*, 81(18):3876–3879, NOV 2 1998.

- [66] NK Tierney and RA Register. Ion hopping in ethylene-methacrylic acid ionomer melts as probed by rheometry and cation diffusion measurements. *Macromolecules*, 35(6):2358–2364, MAR 12 2002.
- [67] R. D. Groot and W. G. M. Agterof. Monte Carlo study of associative polymer networks. 1. Equation of state. *Journal of Chemical Physics*, 100(2):1649–1656, JAN 15 1994.
- [68] Y Liu and RB Pandey. Sol-gel phase transitions in thermoreversible gels: Onset of gelation and melting. *Journal of Chemical Physics*, 105(2):825–836, JUL 8 1996.
- [69] Kumar, Sanat K. and Douglas, Jack F. Gelation in physically associating polymer solutions. *Phys. Rev. Lett.*, 87:188301, Oct 2001.
- [70] C Manassero, G Raos, and G Allegra. Structure of model telechelic Polymer melts by computer simulation. *Journal of Macromolecular Science-Physics*, B44(6):855–871, 2005.
- [71] L Guo and E Luijten. Reversible gel formation of triblock coPolymers studied by molecular dynamics simulation. *Journal of Polymer Science Part B-Polymer Physics*, 43(8):959–969, APR 15 2005.
- [72] SM Loverde, AV Ermoshkin, and MO De La Cruz. Thermodynamics of reversibly associating ideal chains. *Journal of Polymer Science PART B-Polymer Physics*, 43(7):796–804, APR 1 2005.
- [73] Arlette R. C. Baljon, Danny Flynn, and David Krawzsenek. Numerical study of the gel transition in reversible associating Polymers. *Journal of Chemical Physics*, 126(4), JAN 28 2007.

- [74] Monojoy Goswami, Sanat K. Kumar, Aniket Bhattacharya, and Jack F. Douglas. Computer simulations of lonomer self-assembly and dynamics. *Macromolecules*, 40(12):4113–4118, JUN 12 2007.
- [75] J. Billen, M. Wilson, A. Rabinovitch, and A. R. C. Baljon. Topological changes at the gel transition of a reversible Polymeric network. *Europhys. Lett.*, 87(6), SEP 2009.
- [76] Mark Wilson, Avinoam Rabinovitch, and Arlette R. C. Baljon. Aggregation kinetics of a simulated telechelic Polymer. *Phys. Rev. E*, 84(6, Part 1), DEC 5 2011.
- [77] R. D. Groot and W. G. M. Agterof. Monte Carlo study of associative polymer networks. 2. Rheologic aspects. *Journal of Chemical Physics*, 100(2):1657–1664, JAN 15 1994.
- [78] D Bedrov, GD Smith, and JF Douglas. Influence of self-assembly on dynamical and viscoelastic properties of telechelic Polymer solutions. *Europhys. Lett.*, 59(3):384–390, AUG 2002.
- [79] R. S. Hoy and G. H. Fredrickson. Thermoreversible associating polymer networks. i. interplay of thermodynamics, chemical kinetics, and polymer physics. *J. Chem. Phys.*, 131:224902, 2009.
- [80] Zhenlong Li, Hadrian Djohari, and Elena E. Dormidontova. Molecular dynamics simulations of supramolecular polymer rheology. *The Journal of Chemical Physics*, 133(18):184904, 2010.
- [81] K. Kremer and G. S. Grest. Dynamics of entangled linear polymer melts - a molecular-dynamics simulation. *J. Chem. Phys.*, 92(8):5057–5086, 1990.

- [82] Michael Rubinstein and Ralph H. Colby. *Polymer Physics*. Oxford University Press, Oxford New York, 1 edition, 2003.
- [83] M. E. Cates. Reptation of living polymers: dynamics of entangled polymers in the presence of reversible chain-scission reactions. *Macromolecules*, 20(9):2289–2296, 1987.
- [84] Hiroshi Watanabe, Yumi Matsumiya, Yuichi Masubuchi, Osamu Urakawa, and Tadashi Inoue. Viscoelastic Relaxation of Rouse Chains undergoing Head-to-Head Association and Dissociation: Motional Coupling through Chemical Equilibrium. *Macromolecules*, 48(9):3014–3030, MAY 12 2015.
- [85] Guohua Deng, Chuanmei Tang, Fuya Li, Huanfeng Jiang, and Yongming Chen. Covalent Cross-Linked Polymer Gels with Reversible Sol-Gel Transition and Self-Healing Properties. *Macromolecules*, 43(3):1191–1194, FEB 9 2010.
- [86] Fuyong Liu, Fuya Li, Guohua Deng, Yongming Chen, Baoqing Zhang, Jun Zhang, and Chen-Yang Liu. Rheological Images of Dynamic Covalent Polymer Networks and Mechanisms behind Mechanical and Self-Healing Properties. *Macromolecules*, 45(3):1636–1645, FEB 14 2012.
- [87] D. J. M. van Beek, A. J. H. Spiering, Gerrit W. M. Peters, Klaas te Nijenhuis, and Rint P. Sijbesma. Unidirectional dimerization and stacking of ureidopyrimidinone end groups in polycaprolactone supramolecular Polymers. *Macromolecules*, 40(23):8464–8475, NOV 13 2007.
- [88] MarkoM.L. Nieuwenhuizen, TomF.A. deGreef, RobL.J. vanderBruggen, JosM.J. Paulusse, WilcoP.J. Appel, MaartenM.J. Smulders, RintP. Sijbesma, and E.W. Meijer. Self-assembly of ureido-pyrimidinone dimers into one-

- dimensional stacks by lateral hydrogen bonding. *Chemistry - A European Journal*, 16(5):1601–1612, 2010.
- [89] R. Everaers, S. K. Sukumaran, G. S. Grest, C. Svaneborg, and A. Sivasubramanian ANDK. Kremer. Rheology and microscopic topology of entangled polymeric liquids. *Science*, 303(5659):823–826, 2004.
- [90] Alexei E. Likhtman, Sathish K. Sukumaran, and Jorge Ramirez. Linear viscoelasticity from molecular dynamics simulation of entangled polymers. *Macromolecules*, 40:6748–6757, 2007.
- [91] M. P. Allen and D. J. Tildesley. *Computer Simulation of Liquids*. Clarendon Press, Oxford, 1987.
- [92] E.A. Koopman and C.P. Lowe. An algorithm for detecting percolating structures in periodic systems application to polymer networks. *Journal of Computational Physics*, 274(0):758 – 769, 2014.
- [93] R. B. Pandey and D. P. Landau. Directed growth in kinetic gelation. *Journal of Physics A: Mathematical and General*, 18(7):L399, 1985.
- [94] Evgeny B. Stukalin, Li-Heng Cai, N. Arun Kumar, Ludwik Leibler, and Michael Rubinstein. Self-healing of unentangled polymer networks with reversible bonds. *Macromolecules*, 46(18):7525–7541, 2013.
- [95] Jacob N. Israelachvili, D. John Mitchell, and Barry W. Ninham. Theory of self-assembly of hydrocarbon amphiphiles into micelles and bilayers. *J. Chem. Soc., Faraday Trans. 2*, 72:1525–1568, 1976.
- [96] Michael Lang. Monomer fluctuations and the distribution of residual bond orientations in polymer networks. *Macromolecules*, 46:9782–9797, 2013.

- [97] I. A. Nyrkova and A. N. Semenov. Correlation effects in dynamics of living Polymers. *Europhys. Lett.*, 79(6):66007, 2007.
- [98] Sebastian Hackelbusch, Torsten Rossow, Peter van Assenbergh, and Sebastian Seiffert. Chain Dynamics in Supramolecular Polymer Networks. *Macromolecules*, 46(15):6273–6286, AUG 13 2013.
- [99] Torsten Rossow, Axel Habicht, and Sebastian Seiffert. Relaxation and dynamics in transient polymer model networks. *Macromolecules*, 47(18):6473–6482, 2014.
- [100] J. Ramirez, S. K. Sukumaran, Bart Vorselaars, and A. E. Likhtman. Efficient on the fly calculation of time correlation functions in computer simulations. *J. Chem. Phys.*, 133(15):154103, 2010.
- [101] L. Leibler, M. Rubinstein, and R. H. Colby. Dynamics of telechelic ionomers. can polymers diffuse large distances without relaxing stress. *J. Phys. II Frances*, 3:1581–1590, 1993.
- [102] M. Rubinstein and S. Panyukov. Elasticity of polymer networks. *Macromolecules*, 35(17):6670–6686, 2002.
- [103] Fred. T. Trouton. On the coefficient of viscous traction and its relation to that of viscosity. *Proceedings of the Royal Society of London. Series A, Containing Papers of a Mathematical and Physical Character*, 77(519):pp. 426–440, 1906.
- [104] D.F. James and K. Walters. A critical appraisal of available methods for the measurement of extensional properties of mobile systems. In A.A. Collyer, editor, *Techniques in Rheological Measurement*, pages 33–53. Springer Netherlands, 1993.

- [105] Donghua Xu, Jennifer L. Hawk, David M. Loveless, Sung Lan Jeon, and Stephen L. Craig. Mechanism of shear thickening in reversibly cross-linked supramolecular polymer networks. *Macromolecules*, 43(7):3556–3565, 2010. PMID: 20479956.
- [106] Anubhav Tripathi, Kam C Tam, and Gareth H McKinley. Rheology and dynamics of associative polymers in shear and extension: theory and experiments. *Macromolecules*, 39(5):1981–1999, 2006.
- [107] Donghua Xu, Chen-Yang Liu, and Stephen L. Craig. Divergent shear thinning and shear thickening behavior of supramolecular polymer networks in semidilute entangled polymer solutions. *Macromolecules*, 44(7):2343–2353, 2011. PMID: 21547008.
- [108] F. Tanaka and S. F. Edwards. Viscoelastic properties of physically crosslinked networks. 1. transient network theory. *Macromolecules*, 25(5):1516–1523, 1992.
- [109] J. Sprakel, E. Spruijt, M. A. Cohen Stuart, N. A. M. Besseling, M. P. Lettinga, and J. van der Gucht. Shear banding and rheochaos in associative polymer networks. *Soft Matter*, 4:1696–1705, 2008.
- [110] G. Marrucci, S. Bhargava, and S. L. Cooper. Models of shear-thickening behavior in physically crosslinked networks. *Macromolecules*, 26(24):6483–6488, 1993.
- [111] K. C. Tam, M. A. Jenkins, R. D. and Winnik, and D. R. Bassett. A structural model of hydrophobically modified urethaneethoxylate (heur) associative polymers in shear flows. *Macromolecules*, 31(13):4149–4159, 1998.
- [112] J.G Hernández Cifre, Th.M.A.O.M Barenbrug, J.D Schieber, and B.H.A.A van den Brule. Brownian dynamics simulation of reversible polymer net-

- works under shear using a non-interacting dumbbell model. *Journal of Non-Newtonian Fluid Mechanics*, 113(23):73 – 96, 2003.
- [113] Sebastian Seiffert and Joris Sprakel. Physical chemistry of supramolecular polymer networks. *Chem. Soc. Rev.*, 41:909–930, 2012.
- [114] T. A. Witten Jr. and M. H. Cohen. Crosslinking in shear-thickening ionomers. *Macromolecules*, 18(10):1915–1918, 1985.
- [115] H. Manfred Wagner, Heike Bastian, Peter Hachmann, Joachim Meissner, Stefan Kurzbeck, H. Münstedt, and F. Langouche. The strain-hardening behaviour of linear and long-chain-branched polyolefin melts in extensional flows. *Rheologica Acta*, 39(2):97–109, 2000.
- [116] D. J. Evans and G. P. Morris. *Statistical Mechanics of Nonequilibrium Liquids*. Academic Press, London, 1990.
- [117] Thomas Soddemann, Burkhard Dünweg, and Kurt Kremer. Dissipative particle dynamics: A useful thermostat for equilibrium and nonequilibrium molecular dynamics simulations. *Phys. Rev. E*, 68:046702, Oct 2003.
- [118] B. D. Todd and Peter J. Daivis. The stability of nonequilibrium molecular dynamics simulations of elongational flows. *The Journal of Chemical Physics*, 112(1), 2000.
- [119] Andrs Baranyai and Denis J. Evans. New algorithm for constrained molecular-dynamics simulation of liquid benzene and naphthalene. *Molecular Physics*, 70(1):53–63, 1990.
- [120] B. D. Todd and Peter J. Daivis. Homogeneous non-equilibrium molecular dynamics simulations of viscous flow: techniques and applications. *Molecular Simulation*, 33(3):189–229, 2007.

- [121] A W Lees and S F Edwards. The computer study of transport processes under extreme conditions. *Journal of Physics C: Solid State Physics*, 5(15):1921, 1972.
- [122] Jing Cao and Alexei E. Likhtman. Simulating startup shear of entangled polymer melts. *ACS Macro Letters*, 4(12):1376–1381, 2015.
- [123] A.M. Kraynik and D.A. Reinelt. Extensional motions of spatially periodic lattices. *International Journal of Multiphase Flow*, 18(6):1045 – 1059, 1992.
- [124] B.D. Todd and Peter J. Daivis. A new algorithm for unrestricted duration nonequilibrium molecular dynamics simulations of planar elongational flow. *Computer Physics Communications*, 117(3):191 – 199, 1999.
- [125] Alexei E. Likhtman and Jorge Ramirez. Rheology of entangled polymers: Toolkit for analysis of theory & experiment.
- [126] Aamir Shabbir, Hadi Goldansaz, Ole Hassager, Evelyne van Ruymbeke, and Nicolas J. Alvarez. Effect of hydrogen bonding on linear and nonlinear rheology of entangled polymer melts. *Macromolecules*, 48(16):5988–5996, 2015.
- [127] Douglas E. Smith, Hazen P. Babcock, and Steven Chu. Single-polymer dynamics in steady shear flow. *Science*, 283(5408):1724–1727, 1999.
- [128] Jens Kromann Nielsen, Henrik Koblitz Rasmussen, Ole Hassager, and Gareth H. McKinley. Elongational viscosity of monodisperse and bidisperse polystyrene melts. *Journal of Rheology*, 50(4), 2006.
- [129] Anders Bach, Kristoffer Almdal, Henrik Koblitz Rasmussen, and Ole Hassager*. Elongational viscosity of narrow molar mass distribution polystyrene. *Macromolecules*, 36(14):5174–5179, 2003.

- [130] M. H. Wagner and J. Schaeffer. Rubbers and polymer melts: Universal aspects of nonlinear stress-strain relations. *Journal of Rheology*, 37(4), 1993.
- [131] Giuseppe Marrucci and Giovanni Ianniruberto. Interchain pressure effect in extensional flows of entangled polymer melts. *Macromolecules*, 37(10):3934–3942, 2004.
- [132] Manfred H. Wagner, Saeid Kheirandish, and Ole Hassager. Quantitative prediction of transient and steady-state elongational viscosity of nearly monodisperse polystyrene melts. *Journal of Rheology*, 49(6), 2005.
- [133] J. Meissner, S.E. Stephenson, A. Demarmels, and P. Portman. Multiaxial elongational flows of polymer melts: classification and experimental realization. *Journal of Non-Newtonian Fluid Mechanics*, 11(3):221 – 237, 1982.
- [134] L. J. Fetters, D. J. Lohse, D. Richter, T. A. Witten, and A. Zirkel. Connection between polymer molecular weight, density, chain dimensions, and melt viscoelastic properties. *Macromolecules*, 27(17):4639–4647, 1994.
- [135] Ralf Everaers, Sathish K. Sukumaran, Gary S. Grest, Carsten Svaneborg, Arvind Sivasubramanian, and Kurt Kremer. Rheology and microscopic topology of entangled polymeric liquids. *Science*, 303(5659):823–826, 2004.
- [136] Zuowei Wang, Alexei E. Likhtman, and Ronald G. Larson. Segmental dynamics in entangled linear polymer melts. *Macromolecules*, 45(8):3557–3570, 2012.
- [137] Jing Cao and Alexei E. Likhtman. Time-dependent orientation coupling in equilibrium polymer melts. *Phys. Rev. Lett.*, 104:207801, May 2010.
- [138] Jing Cao. *Molecular dynamics study of polymer melts*. PhD thesis, University of Reading, 2011.

- [139] M.L. Matin, P.J. Daivis, and B.D. Todd. Cell neighbor list method for planar elongational flow: rheology of a diatomic fluid. *Computer Physics Communications*, 151(1):35 – 46, 2003.
- [140] Joshua A. Anderson, Chris D. Lorenz, and A. Travesset. General purpose molecular dynamics simulations fully implemented on graphics processing units. *Journal of Computational Physics*, 227(10):5342 – 5359, 2008.
- [141] Morton. A computer oriented geodetic data base and a new technique in file sequencing. Technical Report Ottawa, Ontario, Canada, 1966.
- [142] W. Kahan. Pracniques: Further remarks on reducing truncation errors. *Commun. ACM*, 8(1):40–, January 1965.
- [143] Peter H. Colberg and Felix Hfling. Highly accelerated simulations of glassy dynamics using gpus: Caveats on limited floating-point precision. *Computer Physics Communications*, 182(5):1120 – 1129, 2011.
- [144] Federico Frascoli and B. D. Todd. Molecular dynamics simulation of planar elongational flow at constant pressure and constant temperature. *The Journal of Chemical Physics*, 126(4), 2007.
- [145] Richard S. Graham, Alexei E. Likhtman, Tom C. B. McLeish, and Scott T. Milner. Microscopic theory of linear, entangled polymer chains under rapid deformation including chain stretch and convective constraint release. *Journal of Rheology*, 47(5), 2003.
- [146] E. van Ruymbeke, J. Nielsen, and O. Hassager. Linear and nonlinear viscoelastic properties of bidisperse linear polymers: Mixing law and tube pressure effect. *Journal of Rheology*, 54(5), 2010.